HEAT AND MASS TRANSFER. VOLUME 7, 1968

A. V. Lykova, et al

Foreign Technology Division
Wright-Patterson Air Force Base, Ohio

20 August 1969

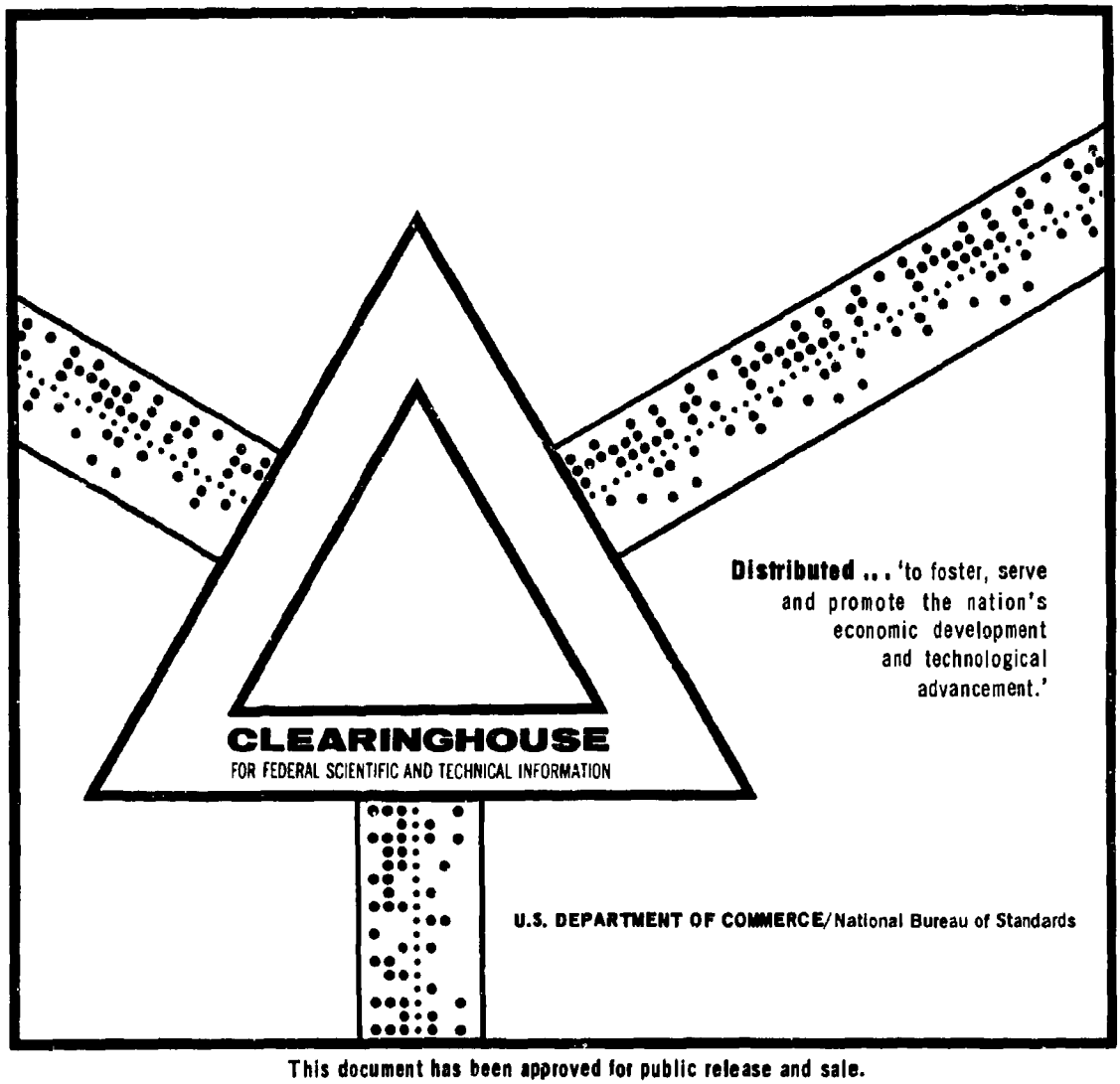

FTD-HT-23-820-68 Part 3 of 3

AD698519

FOREIGN TECHNOLOGY DIVISION

HEAT AND MASS TRANSFER

By

A. V. Lykova, B. M. Smol'kogo

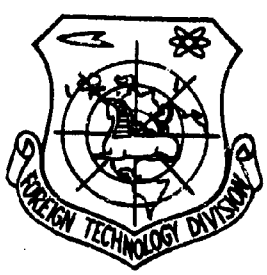

189

FTD-HT-23-820-68
Part 3 of 3

EDITED TRANSLATION

HEAT AND MASS TRANSFER

By: A. V. Lykova, B. M. Smol'kogo

Source: Teplo-I Massoperenos (Heat and Mass Transfer) 1968, Vol. 7, pp. 1 - 609

English Pages: 463 - 649

Translated Under: F33657-68-D-1287

PREPARED BY:

TRANSLATION DIVISION
FOREIGN TECHNOLOGY DIVISION
WP-AFB, OHIO.

Date 20 Aug 19 69

PART THREE

HEAT AND MASS TRANSFER PARAMETERS

THERMOPHYSICAL CHARACTERISTICS OF HEAT-SENSITIVE PAINTS

B. G. Abramovich and L. N. Novichenok

In recent years heat-sensitive paints have found broader use in measuring surface temperatures both in our country and abroad. This method of measuring temperature has one adherence by its simplicity, profitability, and its truly endless possibilities of application. What point measurements achieve by protracted laborious investigations, thermo-paints arrive at almost without any labor involved. They make it possible to obtain a graphic picture of temperature distribution with various units used in measuring temperature on moving and current-bearing parts, etc. Balance study of the properties of these remarkable temperature indicators throw open new vistas of their application.

To evaluate the inertness of thermo-paints and their effect on heat transfer, we determined thermophysical properties of a set of heat-sensitive paints which are now being readied for series production.

In exploring thermophysical properties of heat-sensitive paints, we used a nonsteady-state method [2, 3] the basis of which is the solution of the thermal conductivity problem for a system of bodies consisting of a bounded and a semibounded rod with boundary conditions of the first and fourth orders [1].

Thermophysical characteristics were calculated from the data of one short experiment, using the following formulas:

$$\lambda = \frac{BR}{2AK\sqrt{\sigma}} \quad (1)$$

for the coefficient of thermal diffusivity

$$a = \frac{R^2}{4K^2\tau} \qquad (2)$$

for specific heat

$$C = \frac{26K\sqrt{\tau}}{AR^2}$$
$$A = \frac{2}{\theta}\operatorname{erfc} K - 1 \qquad (3)$$

where k was determined from previously compiled calculation tables [3].

A schematic diagram of the apparatus is shown in Figure 1.

The specific weight of a thermo-paint film was determined by the method of titrating a potassium iodide solution (γ_{AI} = 1500 kg/m^3), in which the thermo-paint film was placed, using water [4]. The method was based on establishing a relationship between the value of the specific weight of the film and the ratio of the volumes of titrated and titrating liquids at the moment the film falls onto the bottom of the vessel.

The calculation made use of the formula

$$\gamma = \frac{\gamma_в V_в + \gamma_{в1} V_{в1}}{V_в + V_{в1}}$$

All the results of the study are shown in tabular form.

Thermophysical characteristics of thermo-paints were determined with an error of approximately 10-15 percent, and the error in determination of their density was approximately 5 percent.

As we can see from the table, the values of the thermal conductivity coefficient lie within the limits 0.19-0.99 w/m·deg, the coefficient of thermal diffusivity -- in the limits $(1.1\text{-}29)\cdot10^{-7}$ m^2/sec, and the specific heat -- $(0.22\text{-}1.45)\cdot10^3$ J/kg·deg.

Table of Thermophysical Characteristics of a Set of Heat-Sensitive Paints

No.	No. of thermo paint	Critical temperature, t_{cr} °C at τ_h = 120 sec and τ_b = 30 d sec	Density γ kg/m³	Coefficient of thermal conductivity λ W/m·deg	Specific heat c J/kg·deg	Coefficient of thermal diffusivity a m²/sec·10⁷
I	I a	45	I445	0,22	I,I2	I,4
2	I7	55	I463	0,22	I,I0	I,4
3	3I	70	I340	0,I9	I,30	I,I
4	46	74	I435	0,24	I,035	I,6
5	32	90	I395	0,2I	I,065	I,4
6	50	II0	I428	0,23	I,I32	I,4
7	4	I30	I4I5	0,22	I,350	I,I
8	30	I30	I460	0,23	I,234	I,3
9	I9	I45	I455	0,26	0,900	2,I
I0	5	I60	I395	0,38	0,587	4,6
II	29	I75	I305	0,83	0,299	I9,9
I2	6	I90	I200	0,27	I,070	2,I
I3	I8	205	I390	0,43	0,585	5,3
I4	230	220	I460	0,52	0,455	7,8
I5	240	225	I450	0,46	0,480	6,7
I6	8	240	I468	0,36	0,635	3,9
I7	320	250	I407	0,3I	0,754	2,9
I8	35	280	I220	0,26	I,040	2,I
I9	33	320	I378	0,24	I,235	I,4
20	26	350	I420	0,24	0,89I	I,9
2I	I2	360	I445	0,84	0,280	20,6
22	230[X]	400	I455	0,52	0,455	7,8
23	470	440	I420	0,39	0,524	5,2
24	480	480	I445	0,30	0,838	2,5
25	490	490	I430	0,34	0,700	3,4
26	I4	550	I455	0,99	0,229	29,0
27	52	555	I450	0,I7	0,8I4	I,5
28	30	570	I460	0,23	I,234	I,3
29	7	690	I428	0,53	0,526	7,0
30	I00	830	I378	0,2I	I,450	I,I

For comparison, we present the values of thermophysical characteristics inherent in the following materials:

a) lacquer and paint coatings and resins (organosilicon lacquer K-55, epoxide resin E-41, etc.)

λ = 0.11-0.17 w/m·deg,

$a = (0.43\text{-}0.87)\cdot 10^{-7}$ m^2/sec,

$c = (1.4\text{-}1.8)\cdot 10^3$ J/kg·deg;

b) heat-insulation materials (asbestos cement, asbestos bakelite, polychlorovinyl plastic, etc.)

λ = 0.032-0.11 w/m·deg,

$a = (0.2 - 0.4)\ 10^{-7} m^2$/sec,

$c = (32 - 1.85)\ 10^3$ J/kg·deg;

c) stainless steel 1Kh18N9T

λ = 9.5 - 12 w/m·deg,

$a = 55\cdot 10^{-7} m^2$/sec,

$c = (0.22 - 0.28)\ 10^3$ J/kg·deg;

From comparison of this data it is clear that heat-sensitive paints have higher coefficients of thermal conductivity and thermal diffusivity than ordinary lacquer-paint coatings and heat-insulating materials, but lower values than steel.

As a result of studies of thermophysical properties of thermo-paints, it has become possible to calculate their dynamic error, which is approximately 0.1 percent, and to establish that thermo-paints practically speaking do not distort the temperature field.

Accordingly, heat-sensitive paints can be regarded as low-inertia temperature transducers suitable for investigating thermal fields of various materials.

Symbols

θ = relative temperature; λ, a, c and γ = coefficients of thermal conductivity, thermal diffusivity, heat capacity and specific weight of heat-sensitive paint; b = thermal activity of etalon material; R = thickness of

thermo-paint layer; τ = time; γ_B = specific weight of water; V_g = volume of water required in titration; V_{KI} = volume of KI solution.

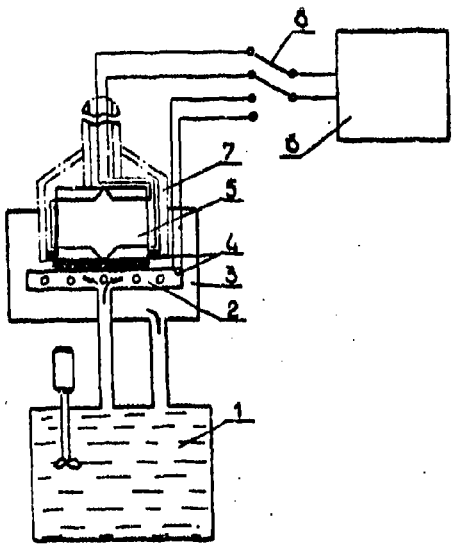

Figure 1. Schematic diagram of apparatus: 1, Thermostat; 2, Base; 3, Vessel; 4, Thermocouples; 5, Specimen; 6, Self-recording potentiometer; 7, Holder; 8, Thermocouple switch

References

1. Lykov, A. V., *Teoriya Teploprovodnosti*, [Theory of Thermal Conductivity], Gostekhnizdat Press, Moscow, 1952.

2. Novichenok, L. N., *IFZh*, Vol. 6, No. 9, 1963.

3. Novichenok, L.N., *Sb. Teplo- i Massoperenos v Kapillyarno-poristykh Telakh*, [Collection: Heat and Mass Transfer in Capillary-Porous Bodies], Nauka i Tekhnika Press, Minsk, 1965.

4. Khoroshaya, Ye. S., G. I. Kovrigina, and V. I. Alekseyenko, *Zavod. Laboratoriye*, Vol. 28, No. 2, p. 205, 1962.

THERMOPHYSICAL CHARACTERISTICS OF FERRITES

Ya. M. Bekker and A. F. Chudnovskiy

The special physical properties of ferrites, in particular, high electrical resistance, make it possible to directly study the lattice component of thermal conductivity, and also effects associated with magnetic ordering and crystallochemical structure.

The present study deals with thermal conductivity and thermal expansion of ferrites, and establishment of their interrelationship with other physical properties.

Materials and Methods of Their Investigation

1. Choice of chemical compositions of the materials in the study was dictated by the necessity to vary within wide limits crystallochemical structure and magnetic properties of solid ferrite solutions. For this purpose, three theories of ferrite compositions were synthesized containing cations with predominant localization in octahedra (Al, Gr, Ni) or in tetrahedra (Zn, Cd), and also cations (Mn, Fe, Mg), the localization of which was determined by technological factors.

Series 1 consisted of solid solutions of ferrite-chromites:

$$Me_{1-yt}\,Fe_{yt}\left[Me_{yt}\,Fe_{(2-t)y}\,Cr_{2(1-y)}\right]O_4\ ,$$

where $0 \leq y \leq 1$ is the concentration of solid solution (varied by 0.1 from specimen to specimen);

$0 \leq t \leq 1$ is the extent of spinel inversion, Me is ions of the metals Ni, Mg, Cd.

Series two -- solid solutions of ferrite-magnesium aluminates:

$$Mg_{1-yt}\,Fe_{yt}\left[Mg_{yt}\,Fe_{(2-t)y}\,Al_{2(1-y)}\right]O_4$$

Series three -- solid solutions of ferrites:

$$y\,NiFe_2O_4 - (1-y)MeFe_2O_4$$

where Me is ions Mg, Zn, Mn.

To exclude the effects of technological factors on measurement results, all specimens of each ferrite system were prepared under the same technological regime, and heat treatment was conducted simultaneously and jointly.

2. The coefficient of thermal conductivity was measured by a method in [1] at room temperature, by a method in [2] in a wide temperature range, and by a method in [3] under exposure to an external magnetic field. The coefficient of thermal expansion was measured on a multi-purpose vacuum dilatometer. The phase composition of the specimens and their crystalline structure were studied on the MIM-7 microscope (porosity, granularity), on the URS-50I X-ray unit (lattice constant, phase composition), and on the YeM-6A electronic microscope (structure of crystallites).

Magnetic parameters in static fields were measured by the ballistic method. The Curie temperature was measured on the NIM-4 bridge. The electrical conductivity and energy of activation were determined by the four-probe method. The rate of propagation of sound longitudinal and transverse waves in the specimens was measured on the UZIS-10 instrument. Microhardness of specimens was determined on the PMT-3 instrument.

Results of Measurements and Their Discussion

1. Thermal conductivity as a function of mean grain size (l_c) is shown in Figure 1.

Microstructural studies revealed that initially grain size growth is accompanied by reduction of its defect content and prolongation of intercrystalline boundaries, which leads to a rise in K. This is in agreement with magnetic measurements. A structure-sensitive magnetic characteristic -- the coercive force (H_c) -- decreased with decrease in defect concentration [4].

Figure 1 (curve 4) makes clear that the course of H_c as a function of l_c corresponds to a drop in K. The appearance of new defects accompanied further grain size growth. Electron-microscopic studies showed that for coarsely crystalline structure (80-120 micromicrons) the specific defect volume rises sharply, which reduces the value of K.

A relationship exists between K and A_c, as predicted by theory. Results of experimental study of this relationship are shown in Figure 2, where the calculated curve: $K \sim A_c^{-1}$ is shown for purposes of comparison. It is clear from this that the relationship $K \sim A_c^{-n}$ is approximately satisfied where $0,6 \leq n \leq 1,5$ In compositions with predominantly ionic bond form A_c proved to have a relatively weak ($n < 1$) effect on K. A_c more markedly affects ($n > 1$) K in those compositions where locally directed covalent bonds are predominant and are stronger than ionic bonds.

3. The crystal lattice constant (a_o) reflects [5] the energy state of the given crystalline structure and, consequently, affects δ and k of ferrites. The mean free phonon path λ_c

$$\lambda_c \sim \frac{\exp \frac{h_o v}{2 K_o a_o T} - 1}{S(\varphi)}$$

decreases with rise in a_o, that is, k is reduced. Additionally, the coefficient of anharmonicity (β) rises with rise in a_o, which increases the phonon scattering cross section ($S(\phi)$) and δ. Figure 3 presents the results of study of δ and the reduced thermal resistance ($W_A = W/A_c$) as a function of a_o. It is clear from the figure that experimental results are in agreement with theory. The functions derived have been confirmed by calculations of the Debye temperature $\vartheta_D = 2,32 \frac{h_o v}{K_o a_o}$ (here the minimum spacing between ions in ferrites $\frac{a_o \sqrt{3}}{2}$ is taken into account). θ_D is reduced with rise in a_o, that is, the number of phonons in the state of statistical equilibrium $N_\varphi \sim (\exp \frac{\theta_D}{T} - 1)^{-1}$ rises and increases their scattering. θ_D for the composition studied lies within the limits $450 \leq \theta_D \leq 700°K$.

4. Analysis of the thermal conductivity components of ferrites in a magnetic field showed that the variation in K in the temperature range studied can be caused by the following:

a) the Maggi-Righi-Leduc effect (MRL) and the $\sigma > \Delta E$ effect. Estimation of the contribution made by the MRL effect to the value of K for iron ferrite, where this contribution must be the maximum, shows that the presumed effect is caused by [7] a supplementary temperature gradient approximately equal to 10^{-2}deg/cm, which is three orders of magnitude less than the applied gradient.

Experimental data shown in Figure 4 demonstrates that the thermal conductivity of ferrites in a magnetic field initially rises $\frac{K_H - K}{K} = \frac{\Delta K_H}{K} > 0$ and then remains unchanged. The quantity ΔK_H -- the effect for cobalt ferrite is greater than for nickel ferrite, the magnetization of which is less than for the cobalt ferrite. These results can be accounted for by the ΔE effect [8], the value of which is determined from the relationship

$$\frac{\Delta E}{E_0} = B_0\left[\left(\frac{I}{I_s}\right)^2 - \frac{1}{3}\right],$$

where B_0 is a numerical constant.

The influence of the ΔE effect lies in the fact that when ferrites are magnetized, their modulus of elasticity and shear modulus determining the rate of phonon propagation are changed. The value of the ΔE effect increases with rising H and when $I = I_s$ remains unchanged, $\Delta E = -0.66\, B_0 E_0$, analogous to the observed function of K_H.

If we represent the ΔE effect [9] via microscopic characteristics of ferrites

$$\frac{\Delta E}{E_0} = \frac{2\lambda_s E_s}{5\sigma_i}$$

then it becomes understandable that the value of K of ferrites in a magnetic field depends materially on their magnetostriction (λ_S) since internal

stresses [10] $\sigma_i \approx 10^8$ н/м². Actually [11] for $CoFe_2O_4 \lambda_S = 200 \cdot 10^{-6}$, but for $NiFe_2O_4$, $\lambda_S = -26 \cdot 10^{-6}$, respectively, which is in agreement with the ΔK_h of these ferrites.

5. Thermal conductivity of ferrites follows a distinctive temperature course determined by the state of magnetic ordering. Comparison of K demonstrates a certain correlation -- specimens with greater I are characterized by a higher value of K. This has also been confirmed by measurement of the Curie temperature:

$$\Theta_K = \frac{I_0 N_0 \mu_B}{R \mathfrak{D}}.$$

Specimens marked by high θ_K correspond to a higher K value.

The temperature dependence of K is shown in Figure 5. In the low-temperature region K initially rises with decreasing T owing to an increase in λ_c (T 180°K) with further drop in T, thermal conductivity falls off owing to effective phonon scattering at crystalline defects, since they become commensurable with the size of defects. In the positive temperature region, K decreases with rising T, approximately following the Eucken law. In the θ_k region the temperature dependence of K exhibits the maximum, which is caused by an anomaly of C_v. It can be concluded from measurements of electroconductivity and δ that $C_v = C_\varphi + C_n$. At Θ_k the heat capacity experiences a jump [9], the value of which

$$\Delta C \approx 1{,}5 \frac{\Theta_K}{\mathfrak{D} I_0} \cdot \frac{d I_i^2}{dT}$$

From here it is clear that the maximum on the temperature dependence of K is proportional to 1. Thus, curve 1 relating to zinc ferrite, whose magnetic moment equals zero, does not exhibit a K maximum.

The maximum on the curve K = f(t) for the ferrite $Ni_{0.3}Zn_{0.2}Fe_2O_4$ is greater than for the ferrite $Ni_{0.4}Zn_{0.8}Fe_2O_4$, which is in agreement with their I and Θ_k.

The smearing out of maxima on the experimental curves occurs within the interval 50-80°K. The greater the I, the greater the smearing, which can be accounted for by fluctuations of spontaneous magnetization. Breakdown of the domain structure occurs not at the fixed temperature Θ_k, but within some temperature range.

When ferrite is heated, the ordering of the spinel system is violated, and when $T = \Theta_k$ the energy of thermal agitation becomes comparable with the energy of bulk interaction and long-range order in orientation of spins is wholly absent. However, owing to microstructural inhomogeneities and local degaussing fields short-range order is preserved. Therefore, when $T > \Theta_k$, the thermal conductivity after going through the maximum does not drop off sharply, but diminishes smoothly with rise in temperature.

Conclusions

1. Investigation directly of the phonon component of thermal conductivity and thermal expansion of ferrites has made it possible to establish their interrelationship with other physical properties of ferrites and, in particular, with magnetic properties.

2. An increase in the mean grain size brings about a rise in thermal conductivity, which is accounted for by a reduction in the specific volume of defects in polycrystalline ferrites.

3. A correlation exists between thermal conductivity and mean atomic weight, and in considering this correlation the nature of bonding forces between ions must be borne in mind.

4. The values of coefficients of thermal conductivity and of thermal expansion mutually correlate with each other.

5. Microhardness, thermal conductivity and thermal expansion of ferrites exhibit an interrelationship -- compositions with high microhardness correspond to a greater thermal conductivity, and those with low microhardness correspond to low thermal expansion.

6. Thermal conductivity of ferrites in a magnetic field rises, which is accounted for by the ΔE effect.

7. Compositions with high magnetization correspond to a higher thermal conductivity coefficient. Specimens which have a higher Curie temperature correspond to a higher thermal conductivity coefficient.

Symbols

K = coefficient of thermal conductivity; W = coefficient of thermal expansion; δ = coefficient of thermal expansion; K_H = coefficient of thermal conductivity in the magnetic field H; H = intensity of magnetic field; I = magnetization; I_s = saturation magnetization; I_o = magnetization at 0°K; μ_B = Bohr magneton; No = number of atoms per gram-atom; R = universal gas constant; h_o = Planck constant; k_o = Boltzmann's constant; A_c = mean atomic weight; D = density of mass; C_ϕ = heat capacity of crystal lattice; C_M = heat capacity of magnetic ordering; E = Young's modulus in the field H; E_o = Young's modulus in the absence of a field.

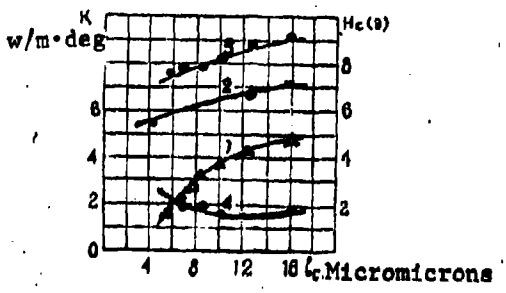

Figure 1. Coefficient of thermal conductivity of ferrites and coercive force as functions of mean grain size: Curves 1, Ferrite 2VT; 2, $MgFe_2O_4$; 3, $NiFe_2O_4$; 4, H_c of ferrite 2VT

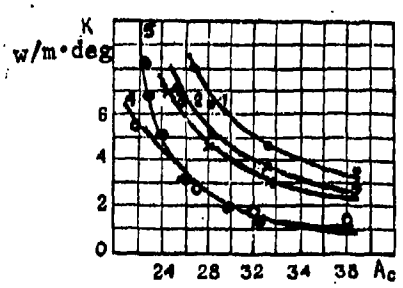

Figure 2. Coefficient of thermal conductivity as a function of mean atomic number of ferrite-chromites and ferrite-aluminites with equal concentration (y) of characterizing ions: Curves 1, y = 0.9; 2, y = 0.6; 3, y = 0.5; 4, y = 0.2; 5, Calculated values

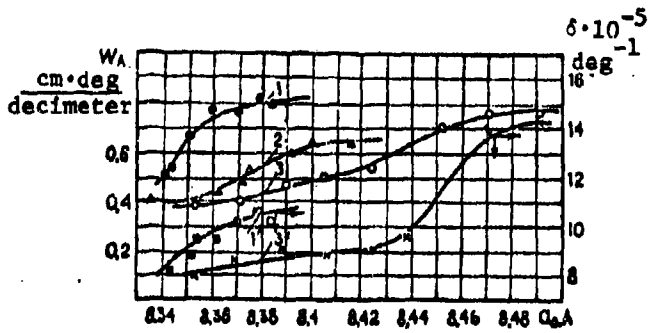

Figure 3. Reduced thermal resistance and thermal expansion as functions of crystal lattice constant

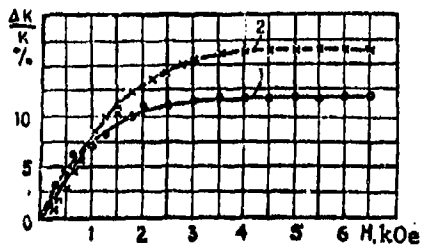

Figure 4. Relative change of thermal conductivity of ferrites in magnetic field: 1, $MnFe_2O_4$; 2, $CoFe_2O_4$

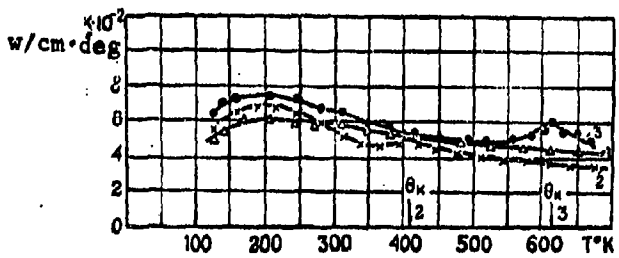

Figure 5. Temperature dependence of thermal conductivity of ferrites: Curves 1 - $ZnFe_2O_4$; 2 - $Zn_{0,8}Fe_{0,4}[Ni_{0,4}Fe_{1,6}]O_4$
3 - $Zn_{0,2}Fe_{0,8}[Ni_{0,8}Fe_{1,2}]O_4$.

References

1. Ioffe, A. V. and A. F. Ioffe, *ZhTF*, Vol. 28, No. 11, p. 2357, 1958.
2. Platunov, Ye. S. and V.V. Kurepin, *Izvestiya Vuzov. Priborostroyeniye*, No. 4, p. 119, 1961.
3. Vishnevskiy, I. I., *Sb. Teplo- i Massobmen v Protessakh Isparenlya*, [Collection: Heat a- d Mass Transfer in Evaporation Processes], p. 236, Academy of Sciences Belorussian SSR Press, Minsk, 1958.
4. Kittel", Ch., *Fizika Ferromagnitnykh Oblastey*, [Collection: Physics of Ferromagnetic Regions], IL Press, Moscow, 1951.
5. Bern, M. and Huang K'un, *Dinamicheskaya Teoriya Kristallicheskikh Reshetok*, [Dynamic Theory of Crystal Lattices], IL Press, Moscow, 1958.
6. Sirota, N. N., *Ferrity Sb. Fizicheskiye i Fizikokhimicheskiye Svoystva*, Ferrites. Collection: Physical and Physicochemical Properties], Academy of Sciences Belorussian SSR, Minsk, 1960.
7. Tsidil'kovskiy, I. M., *Termomagnitnyye Yavleniya v Poluprovodnikakh*, [Thermomagnetic Phenomena in Semiconductors], Fizmatgiz, Moscow, 1962.
8. Bedoy, K. P. *Uprugiye Teplovyye i Elektrivheskiye Yavleniya v Ferromagnetikakh*, [Elastic Thermal and Electrical Phenomena in Ferromagnetics], 1967.
9. Voiskovskiy, S. V., and Ya. S. Shur, *Ferromagnetism*, [Ferromagnetism], GITTL Press, Moscow, 1948.
10. Smolenskiy, G.A. and A. G. Gurevich, *Poluprovodniki v Nauke i Tekhnike*, [Semiconductors in Science and Technology], Vol. 2, Academy of Sciences USSR Press, 1958.
11. Rabkin, L. I., *Vysokochastotnyye Feromagnetism*, [High-grequency Ferromagnetism], Fizmatizdat Press, Moscow, 1960.

EXPERIMENTAL STUDY OF THE VISCOSITY OF THE SYSTEM $N_2O_4 \rightleftarrows 2NO_2 \rightleftarrows 2NO + O_2$ in the Temperature Range 300-780°K and the PRESSURE RANGE 1-50 atm

O. V. Belyayeva, B. G. Maksimov, V. B. Nesterenko,
V. N. Pisarchik, L. A. Pranovich and B. D. Timofeyev

Use of chemically reacting systems of the type $N_2O_4 \rightleftarrows 2NO_2 \rightleftarrows 2NO + O_2$(*) to intensify heat transfer [1], cooling of nuclear reactor channels [2], and as a heat carrier in a gas-turbine engine [3] requires that we know the thermophysical properties of these systems in a wide range of working temperatures and pressures. The present paper deals with an experimental investigation of the viscosity of a chemically reacting system (*) in the temperature range 300-780°K and the pressure range 1-50 atm on a viscosimeter using the dropping load method, the design of which and methods of viscosity measurement have been set forth in detail earlier [4, 5]. Several load designs were studied for use of the viscosimeter with dropping load in investigating the viscosity of the chemically reacting system (*) in the indicated range of temperatures and pressures. These designs differ from each other by the size of the ring gap between the inner diameter of the calibrated channel and the outer diameter of the load, and also by design elements of the centering devices for uniform movement of the load over the measured section.

Prior to and after the experiments on the system (*), the viscosimeter was weighed in nitrogen, helium and carbon dioxide gas. When experimental data on viscosity of the chemically reacting system (*) was treated, the following expression [5] was used:

$$\mu_{p,T} = \frac{A_0 \tau}{[1+\beta(t-t_0)]}\left\{1-\frac{\rho}{\rho_0}[1+3\beta(t-t_0)-f]\right\} - B_0[1+\beta(t-t_0)]\frac{\rho}{\tau} \qquad (1)$$

where the coefficients A_0 and B_0 are found from the viscosimeter weighing data. As has been shown earlier [5], the coefficient B_0 depends on the gas flow regime in the ring channel. For laminar flow, a specific function exists for each load with specific geometric dimensions, and the function can be represented by the following polynomial:

$$B_0 = a_0 + \frac{a_1}{Re^{m_1}} + \frac{a_2}{Re^{m_2}}, \qquad (2)$$

where

$$Re = K \cdot \frac{\rho}{\mu\varepsilon} \cdot [1+\beta(t-t_0)]. \qquad (3)$$

The coefficient K is quite precisely determined based on geometric dimensions of the load and the calibrated channel.

Treatment of weighing data was carried out on the Minsk-22 digital electronic computer at the Institute of Nuclear Power of the Academy of Sciences Belorussian SSR.

The data obtained from weighing the viscosimeter in nitrogen, helium and carbon dioxide gas were used to determine the function $B_0 = f(Re)$, the coefficient A_0, and it was also established that in experiments on load variant IV the dimensionless coefficient of load friction with channel wall $f = 0$ (Figure 1). Here, data on viscosity and the thermodynamic functions of the weighed gases necessary for the calculation were taken from [6] for nitrogen and helium, and from [7] for carbon dioxide gas. The maximum error of individual weighing points when B_0 was used as a function of Re, shown in Figure 1, and the coefficient A_0 obtained did not exceed ±5 percent, while the mean deviation of 112 weighing points in absolute value was 1.9 percent.

Experimental data on the function of nitrogen tetroxide [8-10] were used in treating experimental data on viscosity of the system (*), and in the temperature region of 440°K and the pressure region 1-25 atm, use was made of data calculated according to the method of the Institute of Nuclear Power of the Academy of Sciences Belorussian SSR [11].

Figure 2 presents graphs of experimental data on the viscosity of the chemically reacting system (*) obtained in the Institute of Nuclear Power of the Academy of Sciences Belorussian SSR, on the viscosimeter with falling load variant IV, Petker and Mason [12] used a viscosimeter with a rolling sphere, and Beer [13] -- a viscosimeter with a spiral capillary.

It is clear from Figure 2 that experimental data [12] and [13] embrace the temperature range only from 300-443°K. Satisfactory agreement of experimental data is observed only at room temperature and atmospheric pressure. At pressures of 1 and 5 atm, experimental data of the Institute of Nuclear Power of the Academy of Sciences Belorussian SSR agreed well with [12] throughout the entire temperature range investigated. Experimental data [13] at the maximum temperature of 396°K attained in the experiment differed by 14.4 percent from the experimental data of the Institute of Nuclear Power of the Academy of Sciences Belorussian SSR and the data in [12]. A reduction of the experimental data obtained in [13] obviously must be made because of systematic error not taken into account. First of all, the error must be sought in imprecision of measuring the temperature drop in the capillary by mercury U-shaped manometers, the mercury which was in contact with nitrogen tetroxide during the experiment. Experiments in the Institute of Nuclear Power of the Academy of Sciences Belorussian SSR have shown that during the period of contact of mercury with nitrogen tetroxide when the overall impurity content (water and nitric acid) is about 15 percent salt formation occurs, which for all practical purposes puts the mercury U-shaped manometers out of order.

Conclusions

1. Experimental data obtained at the Institute of Nuclear Power of the Academy of Sciences Belorussian SSR for the chemically reacting system $N_2O_4 \rightleftarrows 2NO_2 \rightleftarrows 2NO + O_2$ agree well with data in [12] at pressures of

1 and 5 atm in the temperature range investigated. These data were obtained for the load variant IV with gas-dynamic stabilization for free motion in a calibrated channel.

2. The mean error of our experimental data on viscosity of the system $N_2O_4 \rightleftarrows 2NO_2 \rightleftarrows 2NO + O_2$ was estimated at 2.5 percent; the maximum error of individual points did not exceed 5 percent throughout the entire range of temperatures and pressures investigated.

In conclusion the authors express their gratitude to Academician of the Academy of Sciences Belorussian SSR A. K. Krasin for constant attention to the study and to Professor D. L. Timrot for his kind consultation and interest in the study.

Symbols

μ = coefficient of dynamic viscosity; A_o and B_o = coefficients of viscosimeter; τ = dropping time of load for uniform motion over the measured section; ρ_o and ρ = density of material of load and of test medium, respectively; f = dimensionless coefficient of friction of load against wall of calibrated channel when the channel is in a vertical position; t = temperature; β = coefficient of thermal expansion of construction material of the load and the calibration channel; Re = Reynolds criterion characterizing the gas flow regime in the circular channel between the load and the calibrated tube.

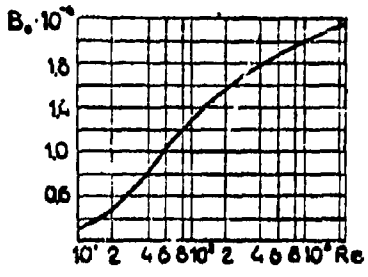

Figure 1. Coefficient B_0 as a function of Re for the load variant IV:

$$A_0 = 8{,}05\ 10^{-6};$$
$$B_0 = 0{,}2388\ 10^{-5} + \frac{0{,}1908\ 10^{-4}}{Re} - \frac{0{,}1275\ 10^{-4}}{Re^{4.8}}$$

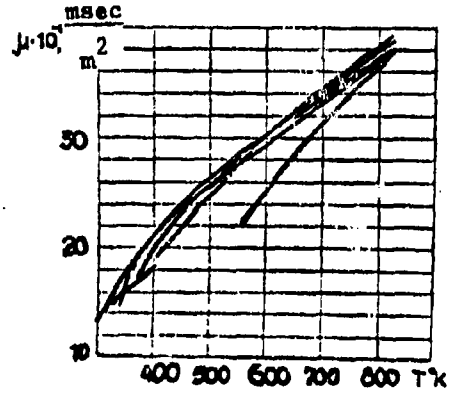

Figure 2. Experimental curves moved over to round va[illegible]or pressures of the chemically reacting system: $N_2O_4 \rightleftarrows 2NO_2 \rightleftarrows 2NO + O_2$ [12] —·—; [13] —··; Institute of Nuclear Power of the Academy of Sciences Belorussian SSR: —— 1 atm, — — — 5 atm, — · — · 10 atm, — ·· — 20 atm, — ··· — 50 atm.

References

1. Schotte, W., *Ind. Eng. Chem.*, Vol. 50, No. 4, 1958.
2. Patent of the Federal Republic of Germany, No. 1.033.344, Class 21d 21/32, dated 26 January 1957. Gaseous Heat Carriers for Nuclear Reactors.
3. Lighthill, M., *Voprosy Raketnoy Tekhniki*, No. 5, 1957.
4. Timogeyev, B. D., *Vestsi AN BSSR, Ser. Fiz. Tekhn. Navuk*, No. 2, 1966.
5. Timogeyev, B. D., *Vestsi AN BSSR, Ser. Fiz. Tekhn. Navuk*, No. 4, 1966.
6. Vargaftik, N. B., *Spravochnik po Teplofizicheskim Svoystvam Gazov i Zhidkostey*, [Handbook on Thermophysical Properties of Gases and Liquids], Fizmatgiz Press, Moscow, 1963.
7. Bukalovich, M. P. and V. V. Altukin, *Teplofizicheskiye Svoystva Dvuokisi Ugleroda*, [Thermophysical properties of Carbon Dioxide], Atomizdat Press, Moscow, 1965.
8. Schlinger, W. G. and B. H. Sage, *Ind. Eng. Chem.*, Vol. 42, p. 2158, 1950.
9. Bubnov, V. P., V. N. Gusarov, G. G. Kuleshov, V. B. Nesterenko, and B. D. Timofeyev, *Vestsi AN SSSR, Ser. Fiz. Tekhn. Navuk*, No. 3, 1966.
10. Tsimarnyy, V. A., *Avtoreferat na Soiskaniye Uchenoy Stepeni k. t. n. Eksperimental'noye Issledovaniye Zavisimosti Chetyrekhokisi Azota pri Temperature 440-580°K i davlenii 50-600 bar*, [Author;s Abstract of Dissertation Defended for the Degree of Candidate of Technical Sciences. Experimental Study of a Function of Nitrogen Tetroxide at Temperatures of 440-580°K and Pressures of 50-600 bar].
11. Maskimov, B. G., L. V. Mishina, and B. D. Timofeyev, *Vestsi AN BSSR*, No. 1, 1966.
12. Petker, I., and D. Mason, *J. Chem. Eng.*, Vol. 9, No. 2, 1964.
13. Beer, H., *Chem. Ing. Techn.*, Vol. 37, No. 10, 1965.

EFFECT OF CRYSTALLINITY ON THERMOPHYSICAL PROPERTIES OF POLYTETRAFLUOROETHYLENE (TEFLON-4)

V. S. Bil', Ye. V. Samardukov, N. Yu. Gasteva
and R. M. Shchonova

Polytetrafluoroethylene (Teflon-4) is a crystallizing polymer, the thermophysical characteristics of which have not been closely studied.

Crystallizing polymers exhibit the same kind of temperature dependencies of thermal diffusivity, heat capacity and density, and different kinds of temperature dependencies of thermal conductivity. Crystallization induces a rise in thermal conductivity, thermal diffusivity, density and the reduction in heat capacity. Thus, for example, from the data in [1] for polyethylene the thermal conductivity, like the low-molecular characteristics of compounds, reduces with temperature rise, but for polytetrafluoroethylene, like low-molecular amorphous compounds, thermal conductivity rises with rise in temperature.

The effect of crystallinity on thermophysical properties of polytetrafluoroethylene have been studied with an instrument described in [2] using a method given in [3] for the temperature range 40-300°C. The density was determined by the hydrostatic weighing method for t < 20°C.

Figure 1 presents experimental data on thermal conductivity of polytetrafluoroethylene as a function of temperature for two density values (crystallinity) of 2140 kg/m^3 and 2180 kg/m^3. (Scatter of experimental points ±4 percent,)

According to the data in [4] for polytetrafluoroethylene, density is unambiguously related to crystallinity by the relationship

$$\rho = 2.0 + 0.3w. \quad (1)$$

This affords the possibility by using experimental data on thermal conductivity to extrapolate temperature dependencies of thermal conductivity for density (crystallinity) values corresponding to amorphous and crystalline phases with the aid of the two-phase model proposed by I. Eiermann [1].

Under the two-phase model it is assumed that a crystalline polymer is a homogeneous mixture consisting of crystalline and amorphous regions, and therefore thermal conductivity can be calculated as the thermal conductivity of the mixture following a formula presented in [1]

$$\lambda = \frac{2\lambda_a + \lambda_k + 2W(\lambda_k - \lambda_a)}{2\lambda_a + \lambda_k - W(\lambda_k - \lambda_a)} \cdot \lambda_a \quad . \qquad (2)$$

The temperature dependencies of λ_k and λ_a were calculated from formula (2) using temperature dependencies of $\lambda(t)$ that we obtained for two density values. The results are indicated in Figure 1 by solid lines.

The results of measuring thermal diffusivity of polytetrafluoroethylene at densities of 2100 kg/m^3, 2118 kg/m^3, and 2160 kg/m^3 shown in Figure 2 demonstrate that within the limits of experimental precision the coefficient of thermal diffusivity depends linearly on temperature within the range investigated. Additionally, the higher the crystallinity (density), the higher the absolute value and the higher the rate of decrease of thermal diffusivity with temperature rise. Experimental points can be described by the following equation with precision of up to ±2 percent:

$$a = \{0{,}685 + 4{,}2(\rho - 2000)\cdot 10^{-3} - [0{,}110 + 10{,}650(\rho - 2000)\cdot 10^{-3}](T°C - 273)\cdot 10^{-3}\}\cdot 10^{-7} \left[\frac{m^2}{sec}\right] \qquad (3)$$

Equation (3) allows us to calculate the temperature dependencies of coefficients of thermal diffusivity of crystalline and amorphous phases, and also the function a(T) for intermediate crystallinity values (Figure 2). (Calculated curves are indicated by solid lines.)

Thus, the experimental and calculated data obtained allow us by using density (crystallinity) of polytetrafluoroethylene to estimate thermal conductivity and thermal diffusivity as function of temperature.

Symbols

λ = thermal conductivity of polymer, w/m·deg; λ_k and λ_a = thermal conductivity of its crystalline and amorphous regions; a = coefficient of thermal diffusivity, m^2/sec; ρ = density, kg/m^3; W = bulk extent of crystallinity; T = temperature (°K); t = temperature (°C).

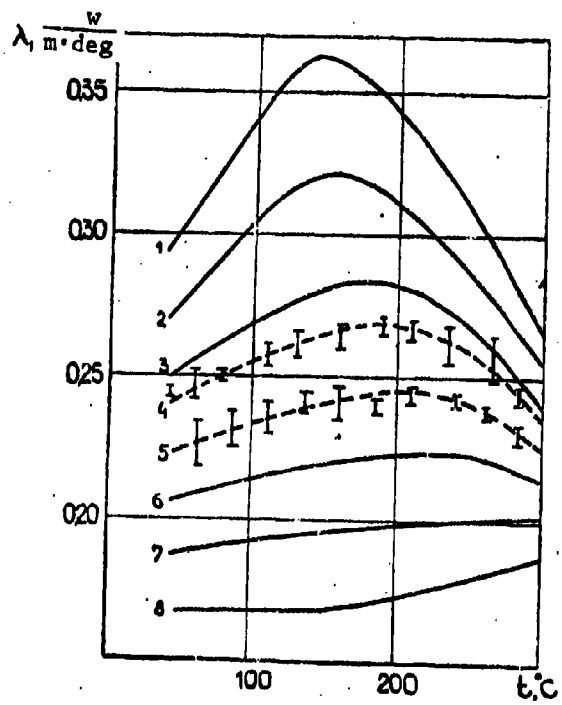

Figure 1. Thermal conductivity of polytetrafluoroethylene as a function of temperature for different densities (crystallinities): 1, ρ = 2300 kg/m^3, wholly crystalline; 2, ρ = 2250 kg/m^3, 83 percent crystallinity; 3, ρ = 2200 kg/m^3, 66 percent crystallinity; 4, ρ = 2180 kg/m^3, 60 percent crystallinity; 5, ρ = 2140 kg/m^3, 46.5 percent crystallinity; 6, ρ = 2100 kg/m^3, 33 percent crystallinity; 7, ρ = 2050 kg/m^3, 16.5 percent crystallinity; 8, ρ = 2000 kg/m^3, wholly amorphous

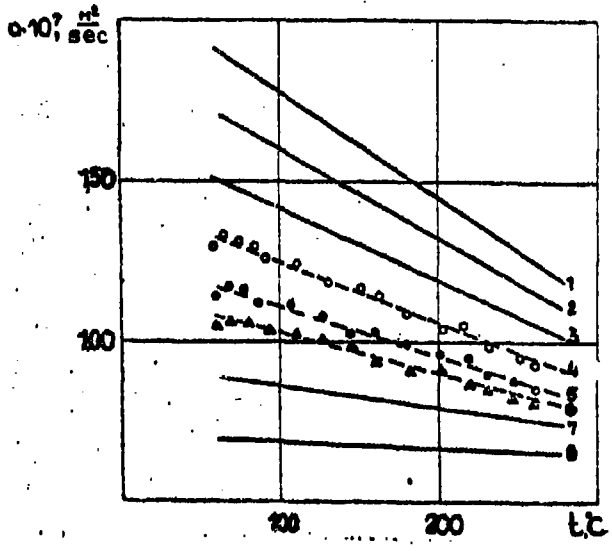

Figure 2. Thermal diffusivity of polytetrafluoroethylene as a function of temperature at different densities (crystallinities): 1, ρ = 2300 kg/m^3, wholly crystalline; 2, ρ = 2250 kg/m^3, 83 percent crystallinity; 3, ρ = 2200 kg/m^3, 66 percent crystallinity; 4, ρ = 2160 kg/m^3, 53 percent crystallinity; 5, ρ = 2118 kg/m^3, 39.2 percent crystallinity; 6, ρ = 2100 kg/m^3, 33 percent cr-stallinity; 7, ρ = 2050 kg/m^3, 16.5 percent crystallinity; 8, ρ = 2000 kg/m^3, wholly amorphous

References

1. Eiermann, K., *Kolloid- Z. and Z. Polymere*, Vol. 201, No. 1, pp. 3-15, 1965.

2. Kurepin, V. V. and Ye. S. Platunov, *Izv. Vuzov. Priborstroyeniye*, No. 5, 1961.

3. Platunov, Ye. S., *Izv. Vuzov. Priborstroyeniye*, No. 1, p. 4, 1961.

4. Heise, B., H. G. Killian, and F. H. Muller, *Kolloid- Z. and Z. Polymere*, Vol. 213, No. 1-2, 1966.

THERMAL CONDUCTIVITY OF THE SYSTEM $N_2O_4 \rightleftarrows 2NO_2 \rightleftarrows 2NO + O_2$ IN THE TEMPERATURE RANGE 300-780°K AND THE PRESSURE RANGE 1-50 atm abs

A. A. Bilyk, F. N. Dresvyannikov, Yu. G. Kotelevskiy,
L. V. Mishina, V. B. Nesterenko and B. D. Timofeyev

Several studies have dealt with experimental investigation of thermal conductivity of nitrogen tetroxide [1-3]. However, all these studies used the heated filament method at low temperature (up to 1 atm abs).

The present study sets forth the results of measurements on the thermal conductivity of the system $N_2O_4 \rightleftarrows 2NO_2 \rightleftarrows 2NO + O_2$ at pressures from 1 to 50 atm abs in the temperature range 300-780°K.

A method of coaxial cylinders using stainless steel of the grade Kh18N10T as the main construction material was selected in studying thermal conductivity at the Institute of Nuclear Power of the Academy of Sciences Belorussian SSR. This material satisfies to the greatest extent requirements posed in investigating chemically reacting gases.

The experimental device consisted of the following assemblies: a) a working thermostat serving to thermostat the experimental section; b) the experimental section; c) a system for control of pressure in the working cavity, housing a model manometer with a membrane divider using carbon tetrachloride as the dividing liquid; d) a vacuum system including a forevacuum pump and a vacuum gauge; e) a system for filling the working cavity with the test gas, consisting of a container filled with condensed nitrogen tetroxide and a thermostat serving to heat it.

The working thermostat was a structure thermally insulated from all sides containing a thick-walled copper cylinder within, over whose external surfaces a four-section heater made of nichrome wire was wound. Activation of the thermostat to the desired regime and maintenance in it of a constant temperature was done automatically with the aid of an electronic temperature control.

The experimental section (Figure 1) consisted of two coaxially arranged cylinders made of stainless steel. The outer diameter of the innermost cylinder was 8 mm and the wall thickness was 1 mm. An approximately 0.8-mm gap between the cylinders was maintained with a ceramic washer (1) placed on the side of the cylinder dead-ends and a thin metal washer (3) on the side of flange joining of the cylinders, which together with the Teflon inserts (4) ensured hermetization of the working cavity within the cylinders. Temperature was measured at the inner surface of the innermost cylinder with the aid of three spring-mounted chromel-alumel thermocouples (7) placed 50 mm from each other.

A rosette of five thermocouples (2) was soldered onto the outer surface of the outermost cylinder using condenser welding at a spacing of 40 mm from each other to record the temperature field along the cylinder length.

A regulated heater (5) was provided to reduce heat losses from the flange side in the lower section of the experimental area.

The heat flux was generated by means of the three-section heater (6) made of 0.23-mm-diameter nichrome enclosed in glass tubing of about 5 mm diameter and placed in the innermost cylinder. To record the power supplied over 100 mm of length, potential leads of copper wire were connected from the central section of the innermost heater.

The inner heater was fed from a storage battery. Measurements of the emf of thermocouples and voltages over the working section and the model coil in the inner heater circuit were made on the R-307 high-ohmic potentiometer.

Choice of the geometry of the experimental section made it possible to exclude convection over the entire range of temperatures and pressures ($Gr \cdot Pr < 1000$).

Use of the relative method of coaxial cylinders made it possible to take into account correction for noncoaxiality of cylinders when weighing for a known material. This correction was included in the apparatus constant.

Since the literature contains no data on the reduced degree of blackness (ε_{red}) for stainless steel passivated by nitrogen tetroxide, the correction

for radiation was provided for by calculation. It was determined thusly.

The overall quantity of heat Q transferred from the inner cylinder to the outer,

$$Q = Q_л + \frac{\lambda \Delta T}{A}, \qquad (1)$$

where A is the apparatus constant, determined by the geometry of the section.

The amount of heat transferred by radiation $Q_л$ was determined from the formula

$$Q_л = B\left[\left(\frac{T_1}{100}\right)^4 - \left(\frac{T_2}{100}\right)^4\right], \qquad (2)$$

where

$$B = \sigma F \varepsilon_{пр}, \qquad (3)$$

For the case when the value of A did not depend on temperature, the coefficients A and B can be determined from the following scheme. Since at temperature drops up to 5°K at low temperatures (up to 373°K), even for oxidized steel which has the highest degree of surface blackness, the contribution of radiation was less than one percent of the total amount of heat. Therefore we can neglect radiation and maintain adequate precision, and determine the value of A from weighing experiments with known material. At high temperatures we can calculate B = B(T) for weighed gas using the value of A obtained at low temperatures.

The value of A was calculated at several points in the temperature range 296-356°K in the weighing experiments with air. A as a function of temperature was not established in our experiments.

The value of B was also determined by weighing experiments in air, and B as a well defined function of temperature was not obtained. A scatter about the mean value was observed.

Thus, the data obtained for A = 0.286 and $B \cdot 10^{-3} = 5.27$ were used in treating measured coefficients of the thermal conductivity of nitrogen tetroxide. To verify the correctness of the determinations of A and B, control experiments with helium were conducted. Results for λ gave satisfactory agreement with known literature data on helium [4].

The measurements made of thermal conductivity of dissociating nitrogen tetroxide in the temperature range 300-780°K at pressures of 1, 10, 30 and 50 atm abs are shown in Figures 2 and 3.

The mean error of experimental data was estimated at 6 percent, and the maximum error at 9 percent.

Experimental data for 1 atm (cf. Figure 2) at temperatures up to ~ 450°K (first stage of the reaction) found quite good agreement with the data of other authors [1, 3] and with calculated data made on the assumption of local chemical equilibrium. The maximum departure from calculated values was approximately 15 percent. No contribution of chemical reaction to thermal conductivity was noted in the second stage in the temperature range 450-780°K, and the experimental points fitted on the curve of the "frozen" component.

Experimental values of λ at a pressure of 50 atm abs in the temperature range 550-780°K are at a level approximately 20 percent higher than at 1 atm abs (Figure 3). The influence of pressure alone cannot account for this increase, but it is obviously necessary to relate it to the contribution of the chemical reaction.

The authors express their gratitude to Academician of the Academy of Sciences Belorussian SSR A. K. Krasin for constant interest in the study.

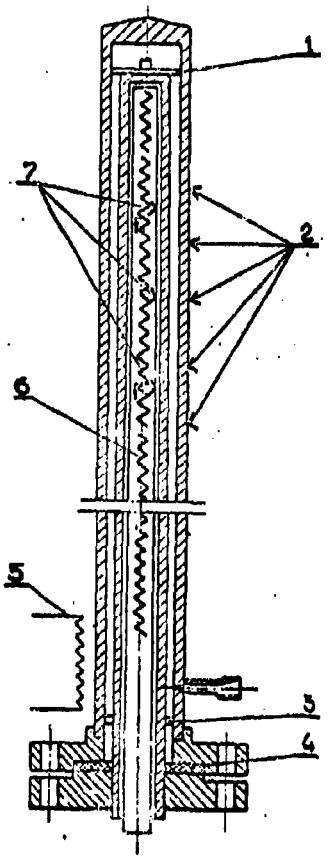

Figure 1. Diagram of experimental section. 1, Ceramic washer; 2, Thermocouples; 3, Metal washer; 4, Teflon inserts; 5, Regulated heater; 6, Three-section heater; 7, Spring-mounted thermocouples

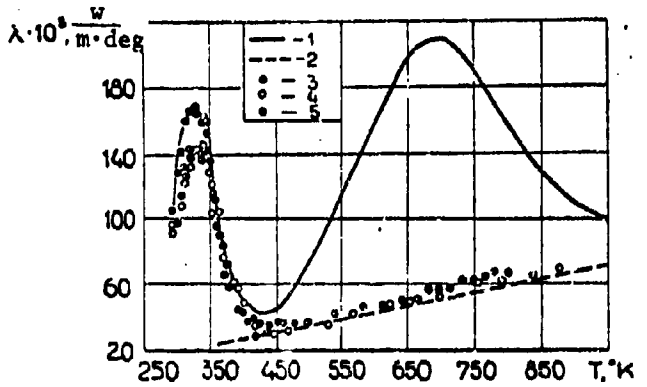

Figure 2. Temperature dependence of coefficient of thermal conductivity of nitrogen tetroxide at P = 1 atm abs: 1, Calculated with the contribution of the chemical reaction taken into account; 2, Calculated for the mixture of "frozen" composition; 3, Data in [1]; 4, Data in [3]; 5, Authors' data

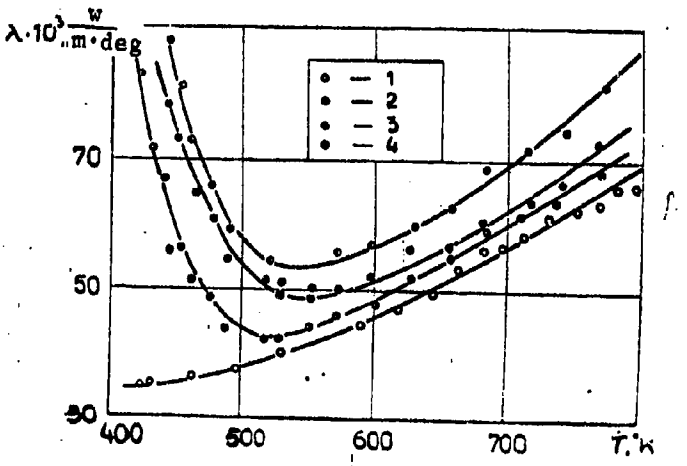

Figure 3. Change of thermal conductivity coefficient for nitrogen tetroxide as a function of temperature and pressure:
1, P = 1 atm abs; 2, P = 10 atm abs; 3, P = 30 atm abs;
4, P = 50 atm abs

References

1. Coffin, K. P. and O'neal, *Natl. Advisory Comm. Aeronaut.* Notes, 4209, 1958.

2. Srivastava, B. N. and A. K. Barua, *J. Chem. Phys.*, Vol. 35, p. 329, 1961.

3. Dresvyannikov, F. N. and G. A. Mukhachev, *Sb. Materialy Vtoroy Konferentsii Molodykh Nauchnykh Rabotnikov*, [Collection of Materials of the Second Conference of Young Scientific Workers], Tatyanigoizdat Press, Kazan', p. 234, 1965.

4. *Teplofizicheskiye Svoystva Veshchestv. Spravochnik pod red. N. B. Vargaftika*, [Thermophysical Properties of Compounds. Handbook, edited by N. B. Vargaftik], Gosenergoizdat, Moscow, 1963.

THERMAL CONDUCTIVITY OF POLYETHYLENE AS A FUNCTION OF ABSORBED RADIATION DOSE

B. A. Briskman and V. D. Bondarev

Data on thermal conductivity λ of polyethylene as a function of temperature and the value of absorbed radiation energy are of interest from two points of view. First, the behavior of polyethylene as an insulator is important in applied problems. Second, study of the λ of polyethylene provides additional information on the structure of this polymer and on physicomechanical and chemical transformations occurring when it is irradiated.

The λ of both high-pressure and low-pressure polyethylene as a function of temperature has often been investigated, for example in the temperature range -190° to +110°-120°C, that is, practically up to the melting point of uncross-linked polyethylene [1, 2]. It has been shown that throughout almost the entire temperature range, with the exception of very low temperatures, the λ of polyethylene drops off monotonically with rise in temperature, while the λ of high-density polyethylene (low-pressure) is considerably higher than the λ of low-density polyethylene (high-pressure).

As we know, polyethylene is a two-phase polymer, a combination of crystalline and amorphous phases. Bearing in mind that: 1) the λ of the crystalline phase is considerably higher than the amorphous phase; 2) the λ of the crystalline phase drops off appreciably with temperature rise; 3) the λ of the amorphous phase rises, but more slowly; 4) the extent of crystallinity drops off [3] with temperature rise all the way to complete failure of crystals in the melting point region, with the foregoing in mind it can be shown that the sign of the temperature effect for the λ of polyethylene depends on the initial phase composition of polyethylene, the rate of degradation of the crystalline phase, and on the temperature coefficients of the crystalline and amorphous phases.

Directing attention to concrete values of the quantities listed above, it must be concluded that the decrease in the λ of polyethylene with temperature rise is due to a reduction in the degree of crystallinity. The mechanism of variation of λ of polyethylene exposed to radiation is more complex. The results of a study of λ of polyethylene as a function of absorbed radiation energy have been presented in [4]. Under the effect of radiation [5], radiation cross-linking of the molecular polyethylene chains takes place, which leads to a reduction in distances between carbon atoms and to higher polyethylene density. At the same time, a decrease in extent of crystallinity occurs [5], leading to a drop in polyethylene density. As has been shown in [4], the λ of polyethylene drops off with rise in absorbed radiation energy at a temperature of approximately 20°C, but at relatively higher temperatures (approximately 150°C) it rises. We must note that the absolute values of polyethylene (below we will discuss low-density polyethylene) vary from 0.26 to 0.47 w/m·°C (for t = 20°C). Such a wide range of polyethylene λ values is accounted for by the dependence of its physico-mechanical properties on the method of preparation, storage, etc. For irradiated polyethylene account must be taken (if the irradiation is conducted in air) of the presence of oxygen compounds (carbonyl groups, especially on the specimen surface, and peroxide bridges between molecular chains). It is very important to allow for the action of gaseous hydrogen formed upon irradiation. To grasp the mechanism of thermal conductivity we must bear in mind also the presence of thermal conductivity anisotropy [6].

The aim of this study is obtaining of additional information on the λ of low-density irradiated polyethylene (γ = 0.920 g/cm^3). Unstabilized block polyethylene in the form of disks of 30 mm diameter and 15 mm thickness was irradiated in a nuclear reactor in air and was used in the same form in the experimental apparatus (Figure 1). The absence of impurities in polyethylene greater than 10^{-5} percent by weight was corroborated by activation analysis. The measurements were made by a steady-state method due to the appreciable dependence of density and heat capacity of polyethylene on temperature. The experimental apparatus was a vacuum-treated chamber (pressure of 10^{-4}-10^{-5} mm Hg) in which the specimens (2) were placed with the heater (5)

located between them. Symmetrical removal of heat was achieved by silver-plated massive copper refrigerators (1). Reduction of heat losses via radiative heat transfer was achieved with the aid of ten cylindrical screens (4) made of polished stainless steel foil (δ = 0.1 mm). Chromel-copel thermocouples (three for each spceimen) are embedded along the specimen axis. The spacing between the hot thermocouple arms is measured by X rays. The measurements were made in the temperature range 25-155°C and the absorbed dose range 0-2300 Mrad. Thermal losses did not exceed 0.5 percent of heater power. The maximum experimental error was ±3.5 percent. Results of measurements are shown in Figures 2 and 3.

As can be seen from Figure 2, at a temperature of 30°C the λ of polyethylene drops off sharply with rise in dose, which is accounted for by the decrease in extent of crystallinity. Beginning with some dose value, depending on temperature, λ is reduced considerably more slowly, this is also the case for the variation of λ with dose for the temperatures 40, 60 and 80°C. At temperatures of 100 and 200°C, λ drops off somewhat up to a dose of 600 Mrad, which is probably explained by the failure of the last crystals. Then λ monotonically rises, revealing a trend toward stabilization. At a temperature of 150°C, λ rises throughout the dose range. We explain the course of all these curves by proceeding from the following considerations. Two competing processes are operative with increase in dose -- radiation cross-linking, leading to rise in λ, and disruption of polyethylene macrostructure owing to gas release upon irradiation. In gas release fine pores appear, the size and number of which rise with increase in received dose [7]. The presence of vacuumed pores and fissures leads, especially at moderate temperatures, to worsening of polyethylene λ. The thermal resistance of pores drops off with rising temperature owing to the ever mounting role of radiative heat transfer, which brings about a rise in λ with increase in dose at relatively high temperatures.

As we can see from Figure 3, λ as a function of temperature is fairly complex, where at temperatures up to 50°C clearly pronounced "valleys" of λ occur, the reliability of which is confirmed by the good reproducibility of the experimental points. At doses of 0 and 100 Mrad, λ drops off owing

to the reduced degree of crystallinity. At a dose of 900 Mrad, the crystals disappear already at a temperature of 40°C and thereafter λ increases. At a dose of 2300 Mrad polyethylene from the very outset is an amorphous phase, whose thermal conductivity rises with temperature. Throughout the range of absorbed doses there is a correlation with the specific volume of polyethylene.

In the future it will be of great interest to study the effect of irradiation conditions on polyethylene thermal conductivity.

We are duty bound to express our gratitude to Professor and Doctor of Chemical Sciences V. L. Karpov for participation in discussion and for valuable counsel.

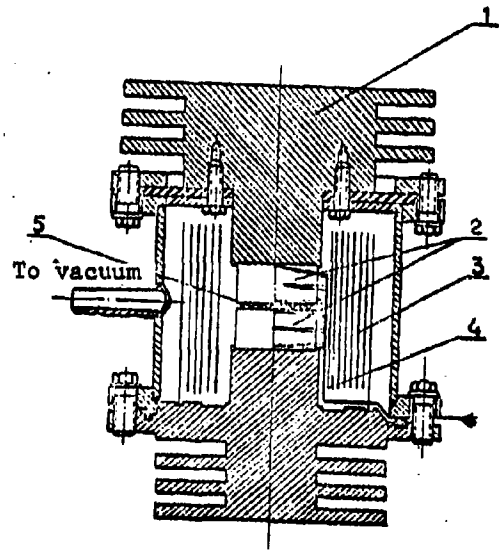

Figure 1. Sketch of experimental apparatus: 1, Copper refrigerators; 2, Polyethylene specimen; 3, Chromel-copel thermocouple; 4, Screen; 5, Heater

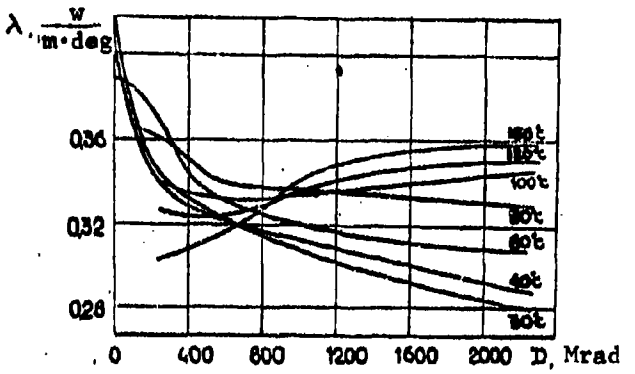

Figure 2. Thermal conductivity of polyethylene as a function of absorbed radiation dose

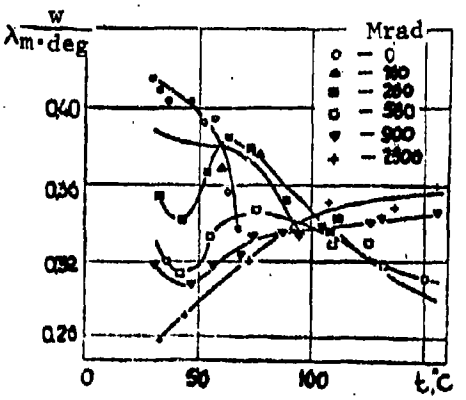

Figure 3. Thermal conductivity of polyethylene as a function of temperature

References

1. Eiermann, K., *Kunststoffe*, Vol. 51, p. 512, 1961.
2. Cherkasova, L., *ZhFKh*, Vol. 33, p. 1928, 1959.
3. Charlesby, A., *Yadernyye Izlucheniya i Polimery*, [Nuclear Radiation and Polymers], IL Press, Moscow, 1962.
4. Tomlinson, J. N., et al., *SPE Transactions*, Vol. 5, p. 44, 1965.
5. Karpov, V. L. and V. I. Zverev, *Sb. Rabot po Radiatsionnoy Khimii*, [Collection of Studies on Radiation Chemistry], Academy of Sciences USSR Press, Moscow, 1955.
6. Kargin, V. A., et al., *DAN SSSR*, Vol. 104, No. 1, p. 96, 1955.
7. Taubman, A. V. and L. P. Uskova, *Tr. I Vsesoyuznogo Soveshchaniya po Radiatsionnoy Khimii*, [Proceedings of the First All-Union Conference On Radiation Chemistry], Academy of Sciences USSR Press, Moscow, 1958.

TOWARD A STATISTICAL THEORY OF THERMAL CONDUCTIVITY OF CONDENSED MEDIA

V. S. Vikhrenko, V. B. Nemtsov and L. A. Rott

Investigation of the thermal conductivity of condensed systems is complex owing to the fact that there are certain difficulties in describing the perturbation of the Hamiltonian of the system, owing to the thermodynamic nature of the perturbations.

The well known Kirkwood theory [1] based on a statistical interpretation of the theory of Brownian motion makes it possible to describe the thermal conductivity phenomenon with satisfactory rigor. But the actual calculation of the coefficient of thermal conductivity is hampered to a large extent owing to the absence of a well defined expression for the binary distribution function.

In the present study the Kirkwood method is applied in a statistical scheme of conventional distributions, which has been developed earlier (cf., for example, [2]).

In essence, the method of conventional distributions amounts to the following. A volume V occupied by system of N particles is divided into cells of volume $v = V/N$. Then the probability density $F_{ij}^{(k,l,\ldots)}(\vec{q}, \vec{p}, \vec{q}^{\,2}, \vec{p}^{\,2}, \ldots, t)$ that at the moment of time t i particles will be found in a certain specific cell v_i, k particles -- in some other cell, l particles in a third cell, and so on in the vicinity of specific coordinates $\vec{q}$ and $\vec{q}_2$ is studied, ..., these particles exhibiting the momenta $\vec{p}$, $\vec{p}^{\,2}$, ... under the condition that in the remaining cells the remaining $N - i - k - l - \ldots$ molecules are distributed arbitrarily, but that no more than j molecules occupy a cell. Here the requirement $i, k, l, \ldots \leq j$ is satisfied.

An attractive feature of the method applied is the possibility of using successive approximations. For example, in the so-called approximation F_{11} employed here, only those system states are taken into account in which each cell contains one molecule. For condensed media the molecular volume v is relatively small and even the F_{11} approximation provides satisfactory results [4].

Use of higher approximations, for example, F_{12} and F_{22} in which the system states are taken into account where each cell can simultaneously have present two molecules allows us even more precisely to describe the behavior of the system.

Hydrodynamic laws of conservation were obtained by using the method of conventional distributions in the F_{11} approximation as well as an expression of the heat flux density, which follows from the equation of the conservation of energy,

$$\vec{j} = \vec{j}^{\text{кин.}} + \vec{j}^{\text{пот.}} \tag{1}$$

Here the kinetic component of the heat flux density

$$\vec{j}^{\text{кин.}} = \frac{m}{2}\int_{\Omega_p}\left(\frac{\vec{p}}{m} - \vec{u}\right)\left(\frac{\vec{p}}{m} - \vec{u}\right)^2 F_{11}(\vec{q}, \vec{p}; t)\, d\vec{p} \tag{2}$$

and the potential component

$$\vec{j}^{\text{пот.}} = \frac{1}{2}\int_{V-V_0}\int\int_{\Omega_p}\left(\frac{\vec{p}}{m} - \vec{u}\right)\Phi(r) F_{11}^{(1)}(\vec{q}, \vec{q} + \vec{r}, \vec{p}, \vec{p}'; t)\, d\vec{p}\, d\vec{p}'\, d\vec{r} + \tag{3}$$

$$+ \frac{1}{V}\int_{V-V_0}\int\int_{\Omega_p}\left[\left(\frac{\vec{p}}{m} - \vec{u}\right) + \left(\frac{\vec{p}'}{m} - \vec{u}\right)\right]\cdot\frac{\vec{r}\vec{r}}{r}\Phi'(r) F_{11}^{(1)}(\vec{q}, \vec{q} + \vec{r}, \vec{p}, \vec{p}'; t)\, d\vec{p}\, d\vec{p}'\, d\vec{r},$$

where $\vec{r} = \vec{q}^{\,2} - \vec{q}$; $\vec{u}$ is the mean molecular velocity. The expression $\vec{r}\vec{r}$ represents a diad, while the expression $\vec{r}\cdot\vec{r}$ is the scalar product; m is the mass of molecule, $\Phi(r)$ is the potential of interaction between molecules. The interaction is presumed to be central and pairwise.

Following the concept of Kirkwood [5], we introduce distribution functions smoothed over the time τ:

$$\bar{F}_{ij}^{(n\ell\ldots)}(\vec{q},\vec{p},\vec{q}^{\,1},\vec{p}^{\,1},\ldots,t)=\frac{1}{\tau}\int_0^{\tau}F_{ij}^{(n\ell\ldots)}(\vec{q},\vec{p},\vec{q}^{\,1},\vec{p}^{\,1},\ldots;t+s)\,ds \qquad (4)$$

The time interval τ over which distribution functions are smoothed must be large in comparison with the relaxation time of intermolecular forces, but much less than the Poincare cycle of the system.

Let H_N represent the Hamiltonian of a system of N particles. Then the distribution function of the dynamic states of the entire system $D_N(\vec{q},\vec{p},\vec{q}^{\,1},\vec{p}^{\,1},\ldots\vec{q}^{\,N},\vec{p}^{\,N};t)$ satisfies the Liouville equation

$$\frac{\partial D_N}{\partial t}=[H_N;D_N],\quad [H_N;D_N]=\sum_{i=1}^{N}\left\{\frac{\partial H_N}{\partial\vec{q}^{\,i}}\cdot\frac{\partial D_N}{\partial\vec{p}^{\,i}}-\frac{\partial H_N}{\partial\vec{p}^{\,i}}\cdot\frac{\partial D_N}{\partial\vec{q}^{\,i}}\right\}, \qquad (5)$$

where the righthand member is the Poisson bracket.

Averaging equation (5) over the time interval τ and integrating it with respect to coordinates and momenta, as shown in [2], we arrive at equations determining the smoothed distribution functions $\bar{F}_n(\vec{q},\vec{p};t)$ and $\bar{F}_n^{(\omega)}(\vec{q},\vec{p},\vec{q}^{\,1},\vec{p}^{\,1};t)$ in the form:

$$\frac{\partial\bar{F}_n}{\partial t}+\frac{\vec{p}}{m}\frac{\partial\bar{F}_n}{\partial\vec{q}}=\frac{\partial}{\partial\vec{p}}\cdot\vec{\Omega}_{1n}$$

$$\vec{\Omega}_{12}=-\frac{N(N-1)}{\tau}\int_0^{\tau}\int_{V_1}\int_{\Delta p}\cdots\int\vec{K}_{12}(\vec{q},\vec{q}^{\,1})D_N(\vec{q},\vec{p},\vec{q}^{\,1},\vec{p}^{\,1},\ldots,\vec{q}^{\,N},\vec{p}^{\,N};t+s)$$
$$\times d\vec{p}^{\,2}\ldots d\vec{p}^{\,N}\sum_{(2)}d\vec{q}^{\,2}d\vec{q}^{\,3}\ldots d\vec{q}^{\,N}ds; \qquad (6)$$

$$\frac{\partial\bar{F}_n^{(\omega)}}{\partial t}+\left(\frac{\vec{p}}{m}\frac{\partial}{\partial\vec{q}}+\frac{\vec{p}^{\,1}}{m}\frac{\partial}{\partial\vec{q}^{\,1}}-\frac{\partial\Phi_{12}}{\partial\vec{q}}\cdot\frac{\partial}{\partial\vec{p}}-\frac{\partial\Phi_{12}}{\partial\vec{q}^{\,1}}\cdot\frac{\partial}{\partial\vec{p}^{\,1}}\right)\bar{F}_n^{(\omega)}=$$
$$=\frac{\partial}{\partial\vec{p}}\cdot\vec{\Omega}_{13}+\frac{\partial}{\partial\vec{p}^{\,1}}\vec{\Omega}_{23}$$

$$\vec{\Omega}_{1s} = -\frac{N(N-1)(N-2)}{\tau}\int_0^{\tau}\int\int\cdots\int\int\cdots\int\int\cdots\int \vec{K}_{1s}(\vec{q}, \vec{q}')$$

$$\times D_N(\vec{q}, \vec{p}, \vec{q}', \vec{p}', \ldots \vec{q}'', \vec{p}''; t+s)\, d\vec{p}\, d\vec{p}' \sum_{(p)} d\vec{q}'' \ldots d\vec{q}''\, ds$$

$\vec{H}S1$ is determined in a similar way. Here Σ denotes summation over all possible rearrangements of particles in cells over which the integration is performed. $\vec{K}_{ij}(\vec{q}^{\,i}, \vec{q}^{\,j}) = -\frac{\partial \varphi(|\vec{q}^{\,i} - \vec{q}^{\,j}|)}{\partial \vec{q}^{\,i}}$ is the force acting on the i-th molecule on the part of the j-th molecule.

The problem consists in transforming the righthand members of equations (6). Assuming that the vicinity of two molecules is readily deviated from the equilibrium state and adopting the Kirkwood method in [5] for the first of the equations (6), we obtain an equation determining the function

$$\vec{F}_{1s}(\vec{q}, \vec{p}; t).$$

$$\frac{\partial \vec{F}_{1s}}{\partial t} + \frac{\vec{p}}{m}\cdot\frac{\partial \vec{F}_{1s}}{\partial \vec{q}} + \frac{\partial}{\partial \vec{p}}\cdot(\vec{K}^{(1)}\vec{F}_{1s}) = \zeta\frac{\partial}{\partial \vec{p}}\cdot\left[\left(\frac{\vec{p}}{m} - \vec{u}\right)\vec{F}_{1s} + kT\frac{\partial}{\partial \vec{p}}\vec{F}_{1s}\right]$$
$$\vec{K}^{(1)} = {}^{(1)}\langle \vec{K}_1 \rangle^{\zeta} + {}^{(1)}\vec{K}^{*} \qquad (7)$$

Here the parentheses ${}^{(1)}\langle \ldots \rangle^{\zeta}$ denote averaging over the equilibrium state of all particles, with the exception of one. $\vec{K}_1$ is the total force acting on the molecule, ${}^{(1)}\vec{K}^{*}$ is nonequilibrium correction stemming from the deviation of the vicinity of two molecules from the equilibrium state.

The scalar coefficient of friction

$$\zeta = \frac{1}{3kT}\int_0^{\infty} {}^{(0)}\langle \vec{K}_1(0)\cdot \vec{K}_1(s) \rangle^{\zeta} ds \qquad (8)$$

The resulting equation (7) agrees with the Chandrasekar equation [6] well known in the theory of Brownian motion. However, equation (7) was

obtained by a statistical method and the coefficient of friction ξ is expressed here via parameters of intermolecular interaction, while in the Chandrasekar equation the coefficient of friction is a phenomenological constant.

Assuming that the vicinity of three molecules is easily deviated from the equilibrium state, and similarly considering two of equations (6), we find an equation determining the function

$$\vec{F}_{ik}^{(\omega)}(\vec{q}_1, \vec{p}_1, \vec{q}_2, \vec{p}_2; t).$$

$$\frac{\partial \vec{F}_{ik}^{(\omega)}}{\partial t} + \left(\frac{\vec{p}_1}{m}\cdot\frac{\partial}{\partial \vec{q}_1} + \frac{\vec{p}_2}{m}\cdot\frac{\partial}{\partial \vec{q}_2} + \vec{K}_1^{(\omega)}\frac{\partial}{\partial \vec{p}_1} + \vec{K}_2^{(\omega)}\cdot\frac{\partial}{\partial \vec{p}_2}\right)\vec{F}_{ik}^{(\omega)} =$$
$$= \xi\frac{\partial}{\partial \vec{p}_1}\cdot\left\{\left[\left(\frac{\vec{p}_1}{m} - \vec{U}_1\right) + kT\frac{\partial}{\partial \vec{p}_1}\right]\vec{F}_{ik}^{(\omega)}\right\} +$$
$$+ \xi\frac{\partial}{\partial \vec{p}_2}\cdot\left\{\left[\left(\frac{\vec{p}_2}{m} - \vec{U}_2\right) + kT\frac{\partial}{\partial \vec{p}_2}\right]\vec{F}_{ik}^{(\omega)}\right\}, \qquad (9)$$
$$\vec{K}_1^{(\omega)} = {}^{(\omega)}\langle \vec{K}_1\rangle^{\circ} + {}^{\omega}\vec{K}_1^{\circ},$$
$$\vec{K}_2^{(\omega)} = {}^{(\omega)}\langle \vec{K}_2\rangle^{\circ} + {}^{\omega}\vec{K}_2^{\circ}.$$

The bent brackets here again denote statistical averaging over the equilibrium state of all particles, except for two.

The forces ${}^{(\omega)}\vec{K}_1^{\circ}$ and ${}^{\omega}\vec{K}_2^{\circ}$ are due to deviation of the state of the three-molecule vicinity from the equilibrium state.

Let us determine the kinetic contribution to the heat flux density. For this purpose, we will multiply equation (7) by $\vec{p}$ and integrated over the momentum space. As a result we have:

$$\frac{\partial \vec{J}_k}{\partial t} + \frac{\partial}{\partial \vec{q}}\cdot\int_{\Delta p}\frac{\vec{p}\vec{p}}{m}\vec{F}_s(\vec{q}, \vec{p}; t)\,d\vec{p} = \frac{\vec{K}^{\omega}\rho}{m}, \qquad (10)$$

where the mass flux density

$$\vec{j}_p = m \int_{\Omega_p} \frac{\vec{p}}{m} \vec{F}_n(\vec{q}, \vec{p}; t)\, d\vec{p}.$$

and the density of the material

$$\rho(\vec{q}, t) = m \int_{\Omega_p} \vec{F}_n(\vec{q}, \vec{p}; t)\, d\vec{p} \tag{11}$$

We will introduce the determination of temperature according to the equality

$$\frac{m}{2} \int_{\Omega_p} \left(\frac{\vec{p}}{m} - \vec{u}\right)\left(\frac{\vec{p}}{m} - \vec{u}\right) \vec{F}_n(\vec{q}, \vec{p}; t)\, d\vec{p} = \frac{3}{2} \kappa T \rho \vec{I}. \tag{12}$$

where $\vec{\vec{I}}$ is a unit tensor.

Comparing (10) and (12) and neglecting the inertia members, and also the squared members in terms of mean velocity $\vec{u}$, after several transformations we find:

$$\vec{K}^{(1)} = \frac{1}{\rho} \frac{\partial}{\partial \vec{q}} (\kappa T \rho) \tag{13}$$

Using (13) in (10) and again neglecting the inertia members and the second and higher order members in terms of mean velocity $\vec{u}$, we similarly obtain an expression for the kinetic component of the heat flux density

$$\vec{j}^{(1)} = \frac{m}{2} \int_{\Omega_p} \left(\frac{\vec{p}}{m} - \vec{u}\right)\left(\frac{\vec{p}}{m} - \vec{u}\right)^2 \vec{F}_n(\vec{q}, \vec{p}; t)\, d\vec{p} = \cdots$$
$$= -\frac{\kappa^2 T}{2 \cdot 3 m} \rho \nabla T + \frac{\kappa^2 T^2}{6 \cdot 3 m} \left(\frac{\partial \rho}{\partial T}\right) \nabla T. \tag{14}$$

To determine the contribution of interaction between molecules to the heat flux density, we integrate the expression (3) over the momentum space and take into account that $\Phi'(r)$ differs from zero in the region of the order of intermolecular distances. Further, we write the expression for the

density of the heat flux potential component in the form:

$$\vec{J}^{(m)} = \frac{1}{2}\int_{V-V_1}\left[\Phi(r)\bar{\bar{I}} - \frac{\vec{r}\vec{r}}{r}\Phi'(r)\right]\cdot(\vec{u}_1^{(m)} - \vec{u})\bar{F}_{11}^{(m)}(\vec{q}, \vec{q}+\vec{r}; t)\,d\vec{r}. \qquad (15)$$

where

$$\vec{u}_1^{(m)}\bar{F}_{11}^{(m)}(\vec{q}, \vec{q}+\vec{r}, t) = \iint_{\Delta_p}\frac{\vec{p}}{m}\bar{F}_{11}^{(m)}(\vec{q}, \vec{q}+\vec{r}, \vec{p}, \vec{p}^1; t)\,d\vec{p}\,d\vec{p}^1;$$

$$\bar{F}_{11}^{(m)}(\vec{q}, \vec{q}+\vec{r}; t) = \iint_{\Omega_p}\bar{F}_{11}^{(m)}(\vec{q}, \vec{q}+\vec{r}, \vec{p}, \vec{p}^1; t)\,d\vec{p}\,d\vec{p}^1.$$

The latter will refer wholly to particles in a six-dimensional configurational space of two molecules (the lowest functions F and $\bar{F}$ can be identified).

We will determine the temperature in the six-dimensional space by the relationship:

$$\iint_{\Omega_p}\frac{\vec{p}\vec{p}}{m}\bar{F}_{11}^{(m)}(\vec{q}, \vec{q}+\vec{r}, \vec{p}, \vec{p}^1; t)\,d\vec{p}\,d\vec{p}^1 = nT\bar{F}_{11}^{(m)}(\vec{q}, \vec{q}+\vec{r}; t)\bar{\bar{I}} \qquad (16)$$

which corresponds to the determination (12) with a precision up to second-order values with respect to the mean velocity $\vec{u}$.

We will introduce an approximation for the distribution function $\bar{F}_{11}^{(1)}$ [4]

$$\bar{F}_{11}^{(m)}(\vec{q}, \vec{q}+\vec{r}; t) = \frac{1}{V}\varphi(\vec{q}, \vec{r}; t)\bar{F}_{11}(\vec{q}; t) \qquad (17)$$

In the equilibrium case we will have

$$\bar{F}_{11}^{(m)}(\vec{q}, \vec{q}+\vec{r}) = \frac{1}{V}\varphi_0(r)\bar{F}_{11}(\vec{q}) \qquad (18)$$

Using equation (9) and making calculations similar to those in [5], we find the function:

$$(\vec{U}'^{(\omega)} - \vec{U}_i)\bar{F}_n^{(\omega)}(\vec{q}, \vec{q}+\vec{r}; t) = \frac{\kappa T}{2\xi V^2}\left[\varphi_n \frac{\partial}{\partial \vec{r}}\left(\frac{\partial(\rho_0 \varphi_n)}{\partial T}\right)\vec{r} - \left(\frac{\partial \varphi_n}{\partial T}\right)\vec{I}\right]\nabla T \qquad (19)$$

Here we take note of the fact that in homogeneous media we can assume

$$\bar{F}_n(\vec{q}) \equiv \frac{1}{V}.$$

Using (19) in the expression for the potential component of the heat flux density (15), we have:

$$\vec{J}^{пот.} = \frac{\pi \kappa T}{3\xi V^2}\left\{\int_{r_n}^{\infty}[\Phi(r) - r\Phi'(r)]r^3\varphi_0(r)\frac{d}{dr}\left(\frac{\partial(\rho_0\varphi_n)}{\partial T}\right)dr - \right.$$
$$\left. - \int_{r_n}^{\infty}[3\Phi(r) - r\Phi'(r)]r^2\left(\frac{\partial \varphi_n}{\partial T}\right)dr\right\}\nabla T; \left(\frac{4\pi}{3}r_n^3 = V\right) \qquad (20)$$

Using the Fourier phenomenological law of thermal conductivity

$$\vec{J} = -\kappa_T \nabla T, \qquad (21)$$

we find an expression for the coefficient of thermal conductivity (according to (14) and (20))

$$\kappa_T = \kappa_{кин} + \kappa_{пот.}$$
$$\kappa_{кин} = \frac{\kappa^2 T}{2\xi m}\rho - \frac{\kappa^2 T^2}{6\xi m}\left(\frac{\partial \rho}{\partial T}\right)$$
$$\kappa_{пот} = \frac{\pi \kappa T}{3\xi V^2}\left\{-\int_{r_n}^{\infty}[\Phi(r) - r\Phi'(r)]r^3\varphi_0(r)\frac{d}{dr}\left(\frac{\partial(\rho_0\varphi_n)}{\partial T}\right)dr + \right. \qquad (22)$$
$$\left. + \int_{r_n}^{\infty}[3\Phi(r) - r\Phi'(r)]r^2\left(\frac{\partial \varphi_n}{\partial T}\right)dr\right\}.$$

The function $\phi_0(r)$ can be approximated by an expression in [3]

$$\varphi_0(r) = A \exp\left\{-\frac{\Phi(r+a)}{kT}\right\}, \tag{23}$$

where a is some small parameter and A is a normalizing multiplier, determined by the normalizing condition

$$\frac{1}{V}\int_{\Omega} \varphi_0(r)\, d\vec{r} = 1 \tag{24}$$

Adopting the approximation (23) and integrating the first term in the potential part of the thermal conductivity coefficient by parts, we arrive at the expression:

$$K_{пот} = \frac{\sqrt{\pi}kT}{3\xi V^2}\left\{\int_{r_0}^{\infty}\left[r\Phi'(r) - \Phi(r)\right] r^2 \frac{\Phi'(r+a)}{kT}\left(\frac{\partial \varphi_0}{\partial T}\right) dr - \right.$$
$$\left. - \int_{r_0}^{\infty}\left[r^2\Phi''(r) + 4r\Phi'(r) - 6\Phi(r)\right] r^2\left(\frac{\partial \varphi_0}{\partial T}\right) dr\right\} \tag{25}$$

Here the derivative with respect to temperature is adopted either at constant volume or at constant pressure, depending on whether we need to know the thermal conductivity at constant volume or at constant pressure.

The coefficient of friction for simple nonpolar liquids has been previously determined in [7]

$$\xi = 12{,}7\sqrt{\frac{M}{T}}\,\frac{\varepsilon}{k}\,\frac{\sigma^4}{r_0^4}\cdot 10^{-5}\ \text{g}\cdot\text{sec}^{-1} \tag{26}$$

where ε/k and σ are parameters of the Lennard-Jones potential (σ = Angstroms, ε/k in degrees, and M = molecular weight).

In higher approximations (F_{12} and F_{22}) calculation of the thermal conductivity coefficient will be considered at a later date.

References

1. Zwanzig, R. W., J. G. Kirkwood, I. Oppenheim, and B. J. Alder, *J. Chem. Phys.*, Vol. 22, No. 5, 1954.
2. Rott, L. A., *ZhFKh*, Vol. 31, p. 1468, 1957; *DAN BSSR*, Vol. 2, p. 58, 1958.
3. Adzerikho, T. S, A. A. Yedinovich, V. B. Nemtsov, and L. A. Rott, *Doklad na Vsesoyuznom Soveshchanii po Fizike Zhidkostey*, [Report Presented at the All-Union Conference on the Physics of Liquids], Kiev, May 1967.
4. Rott, L. A., *Ukr. Fiz. Zh.*, Vol. 7, p. 686, 1962; Vol. 9, p. 354, 1964.
5. Kirkwood, J. G., *J. Chem. Phys.*, Vol. 14, No. 3, p. 180, 1946.
6. Chandrasekar, S., *Stokhasticheskiye Problemy v Fizike i Astrofizike*, [Stochastic Problems in Physics and Astronomy], IL Press, Mosocw, 1947.
7. Rott, L. A., *Sb. Primeneniye Ul'traakustiki i Issledovaniyu Veshchestva*, [Collection: Use of Ultrasonics in Research on Compounds], MOPI Press, No. 22, Moscow, 1967.

THERMOPHYSICAL CHARACTERISTICS OF BINARY SOLUTIONS AS A FUNCTION OF CONCENTRATION

G. V. Grishchenko

In recent years a large number of diverse methods for determining thermophysical characteristics of solids have appeared. But only some of these have been used for determining thermophysical characteristics of liquids. In this respect, the method of the second temperature-time intervals merits attention [1, 2]. The theory of this method allows us to use it in investigating solids, as well as liquids. An important advantage of this method is the fact that this method is comprehensive, that is, all thermophysical characteristics a, λ and c can be determined from a single experiment. This is especially important in studying solutions of polymers, since both such solutions undergo physicochemical changes in the course of heating, and therefore it is necessary to determine all thermophysical characteristics during a single experiment.

Several versions of the method of second temperature-time intervals have been theoretically formulated. For all these versions the method of measurement is the same [1]. Working formulas for calculating thermophysical characteristics are of the form:

$$a = \frac{h^2}{4p\Delta\tau}; \quad \lambda = b\varepsilon\sqrt{a}; \quad c = \frac{\lambda}{a\rho}.$$

The dimensionless parameters p and ε that are part of the working formulas are calculated from working tables, which are of different types for different versions of the method of second temperature-time intervals [3].

A difficulty in measuring thermophysical characteristics of liquids lies in elimination of convection. This requires that the heat flux be

directed from the top downward. In our experiments we used a coolant, placing it downward from the layer of the test liquid or heater, which was placed facing upward. A stream of water from the TS-15 thermostat served as the coolant, and as a heater -- both the stream of water and an electric hot plate with an electronic temperature control.

The thickness of the test liquid layers was 1.5-2 mm, which satisfied the well known relationship $Gr \cdot Pr \leq 600$.

The following were used as reference materials for heat receivers: polymethylmethacrylate, ebonite, quartz sand, vulcanized rubber and marble.

For the one-dimensional case of heat propagation, the lateral surface of the cell and the heat receiver were heat-insulated.

The most promising method for determining thermophysical characteristics of liquids is the generalized method 1. Here the thermocouple is embedded to a certain depth in the heat-receiver material, which makes it possible to conduct studies in very thin layers, free of convection.

Thermophysical characteristics of solutions of sugar and water, gasoline in avtol, and solutions with low stratifying were investigated, such as the following: acetone-water, ethanol-water, pyridine-water, aniline-propyl alcohol. The index of refraction for these compounds is measured at the same time as a function of solution concentration.

It was found that most of the solutions studied reveal a deviation from the additivity rule. For some of them, well defined anomalies on the composition versus property diagrams were revealed.

Figure 1 presents thermophysical characteristics of the acetone-water system. Here also is shown variation of the index of refraction as a function of concentration. It is clear that the nature of the change of the quantity $1/n$ is very close to the change of the quantity a.

Figure 2 presents thermophysical characteristics of the pyridine-water system. We see a well defined nonmonotonic variation of the thermal diffusivity coefficient as a function of solution concentration.

The nonmonotonic nature of thermophysical characteristics as functions of concentration is even more graphically evident in the aniline-propyl alcohol system (Figure 3).

Symbols

λ = thermal conductivity of test compound; a = thermal diffusivity of test compound; c = specific heat; ρ = density; h = thickness of layer; τ = experimentally measured delay time of thermal front; n = index of refraction of solution; b = instrument constant; c = bulk concentration.

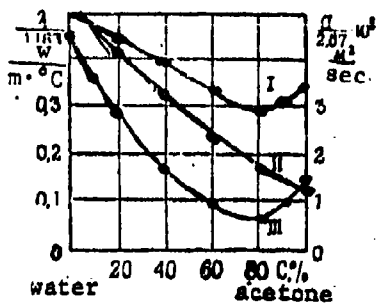

Figure 1. Coefficients λ, a and 1/n as functions of change in bulk concentration for the acetone-water system: I, $a = f_1(c)$; II, $\lambda = f_2(c)$; III, $1/n = f_3(c)$

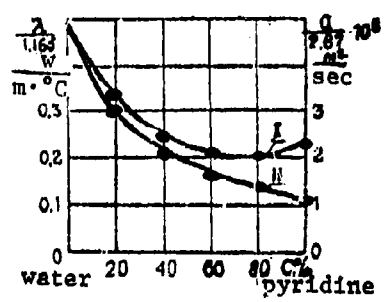

Figure 2. Coefficients λ and a as functions of change in bulk concentration for the pyridine-water system: I, $a = f_1(c)$; II, $\lambda = f_2(c)$

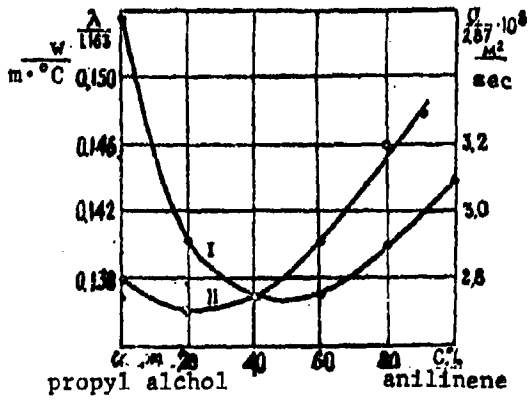

Figure 3. Coefficients λ and a as functions of variation of bulk concentration for the aniline-propyl alcohol system: I, $a = f_1(c)$; II, $\lambda = f_2(c)$

References

1. Vol'kenshteyn, V. S. and N. N. Medvedev, *IFZh*, Vol. 2, No. 10, 1959.
2. Vol'kenshteyn, V. S., *Teplo- i Massoperenos*, [Heat and Mass Transfer], Vol. 7, Nauka i Tekhnika Press, Minsk, 1960, [sic].
3. Vol'kenshteyn, V. S. and N. N. Medvedev, *Sb. Issledovaniya po Teploprovodnosti*, [Collection: Research on Thermal Conductivity], Nauka i Tekhnika Press, Minsk, 1966.

THERMOPHYSICAL PROPERTIES OF SEVERAL NONFILLED AND FILLED AMORPHOUS POLYMERS IN THE GLASSY STATE[1]

V. P. Dushchenko, V. M. Baranovskiy, I. A. Uskov,
V. S. Tytyuchenko, Yu. M. Krasnobokiy, N. I. Shut,
V. V. Levandovskiy and Yu. T. Tarasenko

Thermophysical properties of polymers, especially filled polymers, have not been very closely investigated.

We used the nonsteady-state method of dynamic heating for the investigation [1].

Heat transfer in polymers is determined to a considerable extent by the supermolecular structure and nature of the intra- and intermolecular actions [2].

Heat scattering in a cross-linked polymer -- the ED-5 epoxide resin -- is the greatest, a lower value marks the branched polystyrene (PS), and still lower is linear polyvinyl chloride (PVC). Powders of copper (particles of irregular shape) and iron (particle shape approximately spherical) were used as fillers for these polymers.

The coefficient of thermal conductivity λ of the amorphous polymers investigated in the glassy state region increased slightly with rise in temperature (Figure 1). After the glassy point was reached, when the macromolecules acquire flexibility, λ decreases sharply. This is due to the gradual thawing out of its segmentary vibrations.

These results are in agreement with the Debye phonon theory, if we bear in mind that the specific heat of a polymer rises sharply with temperature, while its density, velocity of propagation of sound and the mean free phonon path decrease slightly.

---

[1]See p. 526

When metal fillers are incorporated into a polymer, a certain rise in thermal conductivity is observed, which is appreciable even at relatively small filler concentrations. Evidently, this is largely associated with the formation in the polymer of domains of oriented structure exhibiting heightened thermal conductivity under the action of the filler, and also with the appreciable thermal conductivity of filler particles.

A substantial rise in the thermal conductivity coefficient was observed for PS and PVC for significant filler contents (40-50 percent). This can be associated with a rise in the proportion of oriented domains around the filler particles in the overall polymer bulk.

The anomaly noted in variation of thermal conductivity coefficients with temperature becomes evident especially forcefully in the transitional region from the glassy state to the highly elastic state. Relaxation effects in amorphous polymers are also most clearly manifest in this temperature range [3]. It is obvious that this anomaly is inherent only to that section of the polymer which undergoes the strong variation of supermolecular structure as a result of the effect of the solid surfaces of filler particles. It can be assumed that in compositions with high filler content the main bulk of a polymer proves to be modified, which leads to a rise in the thermal conductivity coefficient with temperature. As flexibility of macromolecules and their clustered formations grows with rise in temperature, the role of structural changes in the polymer decreases and the filled composition behaves in the ordinary way -- the coefficient of thermal conductivity passes through a maximum and begins to decrease.

A drop in the thermal diffusivity coefficient of polymers ($a = \lambda/c\rho$) with rise in temperature (Figure 2) is accounted for by the temperature dependence of the thermal conductivity coefficient, the specific heat c and the density ρ.

The coefficient of thermal diffusivity of the filled polymers studied decreases with rise in temperature (Figure 2), which is directly associated with variation of the thermal diffusivity coefficients of the components. The coefficient of thermal diffusivity rises for strongly filled compositions when t = const in the form of the appearance of direct contact -- "thermal bridges" between the filler particles.

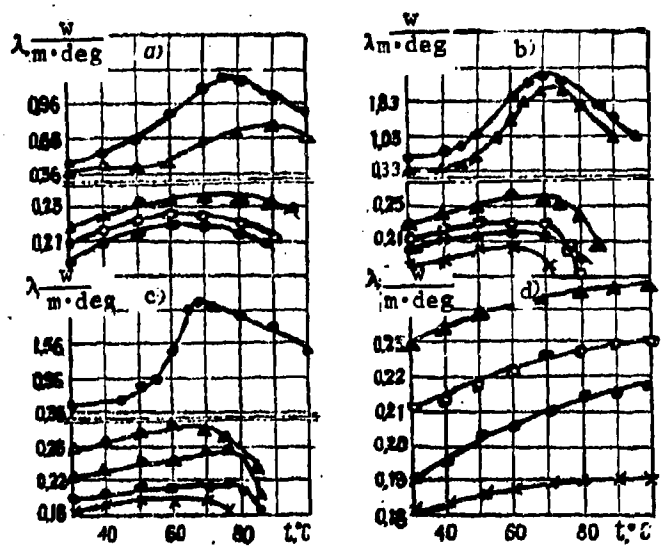

Figure 1. Coefficient of thermal conductivity of polymers as a function of temperature: a, PVC + Fe; b, PVC + Cu; c, PS + Fe; d, ED-5 + Cu: x - 0 percent, • - 10 percent, O - 20 percent, ▲ - 30 percent, Δ - 40 percent, ⊖ - 50 percent (Fe or Cu)

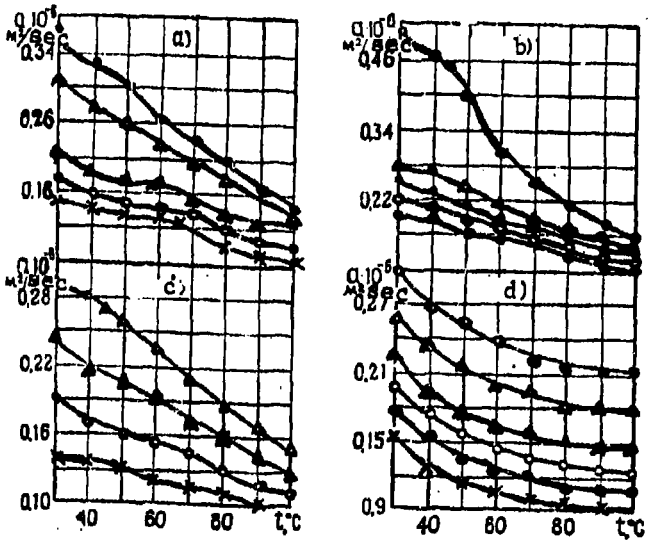

Figure 2. Coefficient of thermal diffusivity as a function of temperature: a, PVC + Fe; b, PVC + Cu; c, PS + Fe; d, ED-5 + Cu: x - 0 percent, • - 10 percent, ○ - 20 percent, ▲ - 30 percent, Δ - 40 percent, ○ - 50 percent (Fe or Cu)

Footnotes

1. To p. 522 The authors feel duty-bound to express their gratitude to G. M. Dul'nev for his kind offer to us of the equipment plans.

References

1. Platunov, Ye. S., *Izv. Vusov. Priborostroyeniye*, Vol. 4, No. 4, 1961.

2. Eiermann, K., *Kolloid- Z und Z. Polymere*, Vol. 198, No. 1-2, 1964.

3. Kargin, V. A. and G. L. Slonimskiy, *Kratkiye Ocherki po Fiziko-khimii polimerov*, [Brief Essays on the Physical Chemistry of Polymers], Moscow State University Press, Moscow, 1960.

MASS TRANSFER CHARACTERISTICS OF PLASTER WITH FILLER

N. P. Zlobina

The intensity of moisture transfer in construction materials characterized by the coefficient of the potential conductivity of mass transfer and the thermal gradient coefficient, which depend on the moisture content and temperature. The aim of this study has been to determine the coefficient of potential conductivity and the thermal gradient coefficient of plaster and its components as functions of moisture content at a temperature of 298°K.

Study of the coefficient of potential conductivity of plaster, gypsum rock and slag sand was carried out by a momentum method. Essentially the method amounts to the following: the end of a rod made of the test material with moisture-insulated side surfaces is wetted with a flat pulsing moisture source.

After a certain time interval of moisture pulse action τ_1, the time of onset of the moisture content maximum in the material layer at a distance x from the moist end of the rod, the coefficient of the potential conductivity is determined from the following relationship [1, 2, 7] from analogy with the momentum method of determining the thermal diffusivity:

$$a_m = \frac{x^2}{2\tau_1}\varphi_a , \qquad (1)$$

where

$$\varphi_a = \frac{\left(\frac{\tau_1}{\tau_{max}}\right)^2}{\left(1-\frac{\tau_1}{\tau_{max}}\right)\ln\frac{1}{1-\frac{\tau_1}{\tau_{max}}}} \qquad (2)$$

The quantities τ_1 and τ_{max} are determined from experiments.

Practically speaking, measurement of the coefficient of potential conductivity by the momentum method is carried out as follows. In a cylinder made of organic glass 6-10 cm high, $\varnothing$ 3.4 cm at a distance x from the moist end, two parallel nichrome wires 1 mm in diameter serving as electrodes are secured. The value of the distance x and the cylinder height depend on the properties of the material and are selected in such a way that, first, the condition of unboundedness which is postulated in solving the differential equation of mass conductivity is not violated, and, second, the distance has to be selected in such a way that the time of onset of moisture content maximum in the selected cross section and the time of moisture pulse action do not coincide, since in this case the function ϕ_s is not determinate. Copper-constantan thermocouples are placed in this same cross section x.

The cylinder prepared in this way is filled with the test material, which is moistened to the desired level of moisture content. Then the ends of the cylinder are sealed hermetically with metal sheets fitted with rubber inserts.

This cylinder is placed in the thermostat at T = 298°K until uniform moisture distribution over the entire specimen is achieved.

In carrying out the experiment, the moist end of the cylinder is lowered into water, and the time of action of the moisture pulse τ_1 is established. Then the cylinder is hermetically sealed and placed in the thermostat. Electrodes are connected to a self-recording PSR-1-01 automatic potentiometer. We know that the electrical resistance of the material depends on its moisture content [4]. Resistance as a function of moisture content for almost all capillary-porous bodies can be expressed by a power function.

$$R = \frac{A}{u^k}, \qquad (3)$$

where A and k are positive constants dependent on the test material and the

conditions of measurement. We see from examination of the function (3) that the resistance minimum corresponds to a moisture content maximum.

Therefore, the time of onset of moisture content maximum is determined from the onset of moisture content maximum is determined from the onset of the electrical resistance minimum. We must note that only the nature of the variation of moisture content in the selected cross section as a function of time is established by this method, and that the moisture content value is not determined.

The nature of variation of electrical resistance in some selected cross section as a function of time for a given time interval of moisture pulse action τ_1 = 7 sec for plaster is shown in Figure 1. In the figure the time of onset of the electrical resistance minimum is easily seen, which corresponds to τ_{max}, the time of onset of the moisture content maximum in the selected cross section.

This method was used to determine the coefficient of potential conductivity of plaster (γ_0 = 1300-1400 kg/m^3) of gypsum rock (water-cement ratio 0.5), slag sand (γ_0 = 1600 kg/m^3) as a function of moisture content at a temperature of 298°K (cf. Figures 2 and 3).

The nature of variation of the coefficient of potential conductivity for plaster, gypsum rock and slag sand correspond to studies made by other authors obtained for different capillary-porous bodies [3, 4, 6] and can be accounted for by the nature of distribution over radii [3].

The thermal gradient coefficient of these materials was determined by a steady-state method. A cylinder 3.4 cm in diameter and 12 cm high made of the test material with the desired level of moisture content, with moisture-insulated total surface and heat-insulated lateral surface, was placed between two heater elements. In our case, hot plates from the desks of Doctor Bokk, the Weiss Company for determining the coefficient of thermal conductivity were used. The temperature of the hot plate was kept constant at 80°C, the temperature of the cold plate was kept at 15°C. For the temperature drop induced in the specimen of test material, redistribution of moisture content occurred only under the action of temperature. After arrival at the steady-state the temperature field was recorded.

Dividing up the cylinder by layers, the moisture content of each layer was determined by a weight method. Based on the data obtained, the following graphs were plotted: $T = f(x)$ and $u = f(x)$, where x is the distance of reference points from the hot end of the cylinder.

The temperature gradients and the moisture content gradients were determined from the graphs.

The thermo-gradient coefficient was calculated from the formula given in [8]

$$\delta = -\frac{\nabla u}{\nabla t}\,\frac{kg/kg}{rpaq}.$$

From the results of investigating the thermal gradient coefficient of plaster and gypsum rock (Figure 4), it follows that in the region of sorption moisture content, the thermal gradient coefficient increases and reaches a maximum for maximum sorption moisture content, but in the super-sorption region the thermal gradient coefficient drops off with rise in moisture content. This kind of variation in thermal gradient coefficient also corresponds to atudies made by other authors [3, 4].

Symbols

a_{in} = coefficient of potential conductivity; τ_1 = time of action of moisture pulse; x = distance from moist end; τ_{max} = time of onset of moisture content maximum in selected cross section x; ϕ_a = auxiliary function; R = electrical resistance; u = moisture content; γ_o = specific weight of material; δ = thermal gradient coefficient.

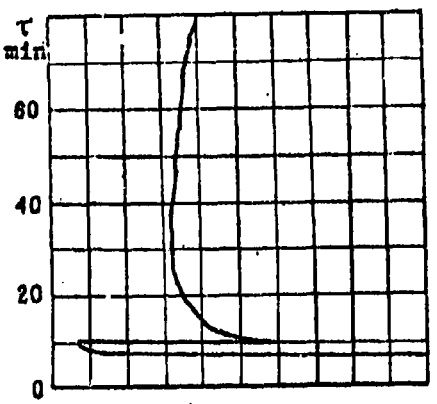

Figure 1. Variation of electrical resistance as a function of time for a given time interval of moisture pulse action τ_1 = 7 sec for plaster

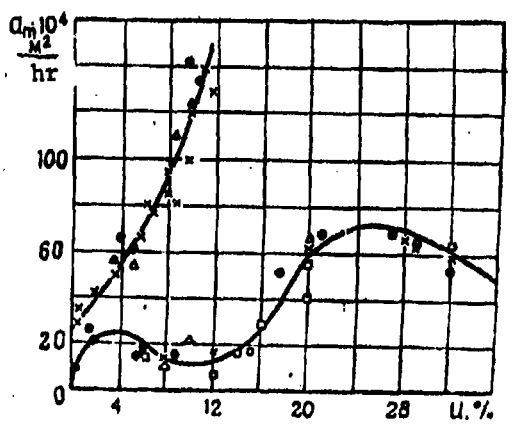

Figure 2. Coefficient of potential conductivity as a function of moisture content for T = 298°K for: 1, Plaster, γ_o = 1300-1400 kg/m^3; 2, Slag sand, γ_o = 1600 kg/m^3

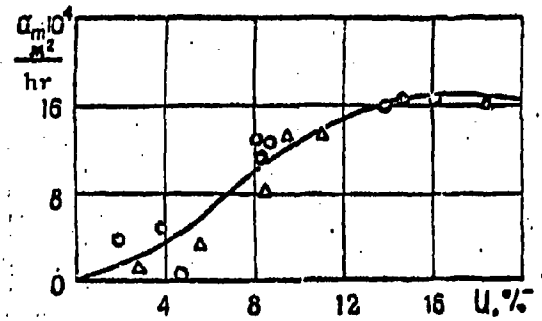

Figure 3. a_m as a function of moisture content for gypsum rock at T = 298°K

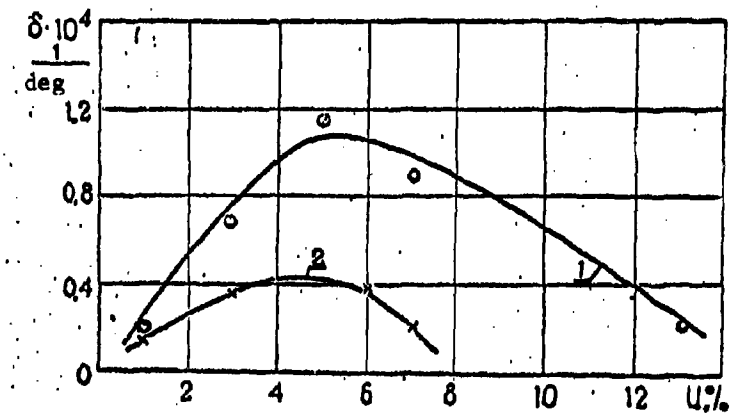

Figure 4. Thermal gradient coefficient as a function of moisture content at T = 313°K for: 1, Plaster; 2, Gypsum rock

References

1. Tsimermanis, L. B., N. P. Zlobina, F. I. Kuznetsov and Ye. I. Fedorov, *Avtorskoye Svidetel'stvo No 174005,* [Author's Certificate No. 174005],

2. Vishnevskiy, N. Ye., *Tr. Vsesoyuznogo Nauchno-issledovatel'skogo kinofotoinstituta,* No. 2 (25), 1958.

3. Lykov, A. V., *Teoriya Teploprovodnosti,* [Theory of Thermal Conductivity], GITTL Press, Moscow, 1952.

4. Lykov, A. V., *Yavleniye Perenos v Kapillyarno-poristykh Telakh,* [Transport Pheonomena in Capillary-porous Bodies], GITTL Press, Moscow, 1954.

5. Lykov, A. V., *Teoriya Sushki,* [Theory of Drying], Gosenergoizdat Press, Moscow-Leningrad, 1950.

6. Berlinf, M. A., *Elektricheskiye Metody i Pribory dlya Izmereniya i Regulirovaniya Vazhnosti,* [Electrical Methods and Instruments for Measurement and Regulation of Moisture Content], Gosenergoizdat Press, Moscow-Leningrad, 1960.

7. *Sb. Teplofizicheskiye Svoystva Veshchestv,* [Collection: Thermophysical Properties of Compounds], Naukova Dumka Press, Kiev, 1966.

8. *Sb. Vazhnostnoye Sostoyaniye i Teplofizicheskiye Svoystva Vspuchennogo Vermikulita, Izdeliy i Konstruktsii iz Nego,* [Collection: Moisture Content and Thermophysical Properties of Swollen Vermiculite, and of Articles and Structures Made Therefrom], Chelyabinsk, 1965.

9. Dmitrovich, A. D., *Teplozashchitnyye Svoystva Stroitel'nykh Materialov i Konstruktsiy,* [Heat-protective Properties of Construction Materials and Structures], Belarus' Press, Minsk, 1963.

TRUE DIFFUSION COEFFICIENTS OF THE He-CO_2 SYSTEM AS A FUNCTION OF TEMPERATURE

N. D. Kosov and A. F. Bogatyrov

Heat transfer by thermal agitation with strict observance of isobaricity of conditions is characterized by true diffusion coefficients [1, 2]. The true diffusion coefficient of one gas in another is not equal, in the general case, to the true diffusion coefficient of the latter gas in the former, and according to Boltzmann [1] for solid spheres with account taken of the persistency of velocities [3, 4] and the mean free path as a function of velocity [3] this coefficient is determined by the following formula:

$$D_1 = \frac{1{,}051\sqrt{8\kappa T}}{3n\pi\sqrt{\pi m_1}\left[(1-\omega_{11})\sqrt{2}C_1\sigma_1^2+(1-\omega_{12})C_2\sigma_{12}^2\sqrt{\frac{m_1+m_2}{m_2}}\right]} \qquad (1)$$

The true diffusion coefficient of the second gas in the first is obtained from formula (1) by replacing the index 1 by the index 2.

True diffusion coefficients as functions of temperature have as yet been poorly investigated.

Below we set forth the results of measurements of true and mutual diffusion coefficients of the He-CO_2 system in the temperature range 290-430°K, and also the values of the baro-effect induced when there is diffusion within closed systems.

Method of Measurements. Results

True diffusion coefficients were measured by a steady-state method under isobaric and isothermal conditions [2]. The difference between our apparatus and that described in [2] lies mainly in the thermostating of its main assemblies (diffusion cell, interference cells, and rheometers) and in the

Table 1. True and Mutual Diffusion Coefficients of the He–CO_2 System at Different Temperatures

T°K	$p \cdot 10^{-2}$ N/m^2	$\bar{D}_1 \cdot 10^4$ m^2/sec			$\bar{D}_2 \cdot 10^4$ m^2/sec			$D_{12} \cdot 10^4$ m^2/sec for pressures given below	
		Experiment at pressures given below		Calculated according to formula (2)	Experiment at pressures given below		Calculated according to formula (2)	Experiment	Normal
		Experiment	Normal		Experiment	Normal			
290	925,0	I,I6	I,06	I,00	0,36	0,33	0,20	0,65	0,59
298	922,5	I,20	I,09	I,02	0,37	0,34	0,2I	0,68	0,62
3I8	923,0	I,3I	I,I9	I,I3	0,40	0,37	0,23	0,76	0,69
343	920,5	I,47	I,34	I,30	0,46	0,4I	0,27	0,86	0,78
363	920,5	I,6I	I,46	I,43	0,50	0,46	0,29	0,94	0,86
388	9I8,2	I,78	I,62	I,59	0,57	0,5I	0,33	I,08	0,96
408	9I7,5	I,92	I,74	I,70	0,63	0,57	0,37	I,I8	I,06
430	920,2	2,08	I,89	I,85	0,70	0,63	0,4I	I,22	I,II

3 percent. The diffusion coefficients of carbon dioxide gas in helium, measured and calculated, differ from each other by 35 percent (precision of $\overline{D}_2$ 5% measurement). However, the theoretical curves of $\overline{D}_2$ as a function of temperature followed the experimental, but was shifted downward almost parallel to itself. This can be accounted for, first of all, by the fact that the carbon dioxide molecule is far from a solid sphere. Secondly, as we see from formulas (2)-(4), the error in determining the effective diameter had a considerably greater effect on the precision of calculation of $\overline{D}_2$.

Thus, the Boltzmann theory correctly reflects to the first approximation the course of the temperature dependence of true diffusion coefficients. However, the deviation observed (in particular for the diffusion of a heavy gas in a light) requires additional investigation.

The Baro-effect at Different Temperatures

One of the interesting problems directly associated with investigation of the temperature dependence of diffusion coefficients is the diffusion baro-effect as a function of temperature. According to the Boltzmann diffusion theory, the baro-effect is a consequence of inequality intrinsic to diffusion flows of the first and second gases. In closed systems, this leads to the induction of pressure on the part of the gas that has the lower true diffusion coefficient, which in turn is the cause of the hydrodynamic flow of the gas mixtures toward the gas that has the higher true diffusion coefficient. In the steady-state, the specific hydrodynamic flow equals the difference between the diffusion flows and for the single-dimensional case can be written as:

$$q_v = (\overline{D}_1 - \overline{D}_2)\frac{\Delta c}{L} \qquad (5)$$

For given gases and given geometry, the hydrodynamic flow will be proportional to the steady-state pressure difference. Bearing in mind equation (5) and taking $\Delta c = 1$, we will obtain

$$\Delta p \sim \overline{D}_1 - \overline{D}_2 \qquad (6)$$

narrow temperature range is well described by the power formula in [6]. From our data, the exponent for the mutual diffusion coefficient was found to be 1.9, which within limits of experimental error agrees with the value of 1.92 found in [7]. This betokens the satisfactory performance of the equipment as a whole. The existing small difference (within the limits of 3 percent) between our data and the data in [7] is accounted for by the fact that we do not introduce corrections for the end effect, and the instrument constant was calculated directly from geometrical parameters while at the same time in [7] the geometric parameter was determined by standardizing.

The true diffusion coefficients of the function of temperature are more complex, as we can see from the curves in Figure 1.

The diffusion coefficient measured in the experiment is integral, and that given by formula (1) is local. The true integral coefficient of diffusion of the first gas in the second obviously equals:

$$\overline{D}_1 = \frac{1}{C_1^{\prime} - C_1^{\circ}} \int_{C_1^{\circ}}^{C_1^{\prime}} D_1(c_1)\,dc_1 = \frac{D_{11}}{(C_1^{\prime} - C_1^{\circ})(1-a_{12})} \ln \frac{(1-a_{12})C_1^{\prime} + a_{12}}{(1-a_{12})C_1^{\circ} + a_{12}}, \qquad (2)$$

where

$$D_{11} = \frac{2(kT)^{\frac{1}{2}}}{3\pi\sqrt{\pi m_1}(1-\omega_{11})\rho\sigma_1^2} = \frac{0{,}375}{\sqrt{m_1}\rho\sigma_1^2}\left(\frac{kT}{\pi}\right)^{\frac{1}{2}}, \qquad (3)$$

$$a_{12} = \frac{1-\omega_{12}}{1-\omega_{11}}\left(\frac{\sigma_1+\sigma_2}{2\sigma_1}\right)^2 \sqrt{\frac{m_1+m_2}{2m_2}} \qquad (4)$$

The true integral diffusion coefficient of the second gas in the first is obtained from formulas (2)-(4) by replacing the index 1 by the index 2.

Coefficients $\overline{D}_1$ and $\overline{D}_2$ calculated from formula (2) are shown in Figure 1 by dashed lines. In the calculations of $\overline{D}_1$ and $\overline{D}_2$, the values of the effective diameters were calculated from the self-diffusion coefficients at the given temperature [6] using formula (3). As we can see from the curves in Figure 1, the true diffusion coefficient of helium in carbon dioxide, calculated from formula (2) differs somewhat (within the limits of 5 percent) from the measured values. The measurement precision of the coefficient $\overline{D}_1$ is

variation of the geometric parameters of the diffusion cell, which simultaneously also fulfill the function of heat exchanger. The thermostating liquid for the diffusion cell was dibutylphthalate, and for the rheometers and interference cells the temperature of which was always kept constant (298°K) -- water. Compressive gaskets were made of Teflon. Preheated to temperatures close to the experimental temperature, the gases were swept through at a constant rate (the bulk rate throughout all the experiments was kept constant at 172×10^{-6} m^3/sec) through the tubings of the diffusion cell in which they took on the desired temperature. The tubings were connected with a set of capillaries in which diffusion was carried out. The capillary sets were made of approximately identical tubes of stainless steel (injection needles) with a total area of 3.77×10^{-5} m^2 (180 tubes in one and 26 tubes in the other). The tube length was 7.05×10^{-2} m. The tubings were slitlike in form (height, width and length, respectively, were $0.002 \times 0.08 \times \times 0.5$ m) and made of brass. Special grooves were ground over the entire outer surface, covered over, and served to channel the dibutylphthalate from the thermostat. To reduce heat losses and equalize temperature, the diffusion cell with the capillary set was carefully heat-insulated. Gases after diffusion were cooled to the temperature of the analysis in a special heat-exchanger and then sent to the interference cells of the interferometer. Establishment of the isobaricity of the conditions and measurement of the concentrations of the diffusing compounds were carried out as in [2].

The coefficients of mutual diffusion were measured on this same equipment using the steady-state method described in [5] for the same temperature range. For this purpose the pressure was varied in one of the tubings until the hydrodynamic flow induced as a consequence equaled the overall transport of a particular gas.

The results of measuring true diffusion coefficients of helium in carbon dioxide gas $\overline{D}_1$ and of carbon dioxide gas in helium $\overline{D}_2$, and also the mutual diffusion coefficients $\overline{D}_{12}$ are presented in Table 1.

Figure 1 presents in logarithmic scale the diffusion coefficients $\overline{D}_1$, $\overline{D}_2$ and $\overline{D}_{12}$ of the system investigated as a function of temperature. The temperature dependence of the mutual diffusion coefficients of gases for a

Another point of view on the nature of the diffusion baro-effect [8, 9] for the same conditions leads to a function of the form

$$\Delta p \sim \overline{D}_{12} \qquad (7)$$

The true diffusion coefficients and the mutual diffusion coefficient varied dissimilarly with temperature. Therefore, formulas (6) and (7) give the baro-effect as different functions of temperature. Therefore it was of definite interest to investigate the baro-effect at different temperatures.

The same apparatus used in measuring mutual diffusion coefficients was employed in measuring the value of the baro-effect at different temperatures (mean capillary radius was equal to $(5.8 \pm 0.5 \times 10^{-4}$ m). In the steady-state method the baro-effect value Δp corresponds to that pressure value at which the overall flows of a given gas are equalized. The pressure difference was measured, as in [2], from the change in the height of the level of gas exiting from the tubing. Figure 2 presents the results of measurement of the baro-effect at different temperatures for the He-CO_2 and He-Ar systems, and the diffusion coefficients of the latter as a function of temperature have been investigated earlier [10]. As we can see from Figure 2, the baro-effect varied linearly with temperature. Figure 3 presents the quantity $\overline{D}_1 - \overline{D}_2$ as a function of temperature plotted from the data in Table 1 and in [10], this function also proving to be linear. The mutual diffusion coefficient is proportional to T^r, where $r > 1.5$ (for the He-CO_2 system $r = 1.92$, for the He-Ar system, $r = 1.75$ [6]). Therefore, according to formula (7), Δp must be proportional to T^r, which was not observed in the experiment.

Symbols

D_1 and D_2 = true local diffusion coefficients; $\overline{D}_1$ and $\overline{D}_2$ = true integral diffusion coefficients; $\overline{D}_{12}$ and D_{11} = coefficients of mutual diffusion and of self-diffusion; ω = persistency of velocities; m and σ = mass and effective diameter of the molecule; n = number of molecules per unit volume; $C_i = n_i / \sum n_i$ = relative concentration; $C_i^b - C_i^a$ = concentration difference at ends of capillary of length L; k = Boltzmann constant; p and T = pressure and absolute temperature.

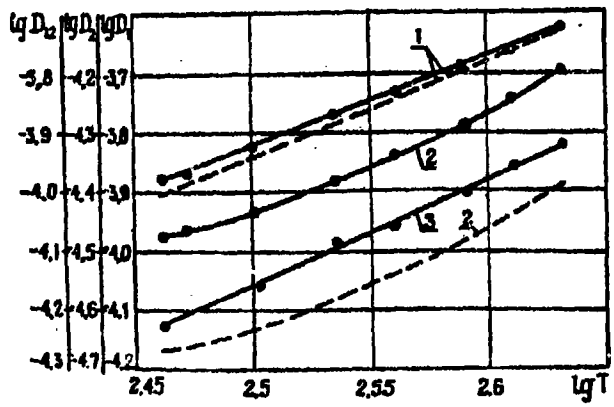

Figure 1. Diffusion coefficients of the He-CO_2 system as a function of temperature: 1, For the true diffusion coefficient of helium in carbon dioxide; 2, For the true diffusion coefficient of carbon dioxide in helium; 3, For the mutual diffusion coefficient. The solid line is experimental values; the dashed line is theoretical values.

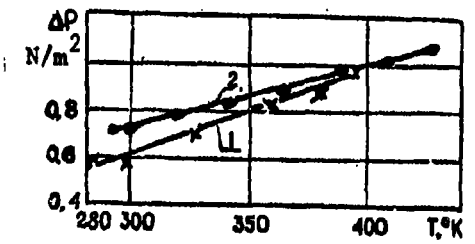

Figure 2. Diffusion baro-effect as a function of temperature for the He-Ar system (1) and for the He-CO_2 system (2)

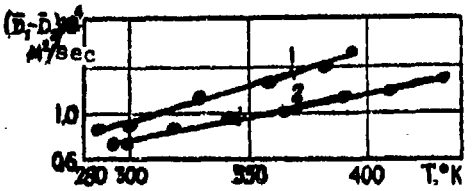

Figure 3. Difference of true diffusion coefficients as a function of temperature for the following systems: 1, For He-Ar; 2, For He-CO_2

References

1. Boltzmann, L., *Lektsii po Teorii Gazov*, [Lectures on the Theory of Gases], GITTL Press, Moscow, 1953.
2. Kosov, N. D. and L. I. Kurlapov, *ZhTF*, Vol. 35, p. 2120, 1965.
3. Jeans, J. H., *The Dynamical Theory of Gases, 4-th Edition*, New York, 1925.
4. Chapman, S. and T. Kauling, *Matematicheskaya Teoriya Neodno-rodnykh Gazov*, Mathematical Theory of Nonhomogeneous Gases], IL Press, Moscow, 1960.
5. Kurlapov, L. I. and N. D. Kosov, *Fizika. Sb. Trudov Aspirantov i Soiskateley*, [Collection of Studies of Graduate Students and Degree-seekers], Ministry of Higher and Secondary Specialized Education Kazakh SSR, No. 3, Alma-Ata, 1967.
6. Vargaftik, N. B., *Spravochnik po Teplofizicheskim Svoystvam Gazov i Zhidkostey*, [Handbook on Thermophysical Properties of Gases and Liquids], Fizmatgiz Press, Moscow, 1963.
7. Saxena, S. C., and E. A. Mason, *Molec. Phys.*, Vol. 2, p. 379, 1959.
8. Kotousov, L. S., *ZhTF*, Vol. 34, p. 2178, 1964.
9. Suyetin, P. Ye and P. V. Volobuyev, *ZhTF*, Vol. 34, p. 1107, 1964.
10. Kosov, N. D. and A. F. Bogatyrev, *Sb. 2. Nekotoryye Voprosy Obshchey i Prikladnoy Fiziki. Tr. Pervoy Respublikanskoy Konferentsii po Voprosam Obshchey Prikladnoy Fiziki, Alma-Ata, 15-19 Maya, 1967*, [Collection 2. Several Problems of General and Applied Physics. Proceedings of the First Republican Conference on Problems of General and Applied Physics, Alma-Ata, 15-19 May, 1967] Nauka Press, Alma-Ata, 1968.

NONISOTHERMAL DIFFUSION IN GASES

N. D. Kosov, A. F. Bogatyrev and L. I. Kurlapov

The diffusion of two gases at constant pressure under isothermal conditions is caused both by a difference in the density of the number of molecules as well as by a difference in their thermal velocities. Both of these factors act simultaneously, therefore they must also be taken into account simultaneously when examining nonisothermal diffusion. Usually nonisothermal diffusion of a binary mixture of gases at constant pressure is called thermodiffusion [1]. If under nonisothermal conditions molecular transport caused by a difference in their population densities and a difference in thermal velocity is taken into account, then even in clean gas a diffusional molecular flux from the cold region to the hot becomes manifest [2]. This molecular transport is conveniently called thermo-self-diffusion (from analogy with self-diffusion under isothermal conditions). The thermo-self-diffusion flux leads to a rise in the molecular population density in the hot region (compared with the equilibrium region at a given temperature) and to a decrease in the cold region, that is, to the appearance of a pressure difference between these two gas domains. The baro-effect induced when there is nonisothermal diffusion is conveniently called the thermodiffusive baro-effect [3].

Thermo-self-diffusion graphically accounts for the mechanism of thermodiffusive separation of gases as the diffusion of each component from the cold region to the hot at its own velocity.

The present study examines a steady-state method of measuring the coefficient of thermo-self-diffusion and the results of experiments analyzing the physical sense of thermodiffusive separation.

Steady-State Method of Measuring the Thermo-Self-Diffusion Coefficient

The thermo-self-diffusion flow (and interms of it the coefficient of thermo-self-diffusion) can be measured on an apparatus designed to measure the thermodiffusive baro-effect in gases [2] and shown schematically in Figure 1, modifying somewhat the method of observation.

Let the left vessel be kept at a constant temperature T_1 (hot region of gas), and the right at a temperature T_2 (cold region of the gas). The vessels are connected by a wide capillary ($2r \gg \lambda$), such that the wall effects can be neglected. Owing to thermo-self-diffusion in section A of the capillary (Figure 1), an increased pressure is induced, and in section B -- a reduced pressure. These pressure changes give rise to hydrodynamic gas flows in the capillary from the cross section A to both sides and to the section B, and also lead to the movement of a drop of inviscous silicon oil in the horizontal tube from the hot vessel to the cold at a specific velocity V. In the steady-state the number of gas molecules intrained by the hydrodynamic flow to both sides from section A equals the number of gas molecules arriving at the section of the cold region owing to thermo-self-diffusion, that is,

$$j_T = j_1 + j_2 \qquad (1)$$

The number of molecules transported per unit time by the hydrodynamic flow through the capillary from region A to region B (regarding the movement in the capillary as of the Poiseuille type), we will have

$$j_1 = \bar{n} \frac{\Delta p r^2 S}{l 8 \bar{\eta}} . \qquad (2)$$

An analogous number of molecules, but transported through the manometric tube, can be written as follows:

$$j_2 = n_0 S_0 V = n_1 \frac{\Delta p_1}{l_1} \frac{r^2 S}{8 \eta_1} = n_2 \frac{\Delta p_2}{l_2} \frac{r^2 S}{8 \eta_2} . \qquad (3)$$

If we assume that the temperature and pressure throughout the capillary length in the steady state vary linearly, as shown in the upper part of Figure 1, then

$$\Delta p = \Delta p_k + \Delta p_1 + \Delta p_2 . \tag{4}$$

The pressure difference Δp_k under the effect of which the drop is moved can be found from its rate of movement through the force of friction $f = \alpha V$

$$\Delta p_k = \frac{f}{S_0} = \frac{\alpha V}{S_0} \tag{5}$$

Determining Δp_1 and Δp_2 from equation (3) and substituting these values as well as Δp_k in equation (4) we find

$$\Delta p = \left[\frac{\alpha}{S_0} + \frac{8 S_0}{3 T r^2}\left(\gamma_1 \ell_1 T_1 + \gamma_2 \ell_2 T_2\right)\right] V . \tag{6}$$

Substituting (6) in (2), and then (2) and (3) in (1), we will find the final expression for the thermo-self-diffusion flow

$$J_T = \frac{p S V}{\kappa T}\left(\frac{\alpha r^2 S}{8 \eta \ell S_0^2} + \frac{\gamma_1 \ell_1 T_1}{2 \ell T_0} + \frac{\gamma_2 \ell_2 T_2}{2 \ell T_0} + \frac{\overline{T}}{T}\right). \tag{7}$$

The thermo-self-diffusion flow can be calculated. By using the ordinary method of the kinetic theory of gas [3], Laranjeira [4] obtained the following expression for the overall flow Γ_i of molecules of the species i per unit area per unit time:

$$\vec{\Gamma}_i = n_i \vec{W} - \frac{1}{3} n_i u_i \left[\lambda_i \nabla \ln c_i + \lambda_i \nabla \ln p - \left(\lambda_i - \frac{\lambda_i}{2}\right) \nabla \ln T\right]. \tag{8}$$

Neglecting baro-diffusion, we obtain from equation (8) the following expression for the thermo-self-diffusion flow:

$$j_T = D_{11}\left(1 - \frac{\lambda'}{2\lambda}\right) S \frac{d\ln T}{dx} = D_T S \frac{d\ln T}{dx} \qquad (9)$$

Equating the righthand members of equations (7) and (9), we find the value of the thermo-self-diffusion coefficient.

To measure thermo-self-diffusion coefficients, two units of equipment were built with different geometric parameters (for one unit: $r = 3.12 \times \times 10^{-4}$ m; $L = 9.5 \times 10^{-2}$ m; $l_1 = l_2 = 2.2 \times 10^{-2}$ m; $S_o = 4.15 \times 10^{-6}$ m^2; for the second: $r = 3.42 \times 10^{-4}$ m; $L = 8.8 \times 10^{-2}$ m; $l_1 = l_2 = 2.5 \times 10^{-2}$ m; $S_o = 2.83 \times 10^{-6}$ m^2). The measurements were conducted at $T_1 = 370°K$, $T_2 = 285°K$, and at different pressures (from 90×10^{-2} to 480×10^{-2} N/m^2). The measured values of the thermo-self-diffusion coefficient prove to be $(0.9 \pm 0.1) \times 10^{-4}$ and $(1.6 \pm 0.2) \times 10^{-4}$ m^2/sec, respectively, for hydrogen and helium.

According to Jeans [3] $\lambda' = 0.745\ \lambda$. Then the self-diffusion coefficients of hydrogen and helium calculated according to formula (9) in terms of the thermo-self-diffusion coefficients prove to be, respectively, 1.4×10^{-4} and 2.5×10^{-4} m^2/sec for a mean temperature of 328°K, which is in agreement with literature data [5].

Physical Meaning of Thermodiffusive Separation of Gases

As we know, no well defined explanation of thermodiffusion has yet been given [6]. Thermo-self-diffusion allows us to account for the phenomenon of thermodiffusive separation as diffusion under nonisothermal conditions of each component from the cold region of the gas to the hot at its own velocity. This leads, as in the case of thermo-self-diffusion, to the induction of the thermodiffusive baro-effect in a gas mixture, whose value depends on the hydrodynamic resistance between the hot and cold regions of the gas. In a closed system under steady-state conditions transport by thermodiffusion of each component from the cold region is equilibrated by reverse transport by the hydrodynamic flow from the hot region of the gas.

The thermodiffusive baro-effect, as a phenomenon that is diffusional in nature, must be inversely proportional to pressure. This does occur for a

clean gas [2]. Measurements of the thermodiffusive baro-effect were made on the two equipment units described above for different pressures for a mixture of 68 percent helium with carbon dioxide gas. The results of the measurements are shown in Figure 2. As we can see from Figure 2, the product $\Delta p \cdot P$ remains constant, which emphasizes the diffusional nature of the thermodiffusive baro-effect also for a gas mixture. The mean deviation from the constant is 13 percent for the upper line (first unit) and 5 percent for the lower (second unit).

The hydrodynamic flow induced as a consequence of the thermodiffusive baro-effect worsens gas separation. The shift in concentrations will be greater if by some method the hydrodynamic flow could be eliminated. In the case of isothermal diffusion the hydrodynamic flow can be eliminated by maintaining the pressure at capillary ends identical and continually sweeping gas through them [7]. We used an analogous diffusion cell in studying the concentration shift as a function of intensity of hydrodynamic gas flow through the capillary.

Let the test mixture sweep through the tubings of the thermodiffusive cell (cf. Figure 3) at a specific bulk flow rate q_a (in the upper tubing at a temperature of T_1 and in the lower -- at a temperature T_2; we set $T_1 > T_2$). The tubings are connected by capillary (to increase measurement precision a set of 51 capillaries is used) in which thermodiffusion and macroscopic movement of the gas mixture occurs. The set of capillaries was made of brass tubes with a mean internal diameter of 3.0×10^{-3} m and a length of 0.15 m, therefore a slight pressure difference is induced at its ends, according to calculations of the order of several hundredths of a dyne/cm^2. It was not possible to employ replacement of the capillary set to establish the condition $\Delta p = 0$, as was done in [7]. Therefore the value of the hydrodynamic flow of gas mixture through the capillary was varied by sucking in the gas at the outlet from the thermodiffusive cell initially from the lower tubing, and then -- from the upper. Further, the bulk flow rate (using the displacement method) at the outlet from the given tubing and the concentration of components in the mixture at the outlet from both tubings were measured.

During all the experiments T_1 and T_2 remained constant (411°K and 286°K, respectively), and the bulk flow rates at the inlet to the thermodiffusive cell in both tubings were identical and equal to 0.908×10^{-6} m^3/sec.

Figure 4 shows the variation in the helium concentration in the upper tubing as a function of change in bulk flow rate $(q_o - q)$ (curve 1) and the variation in carbon dioxide concentration in the lower tubing (curve 2). We note that the bulk flow rate at the inlet to the thermodiffusive cell and at the outlet from the tubings were always measured at the same temperature. Curves 1 and 2 intersect at a point for which $q_o = q$ (within limits of experimental error). Under these conditions thermodiffusion occured in such a way that the bulk flow rates at the outlet from the thermodiffusive cell remained the same as at the inlet. This was possible in two cases.

First when the mixture components under the effect of a temperature gradient diffuse to opposite sides (the light component to the hot region, and the heavy component to the cold) in equal amounts (by numbers of molecules transported) in the absence of a hydrodynamic flow. In this case thermodiffusive flows will be at a maximum and the concentration shifts will be the highest. If, however, thermodiffusive flows are not identical in magnitude but are directed to opposite sides, equilibrating them is possible only by means of the hydrodynamic flow, as in the case of isothermal mutual diffusion. Flows equalized in this way will be characteristics of the overall transport -- by thermodiffusion and by the hydrodynamic flow. In this case the concentration shift will not attain a maximum, since the hydrodynamic flow will mix the mixture being divided. If we eliminate the hydrodynamic flow in some manner (that is, conduct an experiment under strict compliance with isobaricity of conditions) the intrinsic thermodiffusive flows of components will prove to be different in value.

Second, the equality of bulk flow rates at the inlet and outlet is possible also in the case when both components diffuse to the same side, but at different rates, and the hydrodynamic flow moves in the opposite direction, reducing the effectiveness of mixture separation. If an experiment is carried out under conditions of strict isobaricity (that is, in the absence of hydrodynamic flow), the bulk flow rate at the outlet from the upper

("hot") tubing will be increased by the very same amount as the bulk flow rate at the outlet from the upper ("cold") tubing is reduced. In this case the separation will be at a maximum and will be governed by the difference between the thermodiffusive component flows.

The quantity of component equal to the product (c' - c)q was found from data in Figure 4 as a function of velocity at the tubing outlet. Figure 5 presents this function for the light component in the upper tubing (curve 1) and for the heavy component in the lower tubing (curve 2). The curves have maxima that are symmetrically shifted from the intersection point. The intersection point, as we see from the figure, corresponds to the condition $q = q_o$. The maxima correspond to the greatest shift of concentration between the hot and cold regions, which is possible only in the absence of hydrodynamic flow (that is, when $\Delta p = 0$), for any assumption of the direction of thermodiffusive flows. From the x-axis intercept of the maxima it is clear that the velocity at the output from the lower tubing decreases precisely by as much as the velocity rises at the upper tubing. This unambiguously points to the same direction (from the cold region to the hot) as the thermodiffusive flows.

Symbols

j_T = thermo-self-diffusion flow; T_o, T_1, T_2 and $\overline{T}$ = absolute temperatures of the manometric tube, the hot and cold vessels, and the mean temperature, respectively; n_o, n_1, n_2 and $\overline{n}$ = number of molecules per unit volume, respectively, for T_o, T_1, T_2 and $\overline{T}$; p = pressure; r, S and L = radius, area and length of capillary; S_o = cross-sectional area of manometric tubing; η_1, η_2 and $\overline{\eta}$ = coefficient of viscosity at the temperatures T_1, T_2 and $\overline{T}$, respectively; v = linear velocity of drop; f = force of friction; α = coefficient of proportionality between f and V; k = Boltzmann constant; W = velocity of macroscopic flow; u = mean velocity of thermal agitation; λ and λ' = mean free paths for transport of numerical density and momentum; c = relative concentration; D_{11} and D_T = coefficients of self-diffusion and thermo-self-diffusion; q_o and q = bulk flow rates at inlet and outlet from tubing.

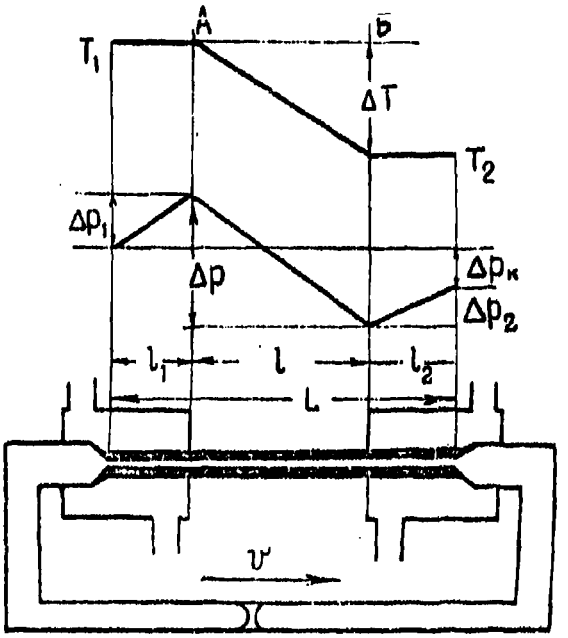

Figure 1. Diagram of the apparatus

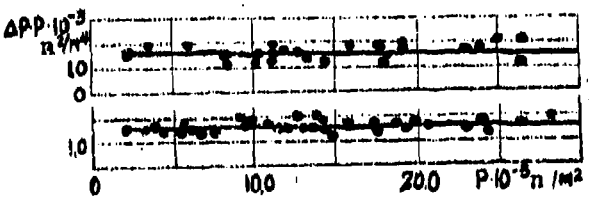

Figure 2. Thermodiffusive baro-effect of the He-CO_2 mixture as a function of pressure

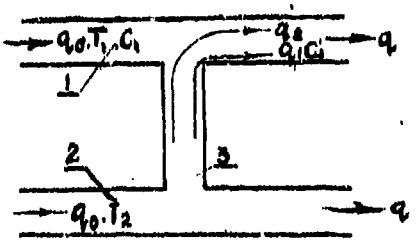

Figure 3. Diagram of thermodiffusive cell: 1, 2, "Hot" and "cold" tubings; 3, Capillary

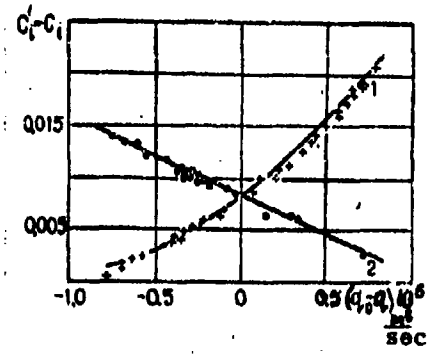

Figure 4. Variation of concentration in tubing as a function of change in velocity at outlet: 1, Change in helium concentration in the "hot" tubing; 2, Change in concentration of carbon dioxide in the "cold" tubing

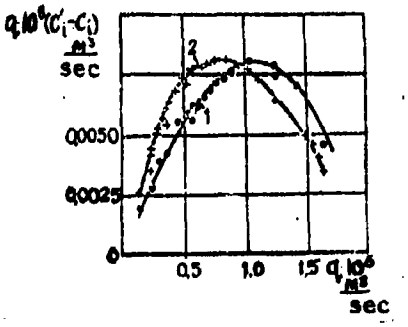

Figure 5. Amount of absorbed component as a function of velocity at outlet: 1, For helium in the "hot" tubing; 2, For carbon dioxide in the "cold" tubing

References

1. Gryu, K. E. and T. L. Ibbs, *Termicheskaya Diffuziya v Gazikh*, [Thermal Diffusion in Gases], GITTL Press, Moscow, 1956.

2. Kosov, N. D., A. F. Bogatyrev, and L. I. Kurlapov, *Sb. 2. Nekotoryye Voprosy Obshchey i Prikladnoy Fiziki. Trudy Pervoy Respublikanskoy Konferentsii po Voprosam Obshchey i Prikladnoy Fiziki, g. Alma-Ata*, [Collection 2. Several Problems of General and Applied Physics. Proceedings of the First Republican Conference on Problems of General and Applied Physics, Alma-Ata, 15-19 May 1967], Nauka Press, Alma-Ata, 1968.

3. Jeans, H. H., *The Dynamical Theory of Gases*, 4th Ed., New York, 1925.

4. Laranjeira, M. F., *Physica*, Vol. 26, p. 409, 1960.

5. Vargaftik, N. B., *Spravochnik po Teplofizicheskim Svoystvam Gazov i Zhidkostey*, [Handbook on Thermophysical Properties of Gases and Liquids], Fizmatgiz Press, Moscow, 1963.

6. Chapman, S. and T. Kauling, *Matematicheskaya Teoriya Neodnorodnykh Gazov*, [Mathematical Theory of Nonhomogeneous Gases], IL Press, Moscow, 1960.

7. Kosov, N. D. and L. I. Kurlapov, *ZhTF*, Vol. 35, p. 2120, 1965.

THERMAL CONDUCTIVITY OF LIQUID ORGANIC COMPOUNDS

G. Kh. Mukhamedzyanov and A. G. Usmanov

A review of methods of determining coefficients of thermal conductivity given in [1, 2] points to the lack of reliable recommendations for precision calculation of λ with temperature change for a wide class of compounds. At present there is no developed system of concepts which would allow us to find coefficients of thermal conductivity even within the limits of a single homologous series.

Therefore, we conducted measurements of λ of various classes of organic compounds within wide limits of variation in number of carbon atoms in the compound molecule n and over wide temperature ranges, on the basis of which we propose to solve the following problems:

1) to establish variation of λ as a function of temperature, and also to discover the effect of various functional groups on thermal conductivity;

2) to derive interpolation equations for calculating thermal conductivity coefficients of the series of compounds studied.

By way of a solution of these problems we have given in previous [illegible] results of investigations on the thermal conductivity of homologous series of saturated hydrocarbons normal-C_nH_{2n+2} (n = 6-24) [3, 4]; normal alcohols normal-$C_nH_{2n+1}OH$ (n = 1-18) [5]; saturated monobasic acids $C_nH_{2n+1}COOH$ (n = 1-18) [6]; complex esters of saturated monobasic acids $C_nH_{2n+1}COOC_nH_{2n+1}$ (n = 3-22) [7]; simple, mixed esters $C_nH_{2n+1}OC_nH_{2n+1}$ (n = 8-16) [8]; and individual representatives of other classes of compounds [9].

This study is a continuation of this series of measurements and includes experimental studies of yet another series of classes of organic liquids: unsaturated hydrocarbons of the olefin series C_nH_{2n} (n = 6-14); aldehydes $C_nH_{2n+1}CHO$ (n = 2-12); ketones $C_nH_{2n+1}COC_nH_{2n+1}$ (n = 3-13); aromatic

C_nH_{2n-6} (n = 6-12) and halogen-substituted hydrocarbons $C_nH_{2n+1}X$ (n = 2-9) where X = I, Br and Cl.

Measurements of the thermal conductivity of these chemically pure liquids were also conducted at atmospheric pressure by the most carefully elaborated method of the heated filament [3]. Special attention was paid to eliminating possible effect of convection on the value of λ. For this purpose the experiments were conducted in a measuring tube of very small diameter (less than 1 mm). The results of λ measurements for different temperature drops in the layer of the test liquids from 4 to 10°C gave good convergence.

Lacking the opportunity to dwell in detail on the method of measurement, we note only that in the experiments possible errors were taken into account. Controlled measurements of λ for several compounds, the thermal conductivity of which have been studied by many authors, revealed that the deviations were within the limits of 1 percent. This is in agreement with the maximum error of our experiment under the most unfavorable conditions, equal to $\pm$1.5 percent.

Tables 1-7 present smoothed experimental data on the organic liquids we investigated.

The thermal conductivity coefficients of particular classes of compounds investigated have been studied by a number of authors. Table 8 presents comparisons of the results of our measurements of thermal conductivity coefficients of these compounds at a temperature of 30°C, λ_{30}, with the data of other authors, λ'_{30}. The λ'_{30} values taken for comparison from [10] were obtained as the result of averaging experimental data of not less than two authors. Deviation of our data, as seen in Table 5, does not exceed experimental error. Tables 1-7 show that the thermal conductivity coefficients decrease with temperature rise.

The nature of the change of the temperature coefficient of thermal conductivity α for normal and associated liquids has been established in [3-9].

A similar picture has been observed also for measurement data. The temperature coefficient α for a given homologous series depends only on the number of carbon atoms in the compound molecule. A decrease of α with rise in n has been observed for all normal compounds.

Identical values of α have been observed for the ketones R-CO-R' apart from any dependence on distribution in the hydrocarbon radicals R and R' for equal n.

Table 1. Thermal Conductivity of Unsaturated Olefinic Hydrocarbons

Compound	Chemical formula	Temperature range of measurement t, °C	Coefficients of Thermal conductivity, λ, w/m·deg
Hexene - I	C_6H_{12}	0 + 60	0.1260 + 0.1070
Heptene - I	C_7H_{14}	0 + 80	0.1290 + 0.1062
Octene - I	C_8H_{16}	0 +120	0.1316 + 0.0995
Decene - I	$C_{10}H_{20}$	0 +160	0.1363 + 0.0976
Dodecene - I	$C_{12}H_{24}$	0 +200	0.1402 + 0.0978
Tetradencene - I	$C_{14}H_{28}$	0 +200	0.1439 + 0.1063

Table 2. Thermal Conductivity of Ketones

Compound	Chemical formula	Temperature range of measurement t, °C	Coefficients of Thermal conductivity, λ, w/m·deg
Acetone	CH_3COCH_3	0 + 40	0.1678 + 0.1541
Methylethylketone	$CH_3COCH_2CH_3$	0 + 80	0.1536 + 0.1304
Methylbutylketone	$CH_3CO(CH_2)_3CH_3$	0 +120	0.1452 + 0.1164
Methylamylketone	$CH_3CO(CH_2)_4CH_3$	0 +140	0.1432 + 0.1100
Methylhexylketone	$CH_3CO(CH_2)_5CH_3$	0 + 160	0.1410 + 0.1044
Diethylketone	$C_2H_5COC_2H_5$	0 + 100	0.1488 + 0.1228
Ethylbutylketone	$C_2H_5CO(CH_2)_2C_2H_5$	0 + 140	0.1426 + 0.1096
Diamylketone	$C_5H_{11}COC_5H_{11}$	20 + 200	0.1390 + 0.1010
Dihexylketone	$C_6H_{13}COC_6H_{13}$	40 + 200	0.1396 + 0.1078
Methylpropylketone	$CH_3CO(CH_2)_2CH_3$	0 + 100	0.1486 + 0.1226

Table 3. Thermal Conductivity of Aldehydes

Compound	Chemical formula	Temperature range of measurements t, °C	Thermal conductivity coefficients, λ, w/m·deg
Acetaldehyde	CH_3CHO	0 + 20	0.1890 + 0.1804
Butyraldehyde	$CH_3(CH_2)_2CHO$	0 + 60	0.1551 + 0.1368
Valeraldehyde	$CH_3(CH_2)_3CHO$	0 + 100	0.1460 + 0.1201
Enantaldehyde	$CH_3(CH_2)_5CHO$	0 + 140	0.1448 + 0.1120
Decylaldehyde	$CH_3(CH_2)_8CHO$	0 + 200	0.1492 + 0.1092
Lauraldehyde	$CH_3(CH_2)_{10}CHO$	60 + 200	0.1454 + 0.1197

Table 4. Thermal Conductivity of Bromine-Substituted Saturated Hydrocarbons

Compound	Chemical formula	Temperature range of measurements t, °C	Thermal conductivity coefficients, λ, w/m·deg
Ethyl bromide	C_2H_5Br	0 + 30	0.1046 + 0.0986
Propyl bromide	C_3H_7Br	0 + 70	0.1062 + 0.0927
Butyl bromide	C_4H_9Br	0 + 100	0.1080 + 0.0900
Amyl bromide	$C_5H_{11}Br$	0 + 120	0.1096 + 0.0896
Hexyl bromide	$C_6H_{13}Br$	0 + 140	0.1114 + 0.0891
Nonyl bromide	$C_9H_{10}Br$	0 + 200	0.1161 + 0.0907

Table 5. Thermal Conductivity of Chlorine-Substituted Saturated Hydrocarbons

Compound	Chemical formula	Temperature range of measurements t, °C	Thermal conductivity coefficients, λ, w/m·deg
Ethyl chloride	C_2H_5Cl	0 + 10	0.1264 + 0.1242
Propyl chloride	C_3H_7Cl	0 + 40	0.1224 + 0.1128
Amyl chloride	$C_5H_{11}Cl$	0 + 100	0.1253 + 0.1048
Amyl iodied	$C_6H_{13}Cl$	0 + 120	0.1265 + 0.1041
Hexyl chloride	$C_7H_{15}Cl$	0 + 140	0.1277 + 0.1022
Nonyl chloride	$C_9H_{19}Cl$	0 + 200	0.1314 + 0.0980

Table 6. Thermal Conductivity of Iodine-Substituted Saturated Hydrocarbons

Compound	Chemical formula	Temperature range of measurements t, °C	Thermal conductivity coefficients, λ, w/m·deg
Ethyl iodide	C_2H_5I	0 + 60	0.0900 + 0.0792
Propyl chloride	C_3H_7I	0 + 100	0.0916 + 0.0744
Butyl iodide	C_4H_9I	0 + 120	0.0933 + 0.0736
Amyl iodide	$C_5H_{11}I$	0 + 140	0.0956 + 0.0740
Hexyl iodide	$C_6H_{13}I$	0 + 180	0.0978 + 0.0716
Heptyl iodide	$C_7H_{15}I$	0 + 200	0.1001 + 0.0723
Octyl iodide	$C_8H_{17}I$	0 + 200	0.1029 + 0.0762
Nonyl iodide	$C_9H_{19}I$	0 + 200	0.1056 + 0.0789

Table 7. Thermal Conductivity of Aromatic Hydrocarbons[1]

Compound	Chemical formula	Temperature range of measurements t, °C	Thermal conductivity coefficients λ, w/m·deg
1,2-dimethylbenzene	$C_4H_4(CH_3)_2$	0 + 140	0.1372 + 0.1057
1,3,5-trimethylbenzene	$C_6H_3(CH_3)_3$	0 + 160	0.1416 + 0.1032
1,2,4-trimethylbenzene	$C_6H_3(CH_3)_3$	0 + 160	0.1350 + 0.0996
Ethylbenzene	$C_6H_5C_2H_5$	0 + 120	0.1364 + 0.1092
n-propylbenzene	$C_6H_5C_3H_7$	0 + 140	0.1290 + 0.0982
Iso-propylbenzene ISO	$C_6H_5C_3H_7$	0 + 140	0.1268 + 0.0962
n-butylbenzene	$C_6H_5C_4H_9$	0 + 180	0.1322 + 0.0944
Sec-butylbenzene	$C_6H_5C_4H_9$	0 + 160	0.1296 + 0.0960
1,2-diethylbenzene	$C_6H_4(C_2H_5)_2$	0 + 180	0.1338 + 0.0942

Table 8

Compound	Thermal conductivity coefficient, λ''_{30} at t = 30°C	Reliability λ''_{30}, %	Our measurements of λ at t = 30°C, w/m·deg	$\frac{\lambda''_{30}-\lambda_{30}}{\lambda_{10}}$ %
Acetone	0.1570	0.3	0.1574	- 0.2
Ethylbenzene	0.1302	0.6	0.1295	0.5
Ethyl bromide	0.0995	0.4	0.0986	0.9

A similar picture has been noted earlier also for homologous series of complex, simple and mixed esters [7, 8]. Maintenance of the constancy of temperature coefficients α was observed also for identical values of n for different halogen-substituted hydrocarbons $C_nH_{2n+1}X$ (X = I, Br and Cl). Naturally, different functional groups also affect thermal conductivity.

The presence of a double bond (olefins) and also replacement of a hydrogen atom by the halogens I, Br and Cl leads to a decrease of thermal conductivity. In the latter case the effect is enhanced with rise in molecular weight of the halogens.

[1] See p. 564

A decrease of thermal conductivity was noted when primary and secondary alcohols are oxidized to aldehydes and ketones. This can be easily seen by comparing data given in Tables 1-7 with the results of measurements published earlier [3-5].

The experimental material obtained on thermal conductivity coefficients of organic liquids allows us to examine the possibility of using different equations in calculating λ.

We compared experimental data with λ values calculated by the equations of Weber [11], Smith [12], Palmer [13], Sakiadis and Coates [14] for liquids representing various calsses of compounds.

The mean error of calculations using the above-cited equations lies within the limits 10-20 percent and often rises to 50 percent. Similar deviations have been noted by Reid and Sherwood [1] and by Bretshnayder [2].

Table 9

Equation	Ethylbenzene				Normal-butyl alcohol			
	Temperature	Coefficient of thermal conductivity, w/m·deg		$\frac{\lambda_{calc}-\lambda_{exp}}{\lambda_{exp}}$, %	Temperature	Coefficient of thermal conductivity w/m·deg		$\frac{\lambda_{calc}-\lambda_{exp}}{\lambda_{exp}}$, %
		λ_{exp}	λ_{calc}			λ_{exp}	λ_{calc}	
Weber [11]	20	0.1320	0.1092	-17.2	40	0.1508	0.1515	0.5
	80	0.1183	0.1136	- 3.8	80	0.1448	0.1531	5.8
Smith [12]	20	0.1320	0.1309	- 0.9	40	0.1508	0.1816	20.4
	80	0.1183	0.1352	14.3	80	0.1448	0.1837	27.0
Palmer[13]	20	0.1320	0.1377	4.3	40	0.1508	0.1489	-1.3
	80	0.1163	0.1414	19.7	80	0.1448	0.1502	3.6
Sakiadis and Coates [14]	20	0.1320	0.1402	6.2	40	0.1408	0.1816	20.4
	80	0.1183	0.1539	30	80	0.1448	0.1782	23.3

In Table 9, by way of example a comparison is presented of our experimental data on ethylbenzene and normal-butyl alcohol [5] with data calculated from the equations in [11-14].

We note that all the equations considered in Table 9 require knowledge of precise values of heat capacity, density and viscosity. Determination of the latter, in turn, involves experimental difficulty and we do not have reliable data for most of the compounds of the classes investigated.

Therefore, on the one hand, the λ values from the equations in [11-14] are reliable to the same extent as are the values of heat capacity, density and viscosity. On the other hand, larger deviations are evidently due to the fact that these methods were not derived by a reliable theoretical approach and, as was noted in [15], in the case of liquids it is impossible to establish the scope of their application.

A method based on similarity considerations was used in [16, 17] to determine the temperature dependence of thermal conductivity coefficients. Its application does not require introduction of any corrections both in the case of normal and associated liquids, as well as their mixtures [17]. It is pointed out in [16, 17] that generalization of experimental data by this method in the coordinates λ/λ_s, and S/S_1 have made it possible to obtain relative thermal conductivity as unique functions of the criterion S/S_1.

For normal liquids and their mixtures this ratio is of the form

$$\lambda = \lambda_{s_1}\left[1{,}75 - 0{,}75\frac{S}{S_1}\right], \qquad (1)$$

for associated liquids and their mixtures

$$\lambda = \lambda_{s_1}\left[1{,}875 - 0{,}375\frac{S}{S_1}\right]. \qquad (2)$$

In Table 10, by way of example, comparisons are given of experimental and calculated data from equations (1) and (2) for individual representatives of the classes of compounds we examined.

Table 10

Liquids	Chemical formula	Temperature t, °C	Thermal conductivity coefficients λ_{exp}	λ_{calc}	$\frac{\lambda_{calc}-\lambda_{exp}}{\lambda_{exp}}$ %
Normal-decane	$_nC_{10}H_{22}$	40	0.1305	0.1300	-0.4
		80	0.1209	0.1209	-
		160	0.1020	0.1028	0.8
Normal-tetracosane	$_nC_{24}H_{50}$	80	0.1506	0.1506	-
		160	0.1373	0.1372	-0.1
		200	0.1306	0.1300	-0.5
Tetradecene-1	$C_{14}H_{28}$	40	0.1363	0.1362	-0.2
		120	0.1214	0.1206	-0.7
		200	0.1063	0.1055	-0.7
Ethyl ester of acetic acid	$CH_3COOC_2H_5$	0	0.1520	0.1518	-0.1
		40	0.1402	0.1408	0.4
		60	0.1346	0.1356	0.7
Normal-octadecyl alcohol	$_nC_{18}H_{37}OH$	80	0.1725	0.1728	0.1
		120	0.1649	0.1662	0.8
		200	0.1497	0.1517	1.4
Acetone	CH_3COCH_3	0	0.1678	0.1678	-
		20	0.1609	0.1620	-0.7
		40	0.1541	0.1556	-0.9
Benzene	C_6H_6	0	0.1505	0.1504	-
		40	0.1404	0.1401	-0.2
		80	0.1302	0.1298	-0.3
Normal-butyric acid	C_3H_7COOH	0	0.1454	0.1450	0.2
		80	0.1356	0.1355	-
		160	0.1260	0.1270	-0.8
Diethyl ester	$C_2H_5OC_2H_5$	0	0.1426	0.1426	-
		20	0.1358	0.1364	-0.4
Acetaldehyde	CH_3CHO	0	0.1890	0.1899	-0.5
		20	0.1804	0.1804	-

It is clear from Table 10 that deviations of experimental data from data calculated using equations (1) and (2) do not exceed the possible experimental error. These equations can be recommended for determination of thermal conductivity of various classes of organic liquids throughout the range of the liquid state at normal pressure. This requires that we have data on λ even though for just one temperature.

We have also applied the method of corresponding states [8, 17]. The relationship we proposed

$$\lambda = A + B(1+\tau) \qquad (3)$$

for calculation of thermal conductivity of all homologous series considered gives good agreement with experiment.

However, we did not use this method in calculating the λ of low representatives of the series in [17]. Therefore, use of equation (3) requires introduction of corrections that allow for the effect of the number of carbon atoms n for low representatives of a series. Additionally, equation (3) also requires knowledge of empirical coefficients that take account of various functional groups and bonds, and for associated liquids -- the effect of the degree of association.

This fact restricts the scope of application of (3) in determining λ and places obstacles in the path of its use in finding the thermal conductivity coefficients of mixtures.

Footnotes

1. To p. 559 Data on benzene, toluene, 1,4-dimethylbenzene are given in [9].

References

1. Reid, R. and T. Sherwood, *Svoystva Gazov i Zhidkostey*, [Properties of Gases and Liquids], Gostekhizdat Press, Moscow, 1964.

2. Bretschneider, S., *Svoystva Gazov i Zhidkostey*, [Properties of Gases and Liquids], Khimiya Press, Moscow, 1966.

3. Mukhamedzyanov, G. Kh., A. G. Usmanov and A. A. Tarzimanov, *Izv. Vuzov. Neft' i Gaz*, No. 9, 1963.

4. Mukhamedzyanov, G. Kh. and A. G. Usmanov, *Izv. Vuzov. Neft' i Gaz*, No. 5, 1967.

5. Mukhamedzyanov, G. Kh., A. G. Usmanov, and A. A. Tarzimanov, *Izv. Vuzov. Neft' i Gaz*, No. 1, 1964.

6. Mukhamedzyanov, G. Kh. and A. G. Usmanov, *Izv. Vuzov. Neft' i Gaz*, No. 1, 1967.

7. Mukhamedzyanov, G. Kh. and A. G. Usmanov, *IFZh*, Vol. 13, No. 2, 1967.

8. Mukhamedzyanov, G. Kh. and A. G. Usmanov, *Sb. Dokladov II Mezhvuzovskoy Konferentsii po Fizike Zhidkogo Sostoyaniya*, [Collection of Papers Presented at the Second Inter-institutional Conference on the Physics of the Liquid State], Samarkand, 1966.

9. Mukhamedzyanov, G. Kh., A. G. Usmanov and A. A. Tarzimanov, *Trudy KKhTI*, No. 32, 1964; *Izv. Vuzov. Neft' i Gaz*, No. 10, 1964.

10. Filippov, L. P., *Vestnik MGU, Seriya 3*, No. 3, 1960.

11. Weber, H. F. and S. Wiedemann, *Ann. Phys. Chem.*, Vol. 68, p 719, 1936.

12. Smith, J. E., *Trans. ASME*, Vol. 56, p. 307, 1934; Vol. 58, p. 719, 1936.

13. Palmer, G., *Ind. Eng. Chem.*, Vol. 40, p. 89, 1948.

14. Sakiadis, B. C. and J. Coates, *AIChE J.*, Vol. 1, p. 275, 1955.

15. Euchen, A., *Forsch. Geb. Ingenieurwesens*, Vol. 113, p. 6, 1940.

16. Usmanov, A. G. and G. Kh. Mukhamedzyanov, *Izv. Vuzov. Khimiya i Khimicheskaya Tekhnologiya*, Vol. 6, 1963.

17. Mukhamedzyanov, G. Kh. and A. G. Usmanov, *Izv. Vuzov. Neft' i Gaz*, No. 4, 1965.

EXPERIMENTAL STUDY OF THE SORFT EFFECT

A. M. Narbekov and A. G. Usmanov

Experimental data on thermal diffusion in the liquid phase are fully described by the Soret coefficient

$$S = -\frac{1}{m}\left(\frac{dm}{dT}\right)_{const} = -\frac{1}{C_1 C_2}\left(\frac{dC_2}{dT}\right)_{const} \qquad (1)$$

which is a measure of the separation effect. Knowing S and the diffusion coefficient D_{12}, we can calculate other thermodiffusion characteristics (α, k_T and D_T) which are necessary in solving several problems of the practical use of the thermodiffusion method in industry.

Experimental study of the Soret effect has given specific material to verify the theories of thermal diffusion in liquids. The expression for the thermodiffusion factor α includes the so-called heat of transfer Q^*_1; however, the overall function for Q^*_1 is lacking, therefore interpretation of Q^*_1 is usually made from the results of measurement of the Soret effect.

For these reasons, obtaining reliable experimental data on thermal diffusion in liquid mixtures has remained as before an urgent problem.

Experimental investigation of the thermal diffusion process in liquids is carried out in cells of two types. The first type of cell [1] consists of two reservoirs divided by a porous partition; one reservoir is heated, the other is cooled, and a temperature gradient is induced in the partition and through it occurs molecular diffusion. In order to sustain the same temperature and concentration in each reservoir, the liquid in the reservoirs is stirred by magnetic mixers. The cell described has the disadvantage that it is difficult to maintain uniform temperature and concentration in the reservoirs and to precisely determine the temperature difference.

The second type of cell [2-4] consisted of two horizontal plates, between which the liquid mixture being separated resides. The horizontal liquid layer thus obtained is subjected to the action of a vertical temperature gradient. The ultimate concentration gradient is determined optically [2, 3, 5-7], conductometrically [4, 8, 9], or by sampling at different levels [10].

Usually, in cells of this type the upper plate is heated and the lower cooled; in this case a thermal conductivity regime always exists in the liquid layer regardless of the value of the temperature difference applied. Cells of the second type are inapplicable for this direction (from bottom to top) of temperature gradient, if the heavier component of the binary mixture accumulates at the heated wall, since reverse mixing of the liquid takes place. We know that when the vertical temperature gradient runs in the opposite direction, a thermal conductivity regime also exists in the liquid layer under specific conditions. For experiments on thermal diffusion a reliable thermal conductivity regime in the horizontal layer of liquid is determined by the following value of the dimensionless product

$$Gr \cdot Pr < 1500.$$

The permissible temperature difference is determined from the equation

$$\Delta T = \frac{Gr \cdot Pr}{gh^3(\rho\beta/\mu a)} \qquad (2)$$

Calculation shows that temperature difference that can be used in this case is slight (for example, for aqueous solutions if the cell height is 0.5 cm, the temperature difference is about 1°C); the separation effect is very slight, that is, use of methods of study sensitive enough for the small changes in concentration of the mixture investigated is necessary.

Thus, in cells with a vertical temperature gradient any temperature gradient direction can be used depending on the nature of the separation. Further, there must be the possibility to establish concentration changes in the course of thermal diffusion with requisite precision.

This requirement can be satisfied when optical methods of investigation are used. In research on the Soret effect, usually two optical methods are employed: the interference method and the method of image shifting. We selected the interference method as providing the possibility of a relatively simple quantitative calculation of the sought-for characteristics of the process under study. The IAB-451 shadow instrument was used as the interferometer, and the LG-75 optical quantum generator served as the light source. Conversion of the IAB-451 into a two-beam diffraction interferometer is described in [11]: transparent diffraction grids R_1 and R_2 were placed in the focal planes of the objectives L_1 and L_2 (Figure 1, a) instead of a slit and a knife, and in the plane of the object was placed the diaphragm D with two windows used to form the two-beam interference field. A beam of light from the optical quantum generator was focused onto the plane of the diffraction grid R_1 with the aid of the short-focal lens L_3.

The cell for investigating thermal diffusion was designed (Figure 1, b) to consist of two plates (1) arranged horizontally and kept at different temperatures, the inserts (2), the partition (3), and two flat-parallel plates (4). These parts formed two cells. The test solution was poured into one of the cells, and the solvent into the other. The vessel was placed in front of the diagram in such a way that the solution-containing cell stood in front of one of its windows, and the solvent-containing cell in front of the other. Both of the solutions in which thermal diffusion took place as well as the solvent were subjected to the same temperature gradient, therefore the interference picture that resulted was a summation of two effects: variation of the index of refraction owing to the concentration gradient established upon thermal diffusion, and that arising from the different temperature dependence of the indices of refraction of the solution and of the solvent. The influence of the second effect is not hard to take into account in interpretation of the interference patterns.

The interference patterns were obtained both when the interference field was adjusted for bands of infinite width (uniformly illuminated fields) as well as for adjustment for bands of finite width. When the bands were adjusted for infinite width variation of the index of refraction associated

with change in concentration of the test solution caused interference bands to appear in the pattern (Figure 2, b) from the arrangement of which the concentration distribution in the cell could be calculated. When the interference patterns were adjusted for finite-width bands (Figure 2, a) the concentration changes could be calculated from the band shifts.

The interference pattern was recorded on moving motion picture film K. The interval between photographs was 30 sec and was provided by the rotating disk B.

The vessel we used was of the following dimensions: height 0.494 cm and light path traveled 3.5 cm. The lower and upper plates of the vessel were kept at different temperatures with the aid of water supplied from thermostats. Constancy of vessel wall temperature was controlled by copper-constantan thermocouples, the signals from which were recorded by the R-307 potentiometer.

Test liquids were aqueous solutions. The solutions were prepared by weighing on analytical balances; the index of refraction was determined on the IRF-23 refractometer.

The process of separation was carried out until the steady-state was achieved. The variation of concentration was measured from the beginning of the experiment according to the equation

$$\Delta C = \frac{K_y \cdot \lambda}{\ell \cdot dn/dc} \qquad (3)$$

Variation of the number of bands (or their displacement) was determined by measurement on the MIR-12 comparator.

We must note the following: our method profitably differs from the early used method in that the interference pattern obtained more fully reproduces the separatory process. The interference pattern (Figure 2, a) shows, for example, that the distribution of concentration by height in separation is uneven: different concentration change occurs at approximately the central line of the cell.

The temperature difference applied on the layer of test liquid is measured optically. For this purpose, the diaphragm is placed in such a way that one of its windows proves to be in front of the cell, and the other remains free, and the beam of light passing through it forms a comparison branch. The interference pattern obtained here consists of a series of horizontal bands characterizing the temperature field. The temperature difference is determined from an equation analogous to (3):

$$\Delta T = \frac{k_e \cdot \lambda}{\ell \cdot dn/dT} \qquad (4)$$

The Soret coefficient is obtained from equation (1). The values of S for single-molar solutions of KCl and KBr (Table 1) agree well with the data in [2]: for KCl, $S = 0.94 \cdot 10^{-3}$ 1/deg, and for KBr, $K = 1.33 \cdot 10^{-3}$ 1/deg ($\Delta T = 14°C$).

Table 1. Experimental and Calculated Data on Determination of the Soret Coefficient for Aqueous Solutions of KCl and KBr

System	Concentration of second component, m	Temperature °K			$\frac{dn}{dm} \cdot 10^2$	$\Delta m \cdot 10^2$	$S \cdot 10^3$ 1/deg
		Cold wall T_1	Temperature difference ΔT	Mean Temperature T_{av}			
Water-KCl	1	290.5	15	298	1,008	1.53	-1.02
Water-KBr	1	290.5	15	298	1.47	2.12	-1.41

These measurements were control values to verify the method used. Later the Soret coefficients were determined for four aqueous solutions (Table 2), for two of which (water-glucose and water-propyl alcohol) literature data are lacking.

Thus, by using the IAB-451 shadow instrument employed as a two-beam diffraction interferometer, the Soret coefficients were obtained for six aqueous solutions of different compounds. The interference pattern of the separation process was quite easily interpreted: necessary information on kinetics of the separation process can be obtained from the nature of variation of the interference pattern with time.

Table 2. Experimental and Calculated Data on the Determination of the Soret Coefficient for Aqueous Solutions of Sugars and Alcohols

System	Concentration of second component, c %	Temperature °K			$\frac{dn}{dc} \cdot 10^3$	$\Delta C \cdot 10^2$	$S \cdot 10^3$ 1/deg
		Cold wall T_1	Difference ΔT	Mean Temperature T_{av}			
Water-saccharose	5	289	8	293	1.48	3.5	-0.92
Water-glucose	5	294	8	298	1.465	2.4	-0.63
Water-ethyl alcohol	10	288	10	293	0.71	33.75	-3.72
Water-propyl alcohol	10	288	10	293	0.925	14.04	-1.56

Symbols

S = Soret coefficient; m = molar concentration; T = temperature; c = weight concentration; α = thermodiffusion factor; k_T = thermodiffusion ratio; D_T = thermodiffusion coefficient; D_{12} = coefficient of concentration diffusion; Q_1^* = heat of transfer; Gr = Grashof criterion; Pr = Prandtl criterion; g = 9.8 m/sec^2; h = height of cell; ℓ = extent of cell along light path traveled; ρ = density; β = coefficient of volumetric expansion; μ = coefficient of viscosity; a = coefficient of thermal diffusivity; k = number of interference bands; λ = wavelength ($6328 \cdot 10^{-10}$ m);

n = index of refraction; the index "st" indicates that the expression in the parentheses was taken in the steady state.

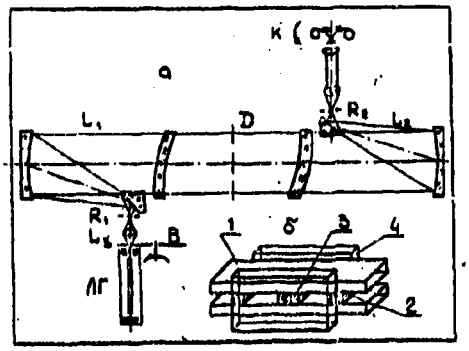

Figure 1. Diagram of apparatus: a, Optical layout; b, Vessel

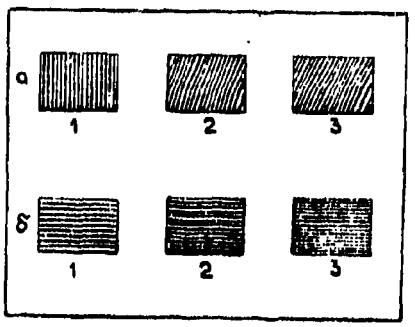

Figure 2. Interference patterns of the thermal diffusion process of an aqueous solution of normal propyl alcohol: a, Adjustment to bands of finite width (1, prior to applying temperature difference; 2, 60 min after applying temperature difference; 3, after completing the separatory process); b, Adjustment for bands of infinite width (1, 2, at different time intervals from the beginning of the separatory process; 3, after completing the separatory process)

References

1. Saxton, R. L., E. L. Dougherty, and H. G. Drickamer, *J. Chem. Phys.*, Vol. 22, p. 1166, 1954.
2. Tanner, C. C., *Trans. Faraday Soc.*, Vol. 23, p. 75, 1927.
3. Longsworth, L. G., *J. Phys. Chem.*, Vol. 61, p. 1557, 1957.
4. Agar, J. N. and J. C. R. Turner, *Proc. Roy. Soc.*, No. A 255, 1960.
5. Gustafsson, S. E., J. G. Bessey and J. A. Bierlein, *J. Phys. Chem.*, Vol. 69, p. 1016, 1965.
6. Whitaker, S. and R. L. Pigford, *Ind. Eng. Chem.*, Vol. 50, 1958.
7. Thomaes, G., *Phys.*, Vol. 17, p. 885, 1951.
8. Chipman, J., *J. Amer. Chem. Soc.*, Vol. 48, p. 2577, 1926.
9. Ikeda, T., *J. Chem. Phys.*, Vol. 30, p. 345, 1959.
10. Bobrova, G. I. and G. D. Rabinovich, *Voprosy Nestatsionarnogo Perenosa Tepla i Massy*, [Problems of Non-steady-state Heat and Mass Transfer], Nauka i Tekhnika Press, 1965.
11. Beketova, A. K., O. A. Klochkova, and N. V. Ryabova, *Optiko-mekhanicheskaya Promyshlennost'*, No. 3, p. 11, 1962.

EFFECT OF THERMOPHYSICAL PROPERTIES ON MASS WEAR PARAMETERS OF GLASSLIKE MATERIALS

Yu. V. Polezhayev and Yu. V. Khramov

Glasslike materials (glass-plastics) are characterized by the fact that exposed to a high-temperature gas flow they disintegrate with the formation of a melt film, the viscosity of which decreases exponentially with rising temperature T:

$$\mu = \exp\left(\frac{\alpha}{T} + \beta\right) \qquad (1)$$

This leads to the fusion parameters as a function of the temperature distribution within the body and, consequently, to the fusion parameters as a function of the thermophysical properties of the condensed phase.

It must be noted that direct measurement of viscosity, thermal conductivity, heat capacity and even the density of the melt at temperatures above 2500°K is practically impossible for a long series of reasons, and in calculations several extrapolated values as a rule are employed. Though compared to viscosity variation of the remaining properties with temperatures not as great (such that they need not be taken into account in the first approximation), the results of calculation depend materially on assumptions made relative to their averaged values.

To determine this effect a large series of parametric calculations were made in which the function of the mass fusion rate G and the surface temperature were studied with thermophysical properties varied relative to certain standard (marked by the index $()_0$ values). Further, density and heat capacity varied by more than twofold, thermal conductivity by more than fivefold, but the exponent in the viscosity law (1) -- by 1.5-2 times.

Calculation of fusion parameters was made following the method in [1] applied to the vicinity of the critical point of a blunt body placed in an axially symmetrical air current with the following retarting parameters: temperature T_e = 6000°K, pressure p_e from 0.001 to 10 bar. This choice of gas flow parameters was based on the fact that the value of the retarding pressure has a substantial effect on the ratio of the quantity of material entrained in liquid and gaseous form, that is, intensifies or weakens the relationship between fusion processes and heat transfer in the solid phase. The variation of the retardingtemperature by 2000°K to either side did not lead to very appreciable rearrangements in the nature of the disintegration and therefore variation of this parameter is not of interest.

Results of calculating the nonsteady-state fusion of glasslike material showed that of all the physical parameters entering into the differential equation and the boundary conditions, the course of the nonsteady-state curve $\overline{G}(\tau)$, where τ = time, is affected only by the thermal conductivity coefficient and, somewhat more weakly, by the density. All the remaining thermophysical properties mainly determine the value of quasi-steady-state, settled velocities and temperatures of disintegration. Taking account of heat capacity C as a function of temperature did not lead to differences either in the instantaneous, or in the quasi-steady-state values of the fusion rate compared to calculation for a constant, mean-integral value over the entire temperature drop in the body. The latter fact somewhat simplifies engineering methods of calculation.

The mass fusion rate and the surface temperature T_w depend very weakly on the density. However, it is natural that this parameter has a more decisive effect on calculation of linear dimensions of the entrained layer.

Thus, two parameters remain: thermal conductivity and viscosity, knowledge of which with adequate precision represents one of the indispensable factors of calculation reliability.

Figure 1 shows how a difference in the value of the thermal conductivity λ from the standard value λ_o can affect the relative fusion rate $\overline{G}/\overline{G}_o$, where $\overline{G}_o$ corresponds to calculations with $\lambda = \lambda_o$. The different curves correspond to variation of pressure of the retarding flow Pe from 0.001 to 10 bar.

Figures 2 and 3 present similar functions for the characteristics of the effect that the parameter β in the viscosity law (1) has on the relative values of the fusion rate $\bar{G}/\bar{G}_o$ (Figure 2) and the temperature of the disintegrating surface T_w/T_o (Figure 3).

It is interesting to note that not one of the thermophysical coefficients, with the exception of viscosity, has an influence greater than ±3 percent on the surface temperature T_w, and therefore this fact can be used in estimating thermophysical properties of glass-plastics at very high temperatures (on the order of 3000°K). Actually, if in comparing the fusion parameters of a certain glass-plastic with a reference material (for example, quartz glass) it turns out that the surface temperatures are close, and the wear rates differ, the difference must be sought for in the nature of the variation of thermal conductivity or in the value of the heat capacity. And, in contrast, if the disintegration surface temperatures differ sharply for the glasslike materials, then the reason for this lies above all in the difference of the viscosity laws of the melts and cannot be explained by other factors.

If in examination nonsteady-state characteristics of fusion are additionally brought into consideration, by comparing parametric calculations with experimental data we can unambiguously determine at least two out of three thermophysical parameters: viscosity and thermal conductivity.

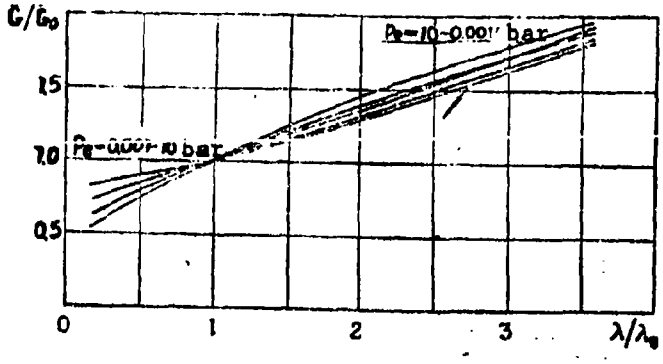

Figure 1. Relative fusion rate $\overline{G}/\overline{G}_o$ as a function of λ/λ_o at different pressures

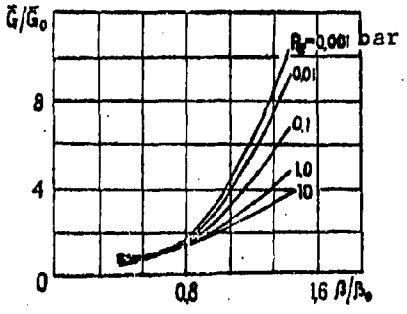

Figure 2. Relative fusion rate $\overline{G}/\overline{G}_o$ as a function of β/β_o at different pressures

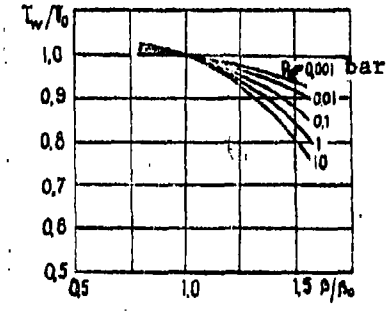

Figure 3. Disintegration surface temperature T_w/T_o as a function of β/β_o at different pressures

References

1. Gorskiy, V. V. and Yu. V. Polezhayev, *TVT*, Vol. 4, No. 2, 1966.

THERMOPHYSICAL PROPERTIES OF MULTICOMPONENT DISPERSE SYSTEMS CONTAINING DIAMOND GRAINS

A. N. Reznikov, V. K. Lyakhov and Yu. I. Ivanov

In solving problems relating to diamond treating processes, we must know the thermophysical properties of diamond wheels and bars. The diamond-bearing layer of a wheel or a diamond bar consists of disperse mixtures made up of several components: binder, filler, diamond grains and air (pores). The relative volume of diamond grains and filler amounts to 50 percent in the diamond-bearing layer of wheels.

This study investigates binders on a bakelite base containing as fillers -- boron carbide and iron powder -- and wheels with bakelite binder containing diamond grains. Since various wheel grades differ in concentration of components, their thermophysical properties vary appreciably.

Determination of thermophysical characteristics of disperse mixtures is of general interest, but it involves a number of difficulties.

Investigations have shown that the bulk weight and specific heat capacity of mixtures can be calculated with adequate precision based on the law of conservation of mass and the additivity rule:

$$\gamma_{cm} = \sum_{i}^{n} \gamma_i P_i \qquad c_m = \frac{\sum_{i}^{n} c_i \gamma_i P_i}{\gamma_{cm}}$$

These formulas are valid if in the mixing process no new chemical compound is formed.

Several theoretical formulas based on different principles are available in calculating the coefficient of thermal conductivity of the mixture at the present time. Calculations based on these formulas give results that differ

appreciably. Therefore, in parallel with the calculation we conducted experimental studies of the thermal conductivity coefficients of mixtures. Here a nonsteady-state method of the a-calorimeter and the steady-state flat layer method were used. Both binary and ternary mixtures were investigated. For binary mixtures bakelite-iron powder and bakelite-boron carbide, five specimens were prepared with filler concentration in the range 0-50 percent.

Graphs (Figure 1, a, b) were plotted from experimental results, and the graphs simultaneously presented calculation results based on the V. I. Odelevskiy formula [1] for a statistical mixture and a matrical system and results from calculations using the K. Likhteneker formula [3].

Results show that within the limits of the concentrations examined the formulas of other authors [2-3], etc.) for a matrical system give approximately identical results, which within the limits of additive concentration of 30-50 percent give values lower than the experimental data. The best agreement with experiments is given by the K. Likhteneker formula

$$\lambda_э = \lambda_1^{p_1} \lambda_2^{p_2} \dots \lambda_n^{p_n} . \qquad (1)$$

Experiments with the ternary mixture bakelite-boron carbide-iron were also conducted with specimens of different concentrations. Experimental results are shown in a graph (Figure 1, c). The iron powder concentration in the specimens was varied in such a way that the overall content of iron powder and boron carbide grains remained constant at 50 percent. This variation in concentrations was characteristic for compositions of various binders of diamond wheels. In the graph (cf. Figure 1, c) experimental data were compared with the results of calculation according to the K. Likhteneker formula (1).

Calculations based on formulas for the matrical system and a statistical mixture give results that differ appreciably from experimental data.

Experiments with the ternary system bakelite-boron carbide-diamond powder were conducted with specimens (diamond wheels) of two concentrations. The results of these experiments and their comparison with calculation based on the K. Likhteneker formula are shown in the table.

Table

No.	Wheel Characteristics	Composition in % of volume			$mw \cdot cm^{-1} \cdot deg^{-1}$	
		Bakelite	Boron carbide	Diamond	Experimental	Calculated
1	AS40-BI-50	50	37.5	12.5	15.6	17.3
2	AS12-BI-50	50	37.5	12.5	17.1	17.3
3	AS4-BI-50	50	37.5	12.5	19.8	17.3
4	AS12-BI-100	50	25.0	25.0	19.5	22.1

Specimens 1, 2 and 3 differed by diamond and boron carbide grain sizes. This was accounted for, in particular, by deviation in experimental data of the first three specimens in which the percentage composition of the components was identical. Specimens 2 and 4 differed in diamond and boron carbide content. Since the percentage content of diamond in the fourth specimen is greater than in the second, and the thermal conductivity coefficient of diamond is greater than the thermal conductivity coefficient of boron carbide, with rise in diamond concentration and with retention of the overall diamond and boron carbide concentration, the equivalent thermal conductivity coefficient rises.

Calculation of the equivalent thermal conductivity coefficient for these tables was made with a five percent air pore content taken into account (the table lists the percentage content of components without including porosity).

Conclusions

1. It follows from our studies that calculations according to the K. Likhteneker formula (1) give satisfactory agreement with experimental data.

2. Calculations based on the formulas of other authors, both for a statistical mixture, as well as for a matrical system, give results that differ considerably from experimental data.

Only in the low-concentration region (Figure 1) is the deviation between experimental data and calculations based on the formulas of various authors small.

Symbols

γ_{mix}; c_{mix}; $\lambda_{\ni}$ = bulk weight, specific heat and equivalent thermal conductivity coefficient of the mixture; γ_1, c_1 and λ_1 = as above, for individual components; p_1 and p_2 = bulk concentrations of components.

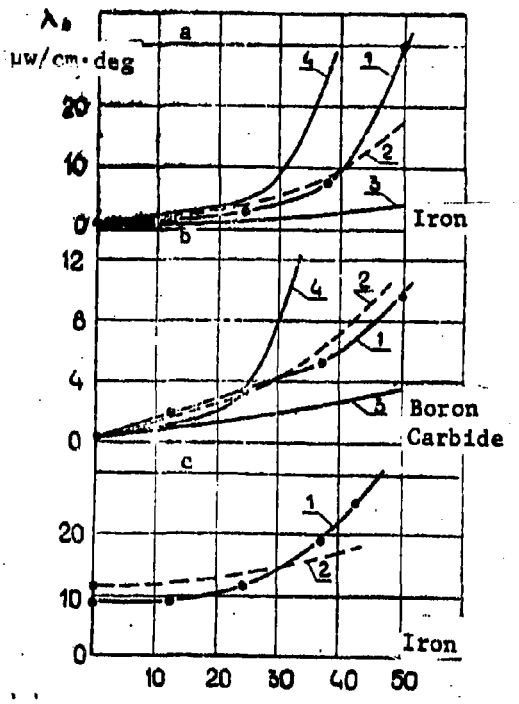

Figure 1. Results of comparison of experimental and calculated data: 1, Experimental results; 2, Calculation based on the K. Likhteneker formula (1); 3, Calculation based on the V. I. Odelevskiy formula [1] for a statistical mixture; 4, Calculation based on the V. I. Odelevskiy formula [1] for a matrical system; a) Bakelite-iron powder mixture; b) Bakelite-boron carbide mixture; c) Bakelite-iron powder-boron carbide mixture

References

1. Odelevskiy, V. I., *ZhTF*, Vol. 31, No. 6, 1954.

2. Bershteyn, R. S., *Koloturbostroyeniye*, No. 1, 1948.

3. Chudnobskiy, A. F., *Teploobmen v Dispersnykh Sredakh*, [Heat Transfer in Disperse Media], Gostoptekhnizdat Press, Moscow, 1954.

STATISTICAL DETERMINATION OF THE DIFFUSION COEFFICIENT

L. A. Rott, V. B. Nemtsov and V. S. Vikhrenko

The possibility of expressing kinetic coefficients of a condensed system by autocorrelation functions is of unquestioned and stimulating interest in the statistical theory of nonequilibrium processes.

This approach was used in calculating diffusion coefficients, which is the main problem area of the present study. But first of all we will consider how we can express viscous properties of the medium in the language of autocorrelation functions (using the well known Kubo method [1]). It is precisely an expression for the coefficient of shear viscosity that is essential for a definitive calculation of the diffusion coefficient.

First we will examine the general case of an anisotropic homogeneous medium. Let a weak mechanical perturbation be applied on the isolated system in which its Hamiltonian H is varied by $\Delta H = -AF(t)$. Then the mean value $\Delta B(t)$ of the variation in the dynamic variable B(t) is determined according to [1] with the aid of the expression

$$\Delta B(t) = -\Theta^{-1}\int_{-\infty}^{t} \langle A(0)\dot{B}(t-s)\rangle F(t-s)\,ds. \qquad (1)$$

where $\Theta = kT$, $\dot{B} = dB/dt$, and the brackets denote the averaging over the equilibrium canonical assemblage.

To explore viscous properties of the system we will examine its behavior when a weak deformation is applied

$$\tilde{X}_n = X_n + \frac{\partial U_n}{\partial q^m} X_m \qquad (2)$$

References

1. Odelevskiy, V. I., *ZhTF*, Vol. 31, No. 6, 1954.

2. Bershteyn, R. S., *Koloturbostroyeniye*, No. 1, 1948.

3. Chudnobskiy, A. F., *Teploobmen v Dispersnykh Sredakh*, [Heat Transfer in Disperse Media], Gostoptekhizdat Press, Moscow, 1954.

STATISTICAL DETERMINATION OF THE DIFFUSION COEFFICIENT

L. A. Rott, V. B. Nemtsov and V. S. Vikhrenko

The possibility of expressing kinetic coefficients of a condensed system by autocorrelation functions is of unquestioned and stimulating interest in the statistical theory of nonequilibrium processes.

This approach was used in calculating diffusion coefficients, which is the main problem area of the present study. But first of all we will consider how we can express viscous properties of the medium in the language of autocorrelation functions (using the well known Kubo method [1]). It is precisely an expression for the coefficient of shear viscosity that is essential for a definitive calculation of the diffusion coefficient.

First we will examine the general case of an anisotropic homogeneous medium. Let a weak mechanical perturbation be applied on the isolated system in which its Hamiltonian H is varied by $\Delta H = -AF(t)$. Then the mean value $\Delta B(t)$ of the variation in the dynamic variable B(t) is determined according to [1] with the aid of the expression

$$\Delta B(t) = -\Theta^{-1}\int_{-\infty}^{t} \langle A(0)\dot{B}(t-s)\rangle F(t-s)\,ds. \qquad (1)$$

where $\Theta = kT$, $\dot{B} = dB/dt$, and the brackets denote the averaging over the equilibrium canonical assemblage.

To explore viscous properties of the system we will examine its behavior when a weak deformation is applied

$$\tilde{X}_n = X_n + \frac{\partial U_0}{\partial q^k} X_m \qquad (2)$$

Here X_n is the component of radius-vector $\vec{r}$ connecting two particles prior to the deformation, and $\tilde{x}_n$ is after the deformation; u_n is the component vector of particle displacement. The particle momenta here are transformed according to the law of canonical transformations in the Lagrange formalism:

$$p_n = \tilde{p}_m \frac{\partial \tilde{x}_m}{\partial x_n} \tag{3}$$

We note that the general approach developed here differs from the particular case based on the use of the Feinman ideas [1, 2].

With a precision that includes neglecting the squared values and the higher powers of deformation, we can write

$$\tilde{p}_i = p_i - \frac{\partial u_i}{\partial q^k} p_k \tag{4}$$

For a system of N particles with pairwise interaction described by the intermolecular potential $\phi(r)$, the Hamiltonian becomes

$$H_N = \sum_{i=1}^{N} \frac{(p_i^\alpha)^2}{2m} + \frac{1}{2} \sum_{i,\mu} \Phi(r^{\mu\nu}) \tag{5}$$

Then $\Delta H = \tilde{H}_N - H_N$ is determined by the following equality with the above-indicated degree of precision

$$\Delta H = \hat{\Pi}_{mn} \frac{\partial u_n}{\partial q^m} , \tag{6}$$

where

$$\hat{\Pi}_{mn} = -\sum_{i=1}^{N} \frac{p_n^\alpha p_m^\alpha}{m} + \frac{1}{2} \sum_{i,\mu} \frac{\Phi'(r) x_m^{\mu\nu} x_n^{\mu\nu}}{r}$$

Taking into account the symmetry of the tensor $\hat{\Pi}_{mn}$, we will represent the expression for ΔH as

$$\Delta H = \hat{\Pi}_{mn} u_{mn} , \tag{7}$$

where

$$u_{mn} = \frac{1}{2}\left(\frac{\partial u_n}{\partial q^m} + \frac{\partial u_m}{\partial q^n}\right)$$

deformation tensor.

Thus,

$$A = -\hat{\Pi}_{mn} \quad , \quad F = u_{mn}$$

Selecting

$$B = \int^{t} \hat{\Pi}_{ik}(s)\,ds . \tag{8}$$

we obtain based on the relationship (1)

$$\Delta B = \Theta^{-1} \int_{0}^{\infty} \langle \hat{\Pi}_{mn}(0)\, \hat{\Pi}_{ik}(s) \rangle\, u_{mn}(t-s)\,ds \tag{9}$$

Let the deformation be cyclic

$$u_{mn} = u_{mn}(0) e^{i\omega t} \tag{10}$$

Then

$$\Delta B = u_{mn}\left[\Theta^{-1} \int_{0}^{\infty} e^{-i\omega t} \langle \hat{\Pi}_{mn}(0)\, \hat{\Pi}_{ik}(t) \rangle\, dt\right] \tag{11}$$

We will compare this equality with the well known phenomenological relationship

$$\int_{-\infty}^{t} \sigma_{ik}\,ds = \eta_{ikmn}\, u_{mn} \qquad (\sigma_{ik} = \eta_{ikmn}\, \dot{u}_{mn}), \tag{12}$$

we obtain an expression for the tensor of viscosity coefficients

$$\eta_{iklmn} = \Theta^{-1}\int_0^\infty e^{-i\omega t}\langle \hat{\Pi}_{mn}(0)\,\hat{\Pi}_{ik}(t)\rangle dt \qquad (13)$$

It is essential to note that the flow $\hat{\Pi}_{mn}$ is determined with a precision up to any value, the divergence of which equals zero. To eliminate this indeterminacy, we can according to [3] rewrite the expression (13) in the following form (the canonical assemblage is used for the averaging):

$$\eta_{iklmn} = \Theta^{-1}\int_0^\infty e^{-i\omega t}\langle \left(\hat{\Pi}_{mn}(0) - \bar{\Pi}(0)\right)\left(\hat{\Pi}_{ik}(t) - \bar{\Pi}_{ik}(t)\right)\rangle dt, \qquad (14)$$

where

$$\bar{\Pi}_{ik} = \sigma^{\circ}_{ik} + \frac{\partial \sigma^{\circ}_{ik}}{\partial \bar{E}}\left(H_N - \bar{E}\right)$$

Here, σ°_{ik} is the equilibrium mean stress tensor and $\bar{E}$ is the mean value of total energy of system H_N.

The expressions presented agree with the results obtained in [4, 5] by another method.

For the isotropic liquid a familiar result for shear viscosity [1] is obtained from the general expression

$$\eta(\omega) = \Theta^{-1}\int_0^\infty e^{-i\omega t}\langle \hat{\Pi}_{12}(0)\,\hat{\Pi}_{12}(t)\rangle dt \qquad (15)$$

The case of slow immersion corresponds to the condition $\omega = 0$.

The expression for bulk viscosity also follows from (14).

For the isotropic liquid, if we use the Stokes model, we can determine the coefficient of friction of a molecule ξ via the coefficient of shear viscosity η. At the same time the coefficient ξ, according to Kirkwood [6], can also be represented by the integral of the autocorrelation function

$$\zeta = \frac{1}{3\kappa T}\int_0^\infty \langle \vec{K}(0)\vec{K}(s)\rangle ds \qquad (16)$$

Here $\vec{K}$ is the force acting at moment s on a selected molecule of the liquid on the part of the remaining molecules in the system. Since the system is isotropic, then the integral encloses a scalar product.

The self-diffusion coefficient (we are considering a single-component system) can be expressed by the integral of the autocorrelation function of molecular velocity, and in the simplest model is equal to it [1], that is,

$$D = \frac{1}{3}\int_0^\infty \langle \vec{V}(0)\vec{V}(s)\rangle ds \qquad (17)$$

Here we also have a scalar product of vectors.

In all the cases cited, attainment of ultimate numerical results involves great and as yet uneliminated difficulties.

Though integral equations determining autocorrelation functions have been obtained (cf., for example [7, 8]), the solution of these equations still remains unclear. Therefore to some extent we can surmount the difficulties by attempting to represent the integral of the autocorrelation function as a product of the mean square of the quantity under consideration and relating to a single arbitrary moment of time for its mean relaxation time.

Here we must forthwith point to the considerable difference in relaxation characteristics for quantities dependent on spatial coordinates (forces) and quantities dependent on velocity. Thus the coefficient of friction of an individual molecule can be represented (for the system states far removed from the critical point) as

$$\zeta = \frac{1}{3\kappa T}\langle \vec{K}^2\rangle \tau_q \qquad (18)$$

We let τ_q represent the mean relaxation time for the force $\vec{K}$ dependent only on spatial coordinates.

The integral for the diffusion coefficient can be written in approximate terms as follows

$$D \approx \frac{1}{3} \langle \vec{V}^2 \rangle \tau_p \qquad (19)$$

Here τ_p is the mean relaxation time of molecular velocity (momentum).

Using the concept of relaxation times τ_q and τ_p, we can determine in an approximate way the autocorrelation function entering into the formula for the shear viscosity coefficient (15) when $w = 0$. The members of the expression for $\hat{\Pi}_{12}$ relates here to a single moment of time and the averaged quantity can be reduced to binomial form with the aid of the procedure described by Zwanzig [9].

The final result is

$$\eta = \frac{\pi \tau_q}{2V} + \frac{2\pi \tau_q}{15V^2} \int_0^\infty \frac{\vec{R}}{dr} \left(r^4 \frac{d\varphi}{dr} \right) \varphi dr \qquad (20)$$

Thus, the problem of determining kinetic characteristics breaks down into two subproblems. One is associated with the need to carry out the procedure of statistical averaging in the equilibrium state of the system, and the other with determination of relaxation time, and the relaxation times τ_q and τ_p differ from each other by two orders of magnitude.

The statistical determination of relaxation time τ_q (for simple liquids it is of the order of 10^{-12} sec) has been given in [10]. The values of τ_q agree with thermal estimates [11]. Here however we will dwell on determination of τ_p. For this purpose we will use the Langevin equation, the statistical approach of which was initially given in the already cited study by Kirkwood. If we do not take into account the member expressing the rapidly oscillating (random) force, the Langevin equation becomes

$$\frac{d\vec{p}}{dt} = -\frac{f}{m} \vec{p} \ , \qquad (21)$$

where $\vec{p}$ is particle momentum, m is particle mass; ξ is equal to the above-given expression (16). From this it is clear that the characteristic momentum relaxation time will be

$$\tau_p = \frac{m}{\xi}; \tag{22}$$

Following the general Kirkwood approach, we can repeat the derivation of the Langevin equation, but now with use of the two-index distribution functions (statistical method of conventional distributions). The friction coefficient for the molecule will then be equal, according to (18), if we carry out the statistical averaging procedure [11], to the following:

$$\xi = \frac{4\pi\tau_q}{3kTV}\int_{r_0}^{\infty}[\varphi'(r)]^2\varphi(r)r^2dr \tag{23}$$

Here $\Phi(r)$ is the pairwise intermolecular potential and v is the molecular volume ($4/3\ \pi r_0^3 = V$).

$$\varphi(r) = V\frac{F_{11}^{(1)}(\vec{q}^1,\vec{q}^2)}{F_{11}(\vec{q}^1)} \qquad r = |\vec{q}^2 - \vec{q}^1| \tag{24}$$

We will recall that in the statistical scheme we used $F_{11}^{(1)}$ denotes the probability density that in the two selected molecular volumes v_1 and v_2 correspondingly surrounding the coordinates q^1cv_1 and q^2cv_2 any two molecules are present, and in the remaining volumes there are also no more than one molecule (this approximation is called the F_{11} approximation). The probability density is similarly determined for a single molecule $F_{11}(q)$. From (24) it is clear that $\phi(r)$ designates the conventional distribution function $F_{11}(q^2/q^1)$. Below, the fixed point q^1 is chosen in the center of a sphere having a volume V.

This approach was used in [11] for calculating the friction coefficient ξ, and then also the shear viscosity coefficient for simple nonpolar liquids on the phase transformation line ultimately equal to

$$\eta = 16\sqrt{\frac{M}{T}}\frac{\xi}{k}\frac{\sigma^6}{V^{4/3}}10^{-6}\ \text{g}\cdot\text{cm}^{-1}\cdot\text{sec}^{-3} \tag{25}$$

where M is the molecular weight, V is the volume of a single mole in cm^3, ε/k and σ are parameters of the Lennard-Jones potential (σ given in Angstroms and ε/k in degrees).

Using the determination of τ_p according to (22) with (23) taken into account, we will find the final expression for the self-diffusion coefficient of a single-component system. Since the mean square of the velocity is 3kT, then

$$D = \frac{kT}{\zeta} \tag{26}$$

or, using the expression for the shear viscosity coefficient (25),

$$D = 0{,}624 \frac{T^{1/2} V^{2/3}}{M^{1/2} \frac{1}{\pi} \sigma^2} 10^{-5} \text{ cm}^2 \text{ cek}^{-1} \tag{27}$$

Below are presented results of calculating the self-diffusion coefficient according to (27) for a number of compounds (argon, hydrogen, nitrogen and carbon dioxide) along the phase transformation line (we individually also present the results of calculating the momentum relaxation time).

Compound	r_o Å	T °K	D $10^8 \frac{cm^2}{sec}$	$T_p 10^{14}$ sec
Ar	2,24	83,78	0,73	-
Ar	2,26	90,03	0,9	4,798
Ar	2,35	III,95	I,72	-
Ar	2,54	I37,67	4,8	-
Ar	2,74	I48,0I	6,28	-
H_2	2,I89	I4,89	2,33	3,807
H_2	2,2585	I9,92	4,43	5,395
N_2	2,346	64,82	0,69	3,6I6
N_2	2,63I	III,98	3,38	I3,3
CO	2,396	68,I7	0,89	4,42

Of no little interest is the fact that the relaxation time τ_p and τ_q are inversely related, since, by combining (18) and (22), we can write

$$\tau_p = \frac{mkT}{\langle R^2 \rangle \tau_q} \tag{28}$$

It appears to the authors that this fact is very significant in accounting for characteristics in the behavior of a compound in its critical state, when diffusion, just like other properties, is manifest in a specific way (cf., for example [12-13]).

Taking into account the approximational nature of the expression (27) adopted, comparison with experimental data [1] must be regarded as wholly satisfactory.

By knowing the coefficient of friction of a molecule we can determine the coefficient of molecule mobility b.

Phenomenologically, the mobility coefficient is defined as the coefficient of proportionality between the diffusion flow and the thermodynamic driving force (the gradient of the chemical potential). Correspondingly, the mobility coefficient can be defined via the diffusion coefficient

$$b = \frac{D}{V^2}\left(\frac{\partial V}{\partial p}\right)_T , \tag{29}$$

where p is the pressure.

If we take the self-diffusion coefficient as the coefficient D, then

$$b = -\frac{kT}{\zeta V^2}\left(\frac{\partial V}{\partial p}\right)_T \tag{20}$$

The transition to the binary isotropic system is based on use, appropriately enough, of a system of two Langevin equations (for the molecules of the a and b species). The friction coefficients were determined with the aid of the sum of two autocorrelation functions

$$\xi_a = \frac{1}{3kT}\int_0^\infty \langle K_{aa}(0)\vec{K}_{aa}(s) + \vec{K}_{ab}(0)\vec{K}_{ab}(s)\rangle ds$$

$$\xi_b = \frac{1}{3kT}\int_0^\infty \langle \vec{K}_{bb}(0)\vec{K}_{(ab)}(s) + \vec{K}_{ba}(0)\vec{K}_{ba}(s)\rangle ds \qquad (31)$$

The expression (14) for the tensor of the viscosity coefficients is easily generalized for the case of a binary mixture. In this case the operator $\hat{\Pi}_{ik}$ becomes:

$$\Pi_{ik} = -\sum_{\mu=1}^{n_1} \frac{P_i^\mu P_k^\mu}{m_1} - \sum_{\nu=1}^{n_2} \frac{P_i^\nu P_k^\nu}{m_2} + \frac{1}{2}\sum_{\mu=1}^{n_1}\sum_{\nu=1}^{n_1} \frac{\Phi_{11}'(r^{\mu\nu})}{r^{\mu\nu}} X_i^{\mu\nu} X_k^{\mu\nu} +$$

$$+ \frac{1}{2}\sum_{\mu=1}^{n_2}\sum_{\nu=1}^{n_2} \frac{\Phi_{22}'(r^{\mu\nu})}{r^{\mu\nu}} X_i^{\mu\nu} X_k^{\mu\nu} + \frac{1}{2}\sum_{\mu=1}^{n_1}\sum_{\nu=1}^{n_2} \frac{\Phi_{12}'(r^{\mu\nu})}{r^{\mu\nu}} X_i^{\mu\nu} X_k^{\mu\nu} \qquad (32)$$

Here n_1 is the number of molecules of species a, n_2 is the number of molecules of species b, and Φ_{ij} is the potential of pairwise molecular interaction of the corresponding species.

The averaging leading to an expression analogous to (20) is conducted here with the aid of two momentum relaxation times of the corresponding ξ_a and ξ_b.

References

1. Kubo, R., *Sb. Termodinamika Neobratimykh Protsessov*, [Collection. Thermodynamics of Irreversible Processes], IL Press, Moscow, 1962.
2. Komarov, L. I., *ZhETF*, Vol. 48, p. 145, 1965.
3. Mc Lennan, J., *Progr. Theor. Phys.*, Vol. 30, p. 408, 1963.
4. Khazanovich, T. N., *PMM*, Vol. 28, No. 6, 1964.
5. De Vault, G. and J. Mc Lennan, *Phys. Rev.*, Vol. 137, p. 724, 1965.
6. Kirkwood, J., *J. Chem. Phys.*, Vol. 14, p. 180, 1946.
7. Berne, B., J. Boon and S. Rice, *J. Chem. Phys.*, Vol. 45, p. 1086, 1966.
8. Singi, K. and M. Tosi, *Phys. Rev.*, Vol. 157, p. 153, 1967.
9. Zwanzig, R. and D. Mountain, *J. Chem. Phys.*, Vol. 43, p. 4464, 1965.
10. Rott, L. A., *Ukr. Fiz. Zh.*, Vol. 12, p. 19, 1967.
11. Rott, L. A., *Sb. Primeneniye Ul'traakustiki k Issledovaniyu Veshchestva*, [Collection: Use of Ultrasonics in Research on Compounds], MOPI Press, Moscow, No. 22, 1967.
12. Khazanova, N. Ye. and L. A. Rott, *IFZh*, No. 6, p. 123, 1963.
13. Krichebskiy, I. R., *ZhFKh*, Vol. 41, No. 10, 1967.

EFFECT OF THE COMPOSITION OF CLOTH AND THE FORM OF BINDING OF ABSORBED MOISTURE ON ITS THERMOPHYSICAL CHARACTERISTICS

N. I. Salivon and M. F. Kazanskiy

The main thermophysical characteristics of cloth determining their heat-protective properties is thermal conductivity λ, thermal diffusivity a and heat capacity c.

Since the values of these characteristics depend decisively on moisture content bound to the solid phase of the cloth in different ways, we conducted a study aimed at discovering how moisture in different forms and types of binding with cloth of different physicochemical character affects the thermophysical properties of the cloth.

The objects of the study were specimens of 100 percent lavsan cloth and woolen combed suit cloth of No. 32/2 weave in the base and in the neck, with interweaving of 2/2 serge for an almost identical density and weight with 10, 30 and 50 percent lavsan content, and also a specimen of cloth of the same structure made of 100 percent wool, woven in the Central Scientific Research Institute of the Garment Industry.

The water-retaining properties of the fabrics were determined by means of isothermal drying thermograms [1] and with the aid of water vapor adsorption isotherms. The results of analysis of the forms in which water is bound with these fabrics are shown in the Table.

Thermophysical coefficients λ, a and c were determined on an apparatus we developed [2] using the method of two temperature-time points [3] for specimens 2-3 mm thick.

The results of a series of experiments with each specimen are shown in Figures 1 and 2 in the form of curves describing the thermal coefficients of functions of moisture content. In the figures the vertical dashed lines

denote the boundaries of moisture of various forms and types of binding with fabric: A is the maximum amount of adsorbed moisture; Γ is the moisture of maximum hygroscopic state.

Table. Amount of Water in Various Forms of Binding with Fabric

Specimen No.	%content of lavsan in mixture with wool	Moisture in mono-molecular adsorption %	Maximum amount of absorbed moisture	Amount of hygroscopic moisture
1	0	5.8	9.6	28.5
2	10	5.4	8.7	24.6
3	30	4.0	6.7	17.4
4	50	2.7	5.1	15.0
5	100	-	0.3	3.8

At low moisture contents (Figure 1, curves 1), when only adsorbed moisture is found in the specimen, the coefficient of thermal conductivity λ remains almost unchanged. An appreciable rise in the thermal conductivity coefficient is observed in the moisture content interval from the adsorbed to the maximum hygroscopic moisture content, when micropores fill up with moisture and thermal contacts between fibers are established via formation of continuous water films. Upon further rise in moisture content, the increase in thermal conductivity coefficient is less intense and is characterized by a tendency toward saturation.

The coefficient of thermal diffusivity a also remains almost unchanged at low moisture contents (Figure 2, curve III). The appreciable rise in the thermal diffusivity coefficient begins from the moment that capillary condensation sets in, when micropores of radius $r < 10^{-5}$ cm begin to be filled in with water. An intensive rise in the thermal diffusivity coefficient with rise in moisture content is observed all the way to attainment of maximum hygroscopic state of the specimen.

The thermal diffusivity maximum for all specimens corresponds to the moisture content close to the maximum hygroscopic state, when all specimen pores are filled with moisture, and when water films are formed between

individual fibers producing thermal contacts. This transition from the three-component system (fabric-water-air) to a two-component system (fabric-water) is characterized by a drop in the thermal diffusivity coefficient.

Due to the diversity of forms and types of binding of fabric-absorbed water, in each of the curves the functions of the thermal conductivity and thermal diffusivity coefficients can be divided into three sections. Here the value of the linear initial section corresponding to the quantity of adsorbed moisture is reduced with rise in lavsan addition both on the thermal conductivity curve and on the thermal diffusivity curve, but for the specimen of pure lavsan there is no such section. The maximum on the thermal diffusivity curve is shifted to the side of lower moisture content with rise in percentage lavsan content, this shift corresponding to the lower moisture capacity of lavsan compared to wool.

The heat capacity for all specimens rises linearly with rise in moisture content (curve II).

Just as for typical capillary-porous and colloidal capillary-porous bodies, the thermophysical coefficients as functions of moisture content for fabrics with different lavsan content are determined above all by the diversity of forms and types of bonding of fabric-absorbed moisture. In this case this diversity depends on the amount of lavsan added to the wool. These conclusions on the effect of lavsan addition on thermophysical coefficients of fabrics can be used in designing suits with desired heat-protective properties.

Symbols

λ = thermal conductivity coefficient; a = thermal diffusivity coefficient; c = specific heat coefficient; r = capillary radius; A = boundary of maximum amount of adsorbed moisture; Γ = boundary of moisture in maximum hygroscopic state.

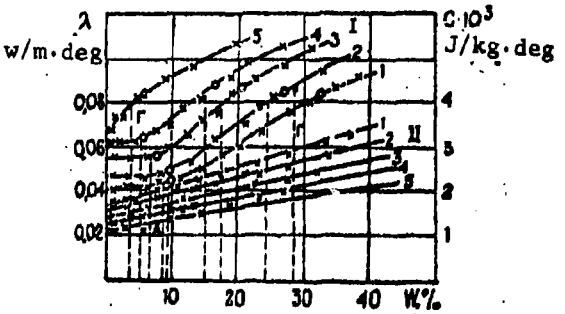

Figure 1. Curves of thermal conductivity (1) and heat capacity (2) as functions of moisture content at a temperature of 298°K for fabric specimens 1-5

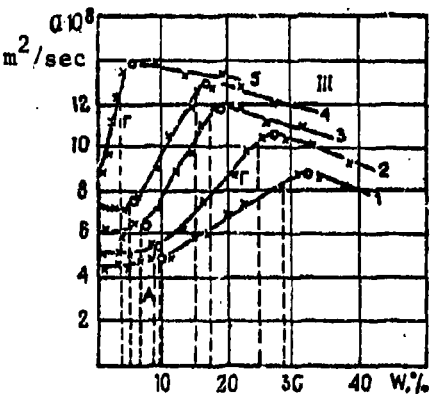

Figure 2. Curves describing thermal diffusivity (III) as functions of moisture content at a temperature of 298°K for fabric specimens 1-5

References

1. Kazanskiy, M. F., *DAN*, Vol. 130, p. 5, 1960.

2. Salivon, N. I. and M. F. Kazanskiy, *Izv. Vuzov*, No. 1, p. 48, 1964.

3. Vol'kenshteyn, V. S. and N. N. Medvedev, *IFZh*, Vol. 2, No. 10, p. 26, 1959.

EFFECTS OF FILLING ON THERMAL CONDUCTIVITY, ELECTROCONDUCTIVITY AND DIELECTRIC CONSTANT OF THIN-LAYER POLYMER COATINGS

F. M. Smekhov, L. N. Novichenok,
L. V. Nitsberg and A. I. Nepomnyashchiy

Variation of thermophysical and electrical properties of filled polymer coatings upon variation of filler content was investigated.

Epoxide resin E-33($\overline{M}_N$ ~ 1000) solidified by the FO-200 polyamide resin ($\overline{M}_N$ ~ 3000) with formation of a reticulate structure was used as the film-forming agent.

The rutile modification of TiO_2 of the R-1 grade served as the filler, and its concentration in the binder varied from 10 to 50 percent by volume.

Experimental Method

The thermal conductivity of coatings λ was measured by a nonsteady-state method for a single temperature-time point in the specimen [1] on an instrument at the Institute of Heat and Mass Transfer of the Academy of Sciences Belorussian SSR. The electroconductivity λ was determined for direct current.

The dielectric permeability ε' and the loss angle of slope tan δ were measured in the frequency range 5-200 KHz. All these characteristics were determined at normal temperature. To investigate the effects of filling, relaxation processes in the polymer were measured as well as the temperature dependence of ε' and tan δ in the temperature range 20-250°C. The specimen temperature was measured by a chromel-copel thermocouple with an error not greater than ±1°C. The error in determining ε' and tan δ did not exceed ±3 percent, and for λ and χ -- ±12 percent.

Experimental Data and Their Discussion

Figure 1 presents the curves of heat and electrical conductivity of coatings, and also their dielectric characteristics as functions of filler concentration.

An increase in the first two indices with rise in TiO_2 content is accounted for by the fact that λ and χ of the filler are approximately two orders of magnitude higher than those for the polymeric binding agent. In addition, introduction of filler evidently leads to a change in the mechanism of thermal conductivity and charge transfer. Thus, according to modern concepts, heat transfer in a polymer occurs mainly via phonon transport [2], to which, with addition of filler, is added heat transfer by weakly bound electrons of the oxide crystals. The process of charge transfer in a polymer, in the view of many authors [3], follows an ionic mechanism; in the case, however, of titanium dioxide electronic conductivity occurs. Thus, introduction of filler leads to complication of heat and charge transfer processes.

The dielectric permeability of the coating rises with rise in TiO_2 content, but the loss slope angle decreases, since for these indices as well the difference in absolute values between the filler and the binder is one to two order of magnitude.

Along with experimental investigation of thermophysical and electrical characteristics of coatings as functions of the filler content, an analytical calculation was made of these same parameters using the formulas proposed by V. I. Odelevskiy for two-phase systems:

a) for matrical distribution with nonelongated inclusions:

$$\Lambda = \Lambda_1 / I + \frac{\theta_2}{\frac{I-\theta_2}{3} + \frac{\Lambda_1}{\Lambda_2 - \Lambda_1}} \qquad (1)$$

b) for statistical distribution of the disperse phase:

$$\Lambda = A + \sqrt{A^2 + \frac{\Lambda_1 \chi \Lambda_2}{2}}; \quad A = \frac{/3\theta_2 - I/}{4} + \frac{/3\theta_1 - I/}{4} \qquad (2)$$

where Λ_1 and Θ_1 are generalized conductivity and bulk fraction of continuous phase. It has been ascertained that the best approximation to experimental data is provided by the relationship (1), cf. the table.

Experimental and Calculated Values of ε' of Coatings

Value of ε'	Bulk Content of Disperse Phase				
	10	20	30	40	50
Experimental Data	4,2	5,3	6,2	7,9	9,1
Calculated Data (Matrical Distribution	4,12	5,18	5,66	8,9	10,7
Calculation (Statistical Distribution)	4,2	6,5	11,0	19,0	31,0

It was shown earlier that the change of effective thermal conductivity of linear polymer (acrylic copolymer AC)-based coatings with rutile filling corresponds to the matrical distribution [4]. This has also been confirmed for the polymer of reticulate structure (Figure 1).

In the calculation filler characteristics taken from literature data were employed. The difference in the rate of change of effective electroconductivity -- both experimental and calculated -- is evidently due to the low degree of precision in determining the χ of rutile [5].

The temperature dependence of ε' and tan δ of coatings at a frequency of 200 KHz is shown in Figure 2. The nature of the variation of dielectric permeability with temperature is identical for coatings with different TiO_2 content. The course of curves describing the temperature dependence of tan δ is precisely analogous both for unfilled and for filled polymers: dielectrical losses rise, reaching a relaxation dipole-segmental maximum.

A further increase in losses is caused by consumption of the electric field energy for continuous electroconductivity. These functions were derived when ε' and tan δ were measured at other frequencies. A decrease in the absolute value of tan δ both in the maximum region and in the region of conductivity losses is observed with rise in filler concentration. Additionally, it was established that introducing small amounts of TiO_2 (10 percent by volume) into the binder produces a shift in the relaxation loss maximum toward the side of lower temperatures. Reduction of the vacancy rate of the three-dimensional network by changing the resin-solidifier ratio leads to a similar result. Evidently, in the solidifying process some of the relaxation-capable groups of resin and solidifier are screened by filler particles. For a 20-percent rutile content the shift of the maximum is less pronounced. A further rise in the filler content leads to a marked drop in the quantity tan δ, and the position of the maximum is difficult to fix. It can be assumed that for an appreciable filler content the reduction in the number of transverse intermolecular bonds ("cross-linking") is compensated by the adsorptive powers of interaction of the molecule and the solid particle. As a result, the segmental mobility does not change and the shift of the dipole-segmental loss maximum is not observed.

Symbols

$\overline{M}_N$ = mean molecular weight of the polymer; λ = thermal conductivity; Λ = generalized conductivity; χ = electroconductivity; Θ = bulk fraction; ε' = dielectric permeability; δ = angle of losses.

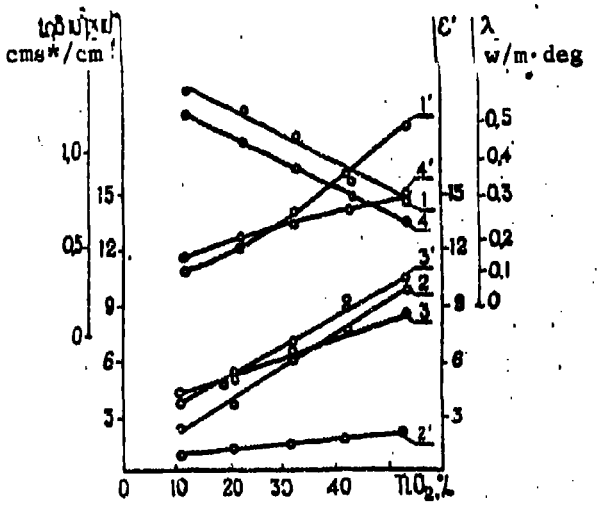

Figure 1. Effect of titanium dioxide content on λ, χ, ε' and tan δ of coatings: 1 and 1^1, Thermal conductivity λ; 2 and 2^1, Electroconductivity χ; 3 and 3^1, Dielectric permeability ε'; 4 and 4^1, Loss slope tan δ at frequency f = 5 KHz. 1, 2, 3, 4 are experimental data; 1^1, 2^1, 3^1, 4^1 are calculated data using the relationship (1).

[1]see p. 609

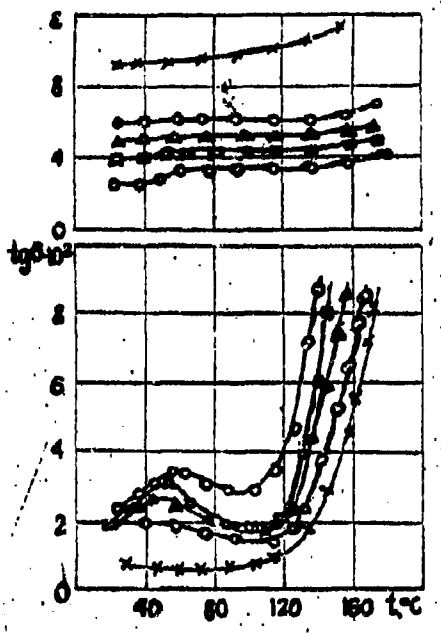

Figure 2. Temperature dependence of ε' and tan δ of coatings at a frequency of 200 KHz: ○, Without filler; □, 10 percent TiO_2; Δ, 20 percent TiO_2; •, 30 percent TiO_2; x, 40 percent TiO_2

Footnotes

1. To p. 607 cms = center of mass system -- Tr.

References

1. Novichenok, L. N., *Sb. Teplo- i Massoperenos v Kapillyarno-poristykh Telakh*, [Collection: Heat and Mass Transfer in Capillary-purous Bodies], Nauka i Tekhnika Press, Minsk, 1965.

2. *Sb. Fizika Nizkikh Temperatur*, [Collection: Low-temperature Physics], IL Press, Moscow, 1959.

3. Sinor, D., *Fortschr. Hochpol.-Forschung*, Vol. 4, No. 3, p. 1, 1966.

4. Nocichenok, L. N., F. M. Smekhov and L. V. Nitsberg, *Lakokrasochnyye Materialy i Ikh Primeneniye*, No. 6, p. 30, 1965.

5. Earle, M. D., *Phys. Rev.*, Vol. 59, No. II., p. 942, 1941.

THERMAL CONDUCTIVITY OF AIR AT TEMPERATURES UP TO 800°K AND PRESSURES UP TO 1000 BAR

A. A. Tarzimanov and V. S. Lozovoy

In recent years thermophysical studies have gained increasing attention. However, investigations dealing with measurements of thermal conductivity λ of gases at P > 500 bar and T > 400°K are very few in number [1, 2]. We have devised a new experimental apparatus using the heated wire method to measure the λ of several gases and liquids, above all, air. The method of measurement is analogous to that adopted in [3].

A diagram of the experimental apparatus is shown in Figure 1. The measuring tube made of "Pyrex" glass was placed within a thick-walled autoclave made of the stainless steel 1Kh18N9T. The autoclave was equipped with three external electric heaters supplied with stabilized alternating current. Control of temperature field uniformity over the autoclave height was maintained by five chromel-alumel thermocouples. The lead-out of the measuring wires from the high-pressure region made use of Teflon sleeves.

A thermocompressor, whose operating principle is analogous to that described in [4], was used to produce high pressure in the system. By means of the thermocompressor it was possible to raise the pressure from 120-150 bar to approximately 500 bar. A further pressure rise to 1000 bar and regulation in the course of the experiments was achieved with the aid of a high-pressure oil press and a U-shaped compressing vessel filled with mercury.

Model manometers at 600, 1000 and 1600 kg/cm^2 were used to measure pressure, and to their readings corrections were added based on calibration of the manometers with the MP-2500 piston manometer of the 0.02 class.

P, bar	T, K	ΔT, K	λ·10⁴ w/m·deg	P, bar	T, K	ΔT, K	λ·10⁴ w/m·deg
I	303,2	6,0I	268	879	505,5	I4,39	697
I	3I0,0	I2,09	272	9I5	500,6	7,65	708
75	306,8	I5,35	306	I	634,8	6,83	493
97	307,7	I6,48	322	98	653,6	9,6I	524
I3I	304,9	I3,78	340	I98	653,I	9,2I	547
I95	304,8	I3,7I	385	26I	652,6	8,99	563
2II	304,0	II,83	393	359	653,0	8,69	58I
232	304,3	I0,02	409	457	652,5	8,32	608
293	303,2	II,6I	452	498	680,6	I2,60	629
3I3	302,4	6,65	462	55I	65I,5	7,94	637
344	303,5	I8,46	48I	586	679,8	I2,I2	655
390	302,2	I0,I3	5I7	684	679,4	II,74	677
4I9	300,3	27,58	537	78I	679,4	II,33	703
487	302,4	7,03	575	785	680,3	I2,88	707
488	30I,2	7,96	58I	879	684,6	I8,62	733
495	305,6	9,I8	583	879	678,8	I2,48	730
535	302,4	6,70	603	I	768,2	22,I5	560
586	298,9	5,26	642	II9	769,I	2I,23	587
683	298,8	4,80	704	2I7	768,7	20,74	609
78I	298,7	4,49	759	3I5	767,7	I9,99	633
879	298,6	4,I7	8I0	4I4	767,I	I9,28	656
I	342,8	I5,05	298	5II	766,9	I8,68	678
I	373,9	34,36	3I5	II8	786,7	I0,43	604
I	40I,3	7,37	34I	I95	786,3	I0,I6	62I
I	508,7	7,20	4II	3I5	786,2	9,85	640
I04	497,8	I3,28	436	413	786,I	9,55	663
I96	496,5	I2,46	463	5I0	786,6	9,26	680
30I	495,3	II,46	502	590	794,I	I9,33	705
396	490,4	I4,40	527	7I2	788,2	I2,82	726
505	489,7	I3,39	567	800	787,9	I2,49	745
586	50I,6	8,84	595	89I	785,7	I2,I8	765
689	499,6	8,33	632	99I	787,4	II,78	790
79I	50I,I	7,93	667	99I	784,2	6,I5	785

The design of the measuring tube is similar to that used in [3]. Its main dimensions are as follows: inner diameter of capillary -- 0.928 mm, outer capillary diameter -- 1.876 mm, diameter of wire of inner resistance thermometer -- 0.100 mm, length of measuring section for the first series of experiments -- 88.9 mm, and after their assembly -- 89.5 mm. The data of control measurements of thermal conductivity of air at atmospheric pressure at temperatures up to 800°K gave satisfactory agreement with known reliable data of other researchers.

For the investigations clean, dried air taken from a high-pressure still for air separation was used. Two drier-filters filled with alumogel were additionally included in the layout (Figure 1). Measurements of the λ of air under pressure are presented on the isotherms. In all the experiments the value of the product of the criteria Gr·Pr did not exceed 1000, which doubtless points to the absence of convective currents within the capillary.

In interpreting the measurement results corrections were introduced that allowed for the removal of heat from the heater ends in the temperature drop at the measuring tube walls, for variation of geometric dimensions with temperature, and for radiative heat transfer. In view of the effect that elongation of the spring has on the inner thermocouple readings, the latter was calibrated during the course of the experiments against the outer resistance thermometer. To verify the effect that high pressures and temperatures have on platinum resistance thermometer readings, a series of special measurements was made. Well defined pressure functions of platinum resistance were obtained in the range T = 300-800°K and p = 1-1000 bar. In calculating the λ of air, a correction was introduced for variation of platinum resistance with temperature. The possible experimental error in our estimation did not exceed 1.5 percent. Figure 2 presents isobars with experimental points given for these pressures. The table lists results of experiments where the following symbols were adopted: p = pressure, T = mean air temperature, ΔT = temperature difference in air layer, and λ = coefficient of thermal conductivity with all the corrections taken into account.

It must be noted that the thermal conductivity of air as a function of pressure has thus far not been adequately studied, which is evidenced by the meagerness of experimental data [5, 6]; further, systematic discrepancy [7] is observed for the data [5, 6].

The data we obtained at pressures up to 1000 bar and temperatures up to 800°K relate mainly to the region of parameters of state uninvestigated thus far. Their comparison with the results of other researchers is most conveniently presented in the form of excess thermal conductivity $\lambda - \lambda_T$ (λ_T is the thermal conductivity at p = 1 bar) as a function of density ρ. As we can see from Figure 3, our experimental points and the data of I. F. Golubev fit along the averaged curve with relatively small scatter, the exception here being the 196°K isotherm [6], the points of which are overstated by up to 8-10 percent. The results in [5] are understated by 5-7 percent.

Close study of the data shows that in the coordinates $(\lambda - \lambda_T) = f(\rho)$, strictly speaking, no single curve is obtained. The isotherms, though very weakly, are stratified (Figure 4). At a density close to the critical point (ρ_{cr} = 313 kg/m^3), stratifying of the 300 and 786°K isotherms amounts to 3 percent. A similar state of affairs has been obtained for the thermal conductivity of nitrogen [1].

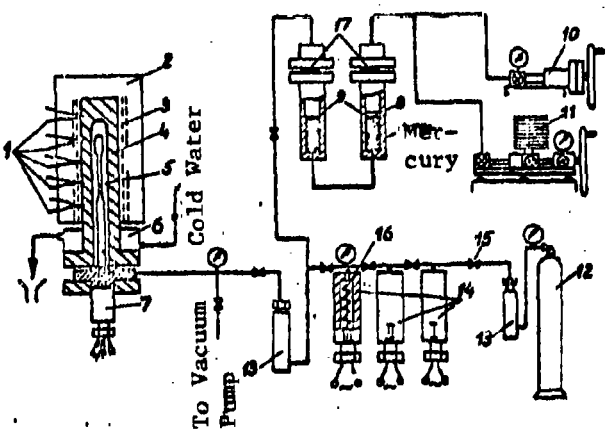

Figure 1. Diagram of experimental apparatus: 1, Thermocouples; 2, Heat insulation; 3, Electric heaters; 4, Autoclave housing; 5, Measuring tube; 6, Cooler; 7, Assembly for leading out of measuring wires; 8, Magnet; 9, Compressing vessel; 10, High-pressure oil press; 11, Piston manometer; 12, Gas cylinder; 13, Filter-driers; 14, Thermocompressor cylinders; 15, Valves; 16, Electric heater; 17, Lens gaskets

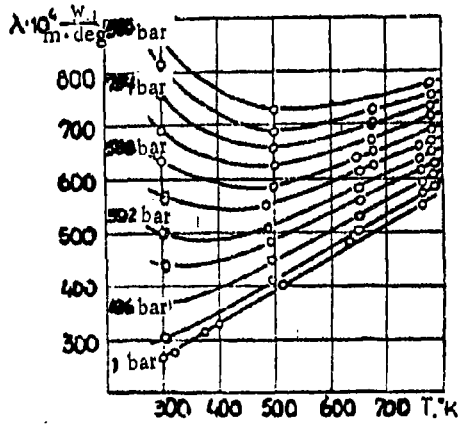

Figure 2. Thermal conductivity of air as a function of temperature (isobars)

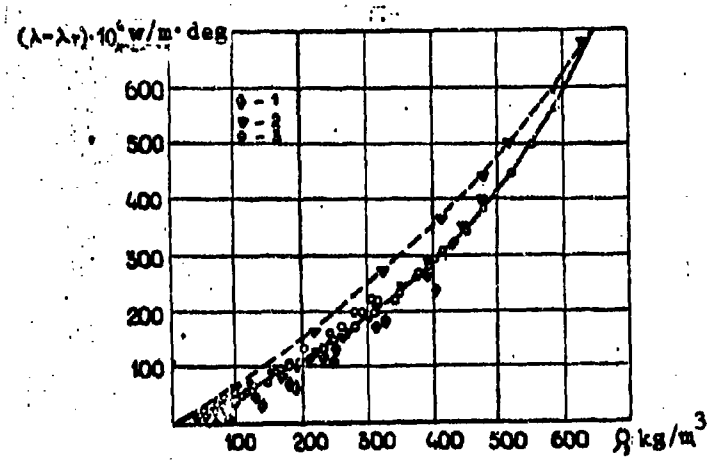

Figure 3. Excess thermal conductivity of air as a function of density: 1, [5]; 2, [6]; 3, Authors' data

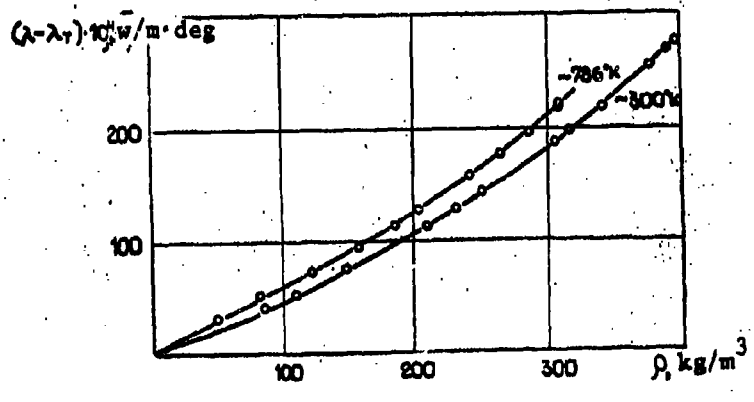

Figure 4. Excess thermal conductivity of air as a function of density for the 300° and 786°K isotherms

References

1. Johannin, R., *Journal des Recherches C.N.R.S.*, Vol. 6, No. 43, p. 116, 1958.
2. Vukalovich, M. P. and L. I. Cherneyeva, *Teploenergetika*, No. 9, 1963.
3. Vargaftik, N. B. and A. A. Tarzimanov, *Teploenergetika*, No. 9, 1959; No. 7, 1960.
4. Boksha, S. S., *Kristallografii*, Vol. 2, No. 1, 1957.
5. Stoylarov, Ye. A., V. V. Ipat'yev, and V. N. Teodorovich, *ZhFKh*, Vol. 24, No. 2, p. 166, 1950.
6. Golubev, I. F., *Teploenergetika*, No. 12, 1963.
7. Vasserman, A. A., Ya. Z. Kazavichinskiy and V. A. Rabinovich, *Teplofizicheskiye Svoystva Vozdukha i Yego Komponentov*, [Thermophysical Properties of Air and Its Components], Nauka Press, Moscow, 1966.

THERMAL CONDUCTIVITY OF THIN BOUNDARY FILMS OF LIQUIDS STABILIZED BY THE SURFACE OF A SOLID

G. T. Timoshenko and M. S. Metsik

Preliminary experiments by one of the authors established the fact of the anomalously high thermal conductivity of films of water on the surface of mica crystals [3]. We made a further careful examination of this effect.

A method of determining thermal conductivity of thin liquid films has been formulated [1-4] based on the general regular regime theory.

Saturating a pile of a large number of identically thick sheets of any material with the test liquid and compressing the pile in a vise, we can get the corresponding thickness of the liquid films. The thermal conductivity of the film liquid is calculated from the formula:

$$\lambda = \frac{c\rho(Z_1 - Z_2)}{2\pi^2\left(\frac{1}{X^2}+\frac{1}{Y^2}\right)} \cdot \frac{m_2 - m_1}{Z_2 - Z_1} + \frac{\lambda^{\perp}}{2\left(\frac{1}{X^2}+\frac{1}{Y^2}\right)}\left(\frac{1}{Z_1}+\frac{1}{Z_2}\right) + \lambda'' \qquad (1)$$

Here:

X, Y and Z are the dimensions of the pile, measured in a direction perpendicular to the sheet plane;

λ'' and $\lambda^{\perp}$ are the components of the thermal conductivity of plates in the longitudinal and normal directions, respectively (given the presence of thermal conductivity anisotropy);

c and ρ are the specific heat and density of the pile with absorbed liquid taken into account;

m_1 and m_2 are cooling rates of the pile in the regular regime for a heat transfer coefficient $\alpha \to \infty$ for the corresponding Z_1 and Z_2 given by compression.

Knowing the cooling rate m_1 and the height Z_1 of the pile at maximum compression (in the limiting case, a continuous specimen, for example a monocrystal of mica), we can determine the mean value of thermal conductivity of liquid films of any thickness, by setting the corresponding pile height Z_2 and experimentally determining the value of the cooling rate m_2. Since according to the conception of the method the thermal conductivity of a pile Z_2 in height saturated with liquid must be compared with the thermal conductivity of a continuous specimen of the same dimension, a correction allowing for reduction of the cooling rate of the continuous specimen when its height is increased to Z_2 is introduced into the measured value of the cooling rate m_1. Studies were made of the thermal conductivity of film liquids on mica. The following method was employed.

The working arm of a differential copper-constantan thermocouple made of 0.1-mm-diameter wires without reinforcement was placed in the center of a previously cleaved mica crystal (muscovite or phlogopite) cut in the form of a rectangular parallelepiped with a base 4×5 cm^2 and about 4.5 cm in height.

Then the crystal was compressed in a vise and according to the regular regime method [5] its cooling rate was determined for 5° in the thermostat whose temperature was kept unchanged to a precision of 0.02 percent, with the specimen heat transfer coefficient $\alpha \to \infty$. A mirror galvanometer with a sensitivity of $0.5 \cdot 10^{-6}$ v/mm was employed. The time intervals were fixed with a precision of 0.2 sec. The cooling rate was determined with an error of 0.002-0.005 sec.

Later the mica crystal was converted into a pile of sheets. For this purpose a muscovite crystal was accurately cut into 30-40 layers 1.0-1.5 mm thick, without varying the mutual positions of the sheets in the pile, the sheets then, in turn, were carefully stacked to a height of 20-30 sheets. However, small (3-5 mm^2) contact sites remained along the margins between the sheets, making it impossible to shift them relative to each other. With careful shaping and using the appropriate compressive force, this pile became the original crystal without visible change in the appearance of the side surfaces.

To stratify a phlogopite crystal the low-temperature swelling effect was used [6, 7]. A swollen phlogopite crystal is an aggregate of a large number of plates fastened to each other along the margin on any one side. Upon being cooled, this crystal is converted into its initial state without any change in the end surfaces.

Saturation of the pile with the test liquid was carried out in vacuum. The cooling rate of the pile for a different bulk concentration of the impregnating liquids was determined under the same set of conditions as for the integral crystal. The Z_1 and Z_2 values were determined with a micrometer with a precision of up to 5 μ. The values of the thermal characteristics of mica were taken from [2]. Interpretation of the results of measuring thermal conductivity of liquid films followed the Kornfel'd method [8] with a reliability of 90 percent out of not less than 30 experiments for each film thickness. The relative error in thermal conductivity measurements was 10-15 percent.

Distilled water, ethyl alcohol, carbon tetrachloride and transformer oil were investigated. To reduce the probability of the test liquid being washed out of the pile with the thermostat water, the experiments with alcohol, carbon tetrachloride and transformer oil were carried out for relatively small film thicknesses.

From the tabulated data it follows that the thermal conductivity of these nonpolar liquids, such as carbon tetrachloride and transformer oil, within limits of experimental error do not change with variation of film thickness and, consequently, no anomalous thermal conductivity was found for them. The thermal conductivity values found from formula (1) for these liquids is approximately one order of magnitude different from the values presented in handbook literature.

A different state of affairs is observed for films of polar liquids. As we see from the table, the effect of anomalous thermal conductivity is quite distinctly evidenced for ethyl alcohol and especially for water. In Figure 1, curve 1 describes the variation of thermal conductivity of water films with film thickness on fresh surfaces of mica sheets. The thermal

conductivity of water rises rapidly with decrease in film thickness and reaches a value of 60-65 w/m·deg for thicknesses less than 0.1 μ, exceeding the thermal conductivity of bulk water (0.6 w/m·deg) by two orders of magnitude and is close to the thermal conductivity of metals.

The thermal conductivity of thin layers of ethyl alcohol on mica surfaces is also ten times higher than its thermal conductivity in the bulk (0.16 w/m·deg) [9]. The possibility of accounting for the anomalous thermal conductivity effect seen in alcohol films by its partial replacement with thermostat water was precluded by the results of experiments with carbon tetrachloride.

The magnitude of the effect cannot be accounted for by possible variation of side surface roughness in the transition from crystal to the pile. The very method of obtaining the pile from the crystal provides for the invariancy of the mutual arrangement of the individual parts of the specimen. Additionally, in previously conducted studies [3] the effect of anomalous thermal conductivity of water film was clearly observed when the pile was made of individual identically fixed sheets of mica and when a pile with greatest compression was taken as the original state. Under these conditions it is obvious that the roughness of the end surfaces remained unchanged. Data given in Figure 2 also evidences the small role of roughness. These data make clear that the cooling rate of a water-saturated pile passes through a maximum with increasing film thickness and for thick enough films (maximum roughness) becomes close to the cooling rate of the uncleaved crystal.

The effect of anomalous thermal conductivity of thin films of polar liquids depends substantially on the state of the crystal surface. The thermal conductivity of water films in a pile was investigated after the mica sheets were rinsed in boiling water. This treatment leaches out the surface and thus weakens the surface field, which leads to a considerable decrease of thermal conductivity of water films (Figure 1, curve 2).

When a pile made of polyethylene sheets is saturated with water, practically no anomaly in thermal conductivity is observed (curve 3).

It is evident that the effect of anomalous thermal conductivity of thin films rises with decrease in temperature, and it can be assumed that it must be most clearly evident that temperatures close to 0°C. The thermal conductivity of water films drops off rapidly, however, with rise in temperature, and at 60-65°C becomes equal to the thermal conductivity of bulk water.

Results of the experiments described confirm the concept of the quasi-crystalline structure of thin films of polar liquids that are in interface with the surface of a solid [10-12].

As we know, in the crystalline state compounds are more heat-conductive compared to the amorphous state. Crystalline quartz, for example, has a thermal conductivity that is an order of magnitude higher than the thermal conductivity of fused quartz [13]. It is obvious that structure-ordered films of polar liquids, and above all water, also exhibit an exceptional capacity to transmit thermal agitations along films. However, with rise in temperature their structure begins to break down, the water films apparently become amorphized. At a temperature of 65°C total amorphization sets in, to which corresponds the rapid drop in thermal conductivity down to the values characteristic of bulk water.

A similar temperature dependence of thermal conductivity has been observed for crystalline compounds in their transition from the solid state to the liquid [13].

Based on the studies made, the following conclusions can be drawn:

1. Experiments with cleaved mica crystals graphically demonstrate the existence of the anomalous thermal conductivity effect for films of polar liquids on mica surfaces.

2. The magnitude of the effect depends on the nature of the liquids and rises with decrease in film thickness; water films about 0.1 μ in thickness on mica surfaces have a thermal conductivity that is one order of magnitude less than that of metal.

Table. Thermal Conductivity of Film Liquids on Mica Crystals

Type of Mica	Test Liquid	Bulk Concentration of Liquid in Pile	Thickness of Liquid Layers, 2h, μ	Cooling Rate of Mica Crystal, $m_1 \cdot 10^2$, sec^{-1}	Cooling Rate of Pile Impregnated With Liquid, $m_2 \cdot 10^2$, sec^{-1}	Mean Thermal Conductivity of Liquid Layer, λ, w/m·deg
Muscovite No. 1	Distilled Water	2,20	0,80	I,605	I,580	I,7
		I,25	0,45	I,6I0	I,620	6,7
		0,65	0,30	I,6I5	I,650	I5,5
		0,55	0,20	I,620	I,680	3I,4
		0,35	0,I2	I,620	I,680	47,3
		0,I5	0,05	I,625	I,660	66,5
	Ethyl Alcohol	0,85	0,30	I,6I5	I,6I0	2,9
		0,55	0,20	I,620	I,625	6,3
		0,30	0,09	I,625	I,635	I3,4
	Carbon Tetrachloride	0,85	0,30	I,6I5	I,600	0,4
		0,55	0,20	I,620	I,6I0	0,0
		0,30	0,09	I,625	I,620	0,0
Muscovite No. 2	Distilled Water	0,90	0,42	I,600	I,620	9,2
		0,50	0,25	I,605	I,640	25,I
		0,38	0,I8	I,605	I,655	38,5
		0,I7	0,08	I,6I0	I,640	54,0
	Transformer Oil	0,70	0,35	I,605	I,595	0,4
		0,40	0,20	I,605	I,600	0,7
		0,20	0,I0	I,6I0	I,605	0,4
Phlogopite	Distilled Water	2,66	-	I,395	I,370	I,7
		I,00	-	I,400	I,4I0	5,8
		0,50	-	I,405	I,445	I8,0
		0,30	-	I,405	I,465	55,2
		0,I5	-	I,4I0	I,445	64,5
	Transformer Oil	0,75	-	I,400	I,395	0,0
		0,50	-	I,405	I,400	0,4
		0,30	-	I,405	I,400	0,0

No anomaly in thermal conductivity is observed for nonpolar liquids.

3. The size of the effect depends on the state of the surface and the nature of the solid. The effect is most graphically evident on "fresh" surfaces of mica crystals. Leaching out the surface leads to a sharp drop in thermal conductivity of film water.

4. The anomalously high thermal conductivity of films of polar liquids is accounted for by the improved quasi-crystalline structure acquired as a result of the action of these liquids on molecules of a strong surface layer of mica. With temperature rise, amorphization of film structure sets in and film thermal conductivity drops off rapidly down to values characteristic of the bulk state.

Symbols

λ = coefficient of thermal conductivity; c = specific heat; ρ = density (bulk weight); m = cooling rate of specimen in regular regime; α = heat transfer coefficient at specimen surface; X, Y and Z = linear dimensions of specimen; 2h = thickness of liquid film between two flat surfaces.

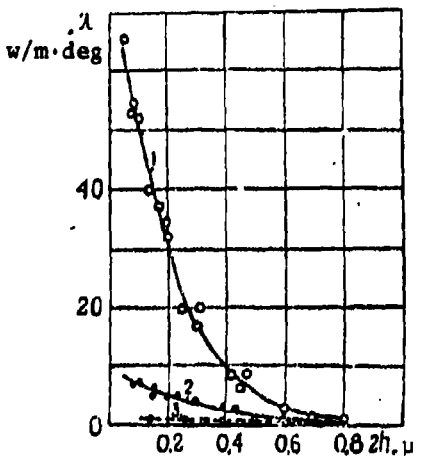

Figure 1. Variation of thermal conductivity of water films with film thickness: 1, On "fresh" surfaces of mice crystals; 2, On surfaces of mica crystals treated in boiling water; 3, On polyethylene surfaces

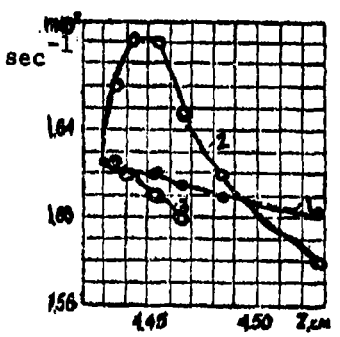

Figure 2. Cooling rate of specimens as a function of their height: 1, For continuous mica crystal at constant density; 2, For cleaved crystal saturated with water; 3, For cleaved crystal saturated with carbon tetrachloride

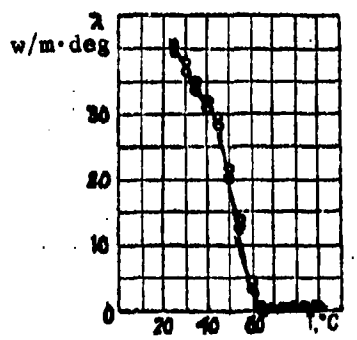

Figure 3. Thermal conductivity of film water on mica crystals as a function of temperature

References

1. Metsik, M. S., *Izv. Vuzov. Fizika* , Vol. 4, p. 29, 1958.
2. Metsik, M. S., *Izv. Vuzov. Fizika*, Vol. 5, p. 131, 1960.
3. Metsik, M. S. and O. S. Aydanova, *Sb. Issledovaniya v Oblasti Poverkhnostnykh Sil*, [Collection: Research on Surface Tension], Institute of Physical Chemistry of the Academy of Sciences USSR, Moscow, 1964.
4. Dimitrovich, A. D., *Opredeleniya Teplofizicheskikh Svoystv Stroitel'nykh Materialov*, [Determination of Thermophysical Properties of Construction Materials], Gosstroyizdat Press, Moscow, 1963.
5. Kondrat'yev, G. M., *Regulyarnyy Teplovoy Rezhim*, [Regular Thermal Regime], Gostekhizdat Press, Moscow, 1954.
6. Lashev, Ye. S., *Slyuda*, [Mica], Promstroyizdat Press, Moscow, 1948.
7. Metsik, M. S. and R. A. Zhidikhanov, *Izv. Vuzov. Fizika*, Vol. 2, p. 66, 1958.
8. Kornfel'd, M. I., *Uspekhi Fizicheskikh Nauk.*, Vol. 85, No. 3, 1965.
9. Key, D. and G. Lebi, *Tablitsy Fizicheskikh i Khimicheskikh Postoyannykh*, [Tables of Physical and Chemical Constants], Fizmatgiz Press, Moscow, 1962.
10. Deryagin, B. V. and Ye. Obukhov, *Kolloidnyy Zhurnal*, Vol. 1, p. 385, 1935.
11. Lykov, A. V., *Yavleniya Perenosa v Kapillyarno-poristykh Telakh*, [Transport Phenomena in Capillary-porous Bodies], Gostekhizdat Press, Moscow, 1954.
12. Metsik, M. S., *Sb. Issledovaniya v Oblasti Poverkhnostnykh Sil*, [Collection: Research on Surface Tension], Academy of Sciences USSR Press, No. 66, 1961.
13. Zhdanov, G. S., *Fizika Tverdogo Tela*, [Solid State Physics], Moscow State University Press, 1961.

THERMAL PROPERTIES OF SOLID AND MOLTEN METALS AT HIGH TEMPERATURES

L. P. Filippov, A. V. Arutyunov, I. N. Makarenko,
I. P. Mardykin, L. N. Trukhanova,
B. N. Khusainova and R. P. Yurchak

The article is a brief description of studies aimed at experimental investigation of the basic regularities underlying the behavior of thermal conductivity, thermal diffusivity, heat capacity and electroconductivity of solid and molten metals and in part of semiconductors at temperatures from 1000° to 3000°K.

A necessary stage in carrying out the projected research program involved an effort aimed at improving existing methods of measurement and devising new, high-temperature methods. The main focus here was given to developing comprehensive methods making it possible to obtain simultaneously the entire totality of main thermal characteristics. At present we have four methods of this type available to us. These methods have been based on the use of the so-called third-order regular thermal regime -- a steady-state periodic process. The main merit of this process is the diversity of information obtained in the experiment. (The following information sources were used: field of mean temperatures, field of amplitudes and phases of several harmonic components of temperature fluctuations [1, 2].) Below follows a brief description of these methods.

The work aimed at devising a method for simultaneous determination of thermal diffusivity and thermal conductivity of methods based on use of temperature fields propagated along the axis of a cylindrical specimen has been published earlier [3]. Usually this kind of process is employed in measuring only thermal diffusivity (the Angstrom method). The possibility of determining also thermal conductivity here involves use of variable heating by electronic bombardment making it possible to determine quite precisely the

value of the heating intensity. The method allows us to measure the parameters indicated for the "long" (several centimeters) and "short" (about one centimeter) specimens with a precision of 6-8 percent at temperatures up to approximately 1500°. Of late, a comparative variant of the method has also been devised making it possible to bypass electronic heating. Study is under way on using the method for molten metals and semiconductors.

The second of the comprehensive methods developed is based on use of temperature fluctuations of cylindrical symmetry -- radial temperature waves. We earlier [3] reported several versions of the use of radial temperature waves in measuring thermal diffusivity. Use of electronic heating in this method allows us to determine, along with thermal diffusivity, also heat capacity and, as a consequence, thermal conductivity. We used a modification of the method in which heating was conducted within a hollow specimen for these comprehensive measurements. For this purpose, the incandescent cathode imitating electrons is placed along the specimen axis. A measured voltage of several hundred volts is applied between the cathode and the specimen. The temperature fluctuations at the outer specimen surface are recorded. Thermal diffusivity is determined from the phase difference between heating intensity fluctuations and temperature fluctuations; heat capacity is found from the value of the amplitude of temperature and heating intensity fluctuations [4]. The maximum error in determining thermal diffusivity is usually 4-6 percent, while the maximum error in heat capacity measurement varies from 3 to 6 percent. A contactless photoelectric method is used in the latter, high-temperature version of the apparatus for recording temperature fulctuations; maximum temperatures here are approximately 1800°K.

The method described was used by the authors mainly in investigating molten metals. Liquid metal was placed in a vessel made of two thin-walled (approximately 0.1 mm) tantalum tubes coaxial with each other. Thermal properties of tin, lead, bismuth, cadmium, antimony, copper and germanium [5, 6] were studied by this method.

One of the main results of this investigation was a conclusion of the weak dependence of thermal conductivity of the materials studied on temperature. Thus, for tin thermal conductivity of a temperature range covering 1100 degrees centigrade varied by not more than 10 percent. The behavior of the Lorentz number of liquid metals is remarkable. At temperatures close

to the melting point the Lorentz number L, as a rule, is close to the theoretical value of $2.45 \cdot 10^{-8}$ w·ohms/deg^2. As the temperature rises, however, a marked progressive drop in L is observed, which provides the necessary formulation of the problem of what causes underlie this regularity.

The third of the comprehensive methods we developed was also based on use of radial temperature waves. In contrast to the former method, these waves are induced by heating a cylindrical specimen in an induction furnace, the power of which is varied periodically (modulated). Owing to the existence of a skin-effect, liberation of heat in the specimen occurs in a relatively thin layer near the surface; accounting for the bulk nature of heat release is nonetheless still necessary. In the version of the method now used, the temperature fluctuations of the outer, heated surface are recorded, though it is possible that there is another modification of the method -- with temperature fluctuations recorded at the specimen axis. A contactless photoelectric method of recording temperature fluctuations is employed. As in the previous method, in determining the thermal diffusivity of the specimen it is enough to know the phase difference between power fluctuations and temperature fluctuations. In determining the power a coil made up of several turns of wire surrounding the specimen is used. The value of the electromotive force recorded from this coil can be associated with the field intensity within the inductor and, ultimately, with the heater power. The measurement method described allows us to determine the thermal diffusivity, thermal conductivity and heat capacity in the temperature range 1000-2500°K with errors of about 6-8 percent and 8-10 percent, respectively. The method is used for systematic measurements of thermal properties of solid refractory metals.

The fourth type of the comprehensive experiment was designed for specimens in wire or foil form. It combines measurements of heat capacity by the alternating current heating method with thermal conductivity measured by the steady-state method. Both methods separately have been described by us [3] (cf. also [7-9]). Lately, these methods have been combined so that both heat capacity and thermal conductivity are determined on the same specimen by means of a single common apparatus, the basis of which is the earlier

described differential optical pyrometer [10, 11]. The electroconductivity of the specimen and its radiative characteristics are also described with the same device (the absolute black body models are used for this purpose). The error of heat capacity determination is 4-6 percent, and 6-8 percent for thermal conductivity; the temperature range is 1000-3000°K.

The comprehensive methods for measuring thermal characteristics described do not exhaust the arsenal of means of investigation used in our work. Thus, in particular, we used the ordinary Angstrom method for molten metals. Recently we have developed a steady-state method of measuring thermal conductivity for molten metals -- the small bridge method, earlier used by Katler and Cheney [6, 12, 13].

Let us proceed to presenting several new specific results obtained only most recently. Figures 1 and 2 present the results of the measurement of thermal conductivity and heat capacity of niobium obtained by different methods. The filled-in symbols in these figures refer to measurements of a massive specimen (rod) of niobium of the following composition: 99.2 percent Nb, 0.3 percent Ta, 0.08 percent Ti, 0.04 percent Fe and 0.04 percent Si (specimen 1). The circles denote values obtained by the variable induction heating method, and the triangles -- values obtained by the electronic heating method. The unfilled-in circles designate the wire specimen[1]. Its composition was as follows: 98.4 percent Nb, 0.6 percent Ta, 0.86 percent W and 0.015 percent Mo (specimen 2).

All the data obtained for thermal conductivity agree quite well with each other, and also with results of measurements in [14]. Agreement on the results of our heat capacity measurements are also quite satisfactory. The data obtained differed from the results of measurements in [15] by 4-7 percent, from the data in [16] by -1.5-+1.5 percent, from the data in [17] by -4-0 percent, and from the data in [18] by -3-+1 percent. The results in [18] are 6-7 percent below ours.

Figures 3 and 4 present the results of thermal conductivity and heat capacity measurements for antimony (Sb 96.8 percent, Pb 2.63 percent, Ag 0.50 percent, Cu 0.05 percent and Fe 0.02 percent), and for germanium

[1]See p.634

(specific resistance at room temperature approximately 10 ohms·cm) in the solid and liquid states obtained by the method of radial temperature waves (electronic heating). In addition to these data, here also are presented results obtained for solid germanium (specific resistance at room temperature 0.005 ohm·cm, alloyed with Sb impurity) by the first of the above-described comprehensive methods[2], and the data for liquid gallium (99.9997 percent). The values found for the thermal conductivity of gallium were secured by the low bridge method. The data are in satisfactory agreement with the results of measurement in [20] obtained up to 200°C. The thermal conductivity results for solid alloyed germanium agree well with the data in [21].

Small changes in heat capacity when antimony and germanium are fused agree with what has been obtained for other elements. The values of molar heat capacity in the molten state, as for most liquid metals, are close to 7-8 cal/mole. When we analyzed the thermal conductivity results, our attention was drawn to the discontinuous increase in germanium thermal conductivity upon fusion. The order of magnitude of thermal conductivity of liquid germanium is the same as for most liquid metals. This thermal conductivity behavior confirms the finding of the metallic nature of conductivity in liquid germanium, which was arrived at based on analysis of electroconductivity and the Hall effect [22]. The behavior of the Lorentz number for liquid antimony and germanium confirmed the regularity found for other liquid metals (cf. above).

Close to the melting point the Lorentz number is close to the theoretical value, but is gradually reduced with rise in temperature. To illustrate this, Figure 4 presents the results of thermal conductivity calculations, indicated by a dashed line, carried out on the assumption of the validity of the Widemann-Franz law.

[2]See p. 634

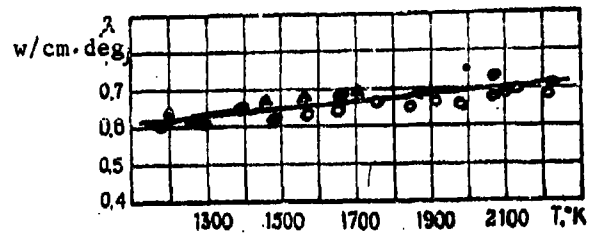

Figure 1. Results of investigating the thermal conductivity of niobium

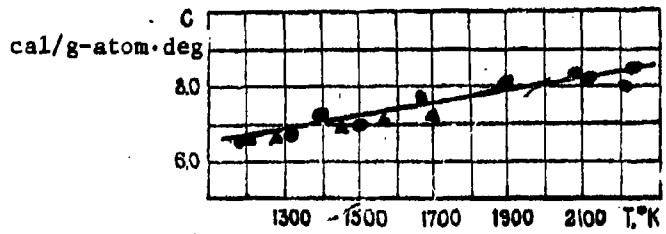

Figure 2. Heat capacity of niobium

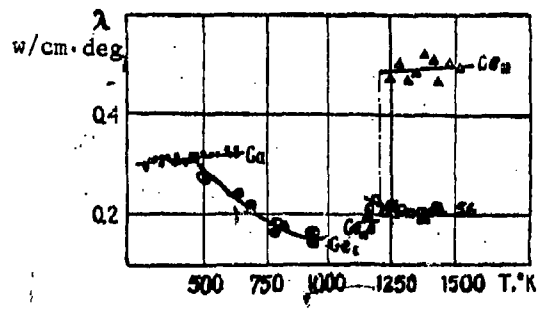

Figure 3. Results of measuring thermal conductivity of solid and liquid germanium, liquid antimony and liquid gallium

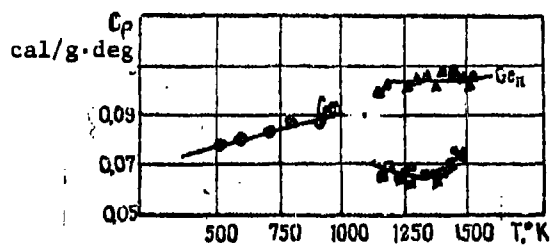

Figure 4. Heat capacity of germanium and antimony

Footnotes

1. To p.631 These data have been obtained with participation of A. G. Sorokin.

2. To p.632 Yu. L. Stakheyev participated in the study.

References

1. Filippov, L. P., *TVT*, No. 5, p. 817, 1964.
2. Filippov, L. P., *Int. J. Heat Mass Transfer*, Vol. 9, p. 618, 1966.
3. Filippov, L. A., *Teplo- i Massoperenos*, [Heat and Mass Transfer, Vol. 7], Energiya Press, Moscow, 1966.
4. Filippov, L. P. and R. P. Yurchak, *Vestnik MGU. Seriya Fizich.*, No. 1, p. 110, 1966.
5. Yurchak, R. P. and L. P. Filippov, *TVT*, No. 5, p. 696, 1964.
6. Yurchak, R. P. and L. P. Filippov, *TVT*, No. 2, p. 323, 1965.
7. Filippov, L. P., N. A. Tugareva and L. I. Markina, *IFZh*, No. 6, p. 3, 1964.
8. Filippov, L. P. and Yu. N. Simonova, *TVT*, No. 2, p. 188, 1964.
9. Filippov, L. P., *Vestnik MGU. Seriya Fizich.*, No. 4, p. 90, 1964.
10. Filippov, L. P. and Yu. N. Simonova, *TVT*, No. 1, p. 3, 1964.
11. Filippov, L. P. and Yu. N. Simonova, *Peredovoy Nauchno-tekhnicheskiy i Proizvodstvennyy Opyt*, No. 18-65-143/19, 1965.
12. Cutler, M., *J. Appl Phys.* Vol. 32, No. 6, p. 1915, 1961.
13. Cutler, M. and G. T. Cheney, *J. Appl. Phys.*, Vol. 34, No. 6, p. 1714, 1963.
14. Voskresenskiy, V. Yu., V. E. Peletskiy and D. L. Timrot, *TVT*, No. 1, p. 46, 1966.
15. Kirillin, V.A., A. G. Sheyndlin, V. Ya. Chekhovskiy and I. A. Zhukova, *TVT*, No. 3, p. 395, 1963.
16. Jarger, F. M. and W. A. Veenstra, *Proc. Acad. Wetens. Amsterdam*, Vol. 37, p. 61, 1934.
17. Lowenthal, G. C., *Austr. J. Phys.*, Vol. 16, p. 47, 1963.
18. Kraftmakher, Ya. A., *FTT*, Vol. 5, No. 3, 1963.
19. Fel'd, P. V. and F. G. Kusenko, *Metallurgiya i Toplivo*, No. 2, p. 79, 1960.

20. Dutchak, Ya. I. and F. V. Fanasyuk, *FTT*, Vol. 8, No. 9, p. 2805, 1966.

21. Beers, D. S., G. D. Cody and B. Ables, *Proc. of Int. Conf. on the Physics of Semiconductors*, p. 41, London, 1962.

22. Cusack, N. E., *Rept. Progr. Phys.*, Vol. 26, p. 361, 1963.

THERMAL CONDUCTIVITY OF STABILIZED ZIRCONIUM DIOXIDE AT HIGH TEMPERATURES

V. Ya. Chaykovskiy and A. M. Banayev

Investigations of the thermal conductivity of refractory oxides in the temperature range 1400-2000°C thus far are very few in number [1, 2], in spite of the fact that data at these temperatures is of special practical interest. The authors of this present study have devised an experimental apparatus for determining the thermal conductivity coefficient at temperatures up to 2100°C. The method of the experiment and the apparatus design have been set forth quite adequately in [3]. The measurements were conducted by the tubing method.

Specimens of the test material, cylindrical in configuration, were in the form of a set of disks 20 mm high, with outer diameter of 50 mm and inner diameter of 4-6 mm. Dead-end vertical openings 2 mm in diameter were made with ultrasonic equipment to measure temperature in the specimens. Tungsten-rhenium (VR-5/20, 0.35 mm in diameter) and platinum-platinum-rhodium thermocouples in two-channel alundum tubings were placed into these apertures.

The apparatus was supplied from a 220-v alternating current network through the AOSK-25 single-phase automatic transformer and the OSU-40 step-down transformer. Determination of the thermal flux value was made electrically, that is, by measuring the current passing through the heater and the voltage drop over its working section. The current value and the voltage drop over the experimental section of the heater were measured by the R-56 type alternating current potentiometer. The emf of the thermocouples was measured by the PMC-48 type direct current potentiometer. The VR-5/20 type thermocouples employed were calibrated with the OP-48 optical pyrometer in the modernized TVV-2 high-temperature vacuum furnace [4].

Table 1. Characteristics of ZrO_2 Specimens and Their Chemical Analysis

Designation of Materials	Maximum Sintering Temp. °C	Maximum Molding Pressure, N/m^2	Grain Size of Original Material, mm	Bulk Weight kg/m^3	Porosity of Specimens, %	Results of X-ray Analysis After Sintering	Chemical Composition in % by Mass							
							SiO_2	Al_2O_3	TiO_2	Fe_2O_3	CaO	MgO	Alkali	ZrO_2
1	2	3	4	5	6	7	8	9	10	11	12	13	14	15
I	I750	$5 \cdot 10^7$	50% 2-0,5; 50% 0,088	$4,3 \cdot 10^3$	22,8	90% Cubic 10% Monoclinic	0,8	0,5	I,I0	0,225	5,37	0,429	0,32	90,94
2	I750	$10 \cdot 10^7$	50% 2-0,5; 50% 0,088	$4,4 \cdot 10^3$	2I,5I	60% Alkali 40% Monoclinic	0,8	0,5	I,I8	0,273	5,23	0,I22	0,I8	9I,48

The experimental values of thermal conductivity obtained relate to the mean arithmetic temperature.

In this study thermal conductivity of refractories based on zirconium dioxide in the temperature range 300-2000° was measured. Table 1 lists the characteristics of the specimens investigated and their chemical composition. As we can see from Table 1, the test materials differed by different ratio of cubic and monoclinic modifications of zirconium dioxide, the amount of impurities in the form of various oxides, and the molding pressure. Crystalline structure had the greatest effect on the results of the study. We first of all must take note of the variation in the course of thermal conductivity as a function of temperature for the polymorphous transformation (1000-1250°C) of the monoclinic modification of zirconium dioxide into the tetragonal modification [5]. Up to the polymorphous transformation, the thermal conductivity of refractories rises linearly with temperature rise, but thereafter it varies so slightly that to the first approximation it remains constant within limits of experimental error. Further, up to the phase transition point the thermal conductivity depends on phase composition: the higher the content of the cubic and the lower the content of the monoclinic modification of zirconium dioxide, the higher the thermal conductivity of the material. We must also take note of the fact that at temperatures above the polymorphous transition experimental data for refractories 1 and 2 are practically the same.

The molding pressure did not affect the thermal conductivity value.

Results of experimental determination of thermal conductivity of the specimens investigated are shown in Figure 1, and Table 2 lists the smoothed values of the thermal conductivity coefficient for rounded temperature values.

The maximum scatter of experimental points relative to the averaged value does not exceed the limiting random error of the experiment, which the authors estimate at 12 percent.

Table 2. Smoothed-Over Values of Thermal Conductivity Coefficients for Zirconium Dioxide

T°C	w/m·deg	
	Material No. 1	Material No. 2
100	1,45	-
200	1,48	-
300	1,52	-
400	1,55	1,06
500	1,57	1,12
600	1,58	1,18
700	1,59	1,25
800	1,59	1,32
900	1,60	1,38
1000	1,60	1,46
1100	1,61	1,52
1200	1,62	1,53
1300	1,63	1,54
1400	1,64	1,55
1500	1,64	1,56
1600	1,65	1,57
1700	1,65	1,58
1800	-	1,59
1900	-	1,61
2000	-	1,62

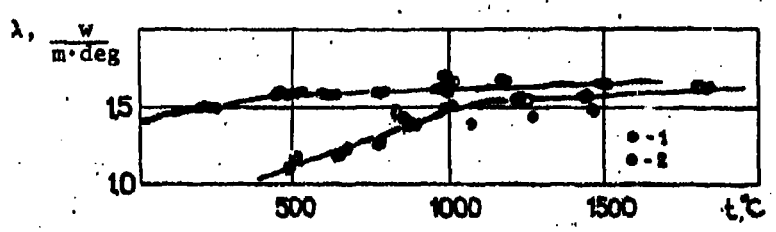

Figure 1. Results of experimental study of thermal conductivity of zirconium dioxide stabilized with calcium oxide: 1, 2, Materials No. 1 and 2 (cf. Table 1); the averaged values of the experimental data obtained are presented on the curves.

References

1. Pustovalov, V. V., *Zavodskaya Laboratoriya*, No. 9, 1957, *Ormeupory*, No. 7, 1957.
2. Kharlamov, A. G., *Teploenergetika*, No. 3, 1961; No. 1, 1962.
3. Chekhovskoy, V. Ya. and A. M. Banayev, *TVT*, Vol. 3, No. 1, 1965.
4. Chekhovskoy, V. Ya. and A. Ye. Sheyndlin, *Zavodskaya Laboratoriya*, Vol. 29, No. 10, 1963.
5. Sukharevskiy, B. Ya. and I. I. Vishnevskiy, *DAN SSSR*, Vol. 147, No. 4, 1962.

THERMAL CONDUCTIVITY OF POLYCAPROAMIDE AS A FUNCTION OF TEMPERATURE AND MOLECULAR WEIGHT

I. I. Chernobyl'skiy, V. I. Kirichenko and A. N. Piven

Modern views of the nature of polymers require some refinement of the heat transfer process in polymers and their melts. Studies of the thermal conductivity of polymers conducted with simultaneous investigation of variations of structure and molecular weight allow us to obtain data supplementing and refining modern concepts of the thermal conductivity method and of polymeric bodies. These studies are necessary both for advancing the overall theory of polymeric properties as a function of polymer structure, and also for substantiating and determining the main parameters of processes of obtaining and processing polymers.

The aim of this study is to investigate the thermal conductivity of polycaproamide as a function of temperature and molecular weight while simultaneously studying the nature of supermolecular structure.

Determination of the thermal conductivity was conducted by the method of heating two plates with a constant-power flat heat source [1]. The thermal conductivity of polycaproamide was studied in this work as a function of molecular weight in the temperature range 20-250°C.

The test specimens were made in the form of flat sheets 49.5 mm in diameter and 3-5 mm thick. By special processing of caprolactam and polycaproamide melts -- degassifying under vacuum -- monolithic crystalline blocks were obtained practically free of moisture (not more than 0.01 percent by weight). The specimens of caprolactam-monomer were obtained by crystallizing the melt in a metal cell with no access to air. The blocks of polycaproamide with the required molecular weight were obtained by polymerization of caprolactam in a special autoclave under specific sets of

conditions. The averaged molecular weig. calculated from the curves of the molecular-weight distribution was adopted as the molecular characteristic of polycaproamide. These curves were obtained by the method of diffusive salting out of a polycaproamide solution developed in the Institute of Monomer and Polymer Chemistry of the Academy of Sciences Ukrainian SSR. The melting point of polycaproamide was determined with the aid of the MIN-8 microscope by observing the fusing process in polarized light. To exclude the effect of crystallinity on thermal conductivity when comparing specimens of polycaproamide of different structures and different molecular weights, specimens with identical density, determined by the gradient tube method, were selected.

Physicochemical characteristics of the test polycaproamide specimens are listed in the table. Microphotographs of the supermolecular structure of polycaproamide were obtained on the MRI-6 microscope in transmitted polarized light.

The thermal conductivity of caprolactam and polycaprolactam as a function of temperature is presented in Figures 1 and 2. The general nature of the curves describing thermal conductivity as a function of temperature corresponds to the concepts of heat transfer in low-molecular and polymeric compounds. It follows from Figure 1 that thermal conductivity of caprolactam varies slightly with temperature rise: in the temperature range up to the melting point (about 69.5°C) thermal conductivity rises, but at temperatures higher than the melting point it drops off with temperature rise. For polycaprolactam, thermal conductivity was observed as a function of temperature (Figure 2) characteristic for most polymers [2, 3], namely: thermal conductivity decreases with temperature rise.

In this present work, the thermal conductivity of caprolactam and polycaprolactam were studied in temperature ranges within which the first-order structural transition takes place -- melting. The presence of this structural transition is due to the characteristic maximum on the thermal conductivity versus temperature curve for caprolactam (Figure 1) and the well defined, successive, minimum and maximum on the very same curves for

polycaproamide (Figure 2). The sharp variation of many properties in this case, including thermal conductivity, results from the abrupt variation of the energy state of the system. The effect of polymer fusion on the heat transfer process is expressed, first of all, in the abrupt drop of the modulus of elasticity of the macromolecules (by 10^3-10^5 times [5]), and also in the considerable rise of mobility of individual segments and of the macromolecules as a whole.

Table

No.	Mean Molecular Weight	Extent of Polydispersity	Melting Point, °C	Density at 20°C	Size of Spherolites, μ
I	I8000	0,20	2I0	I,I590	I50÷200
2	2I000	0,39	2I8	I,I6I0	50÷70
3	25000	0,28	222	I,I593	200÷220
4	32000	0,27	2I5	I,I590	I00÷I20

Near the melting point in polycaproamide melt, high order of macromolecules is possible, as a result of which the thermal conductivity of the polymer must rise sharply all the way to values corresponding to the crystalline state (Figure 2). The probability of the highly ordered state of polycaproamide melt drops off rapidly with temperature rise, and thermal conductivity is already governed by the physical regularity corresponding to the state of the single-phase liquid system, that is, decreases with temperature rise.

Analysis of curves a, b and d in Figure 2 lead to the conclusion that in spite of some differences in structure of specimens there is still a marked tendency toward rise of polycaproamide thermal conductivity with increase in molecular weight. This function is observed even more distinctly for molten polycaproamide, where the effect of the supermolecular structure (spherolite type) is excluded.

It is clear from the microphotographs we have taken (Figure 3) that all the polycaproamide specimens studied have a crystalline structure in the form of spherolites of fibrillary structure and differ in spherolite size. By comparing Figures 2 and 3 it follows that the spherolite sizes have an effect on the polymer thermal conductivity. This effect evidently is accounted for by the fact that the thermal conductivity of polymers, including polycaproamide, are determined by the number and mobility of structure elements (spherolites). All possible changes in the mobility of structural elements can be accounted for by change in their size. When spherolite dimensions are reduced, their mobility and numbers per unit volume rise. This can account for the rise in thermal conductivity for the specimens a and b compared with the thermal conductivity for the specimen (Figure 2). Upon analyzing the effect on thermal conductivity of the supermolecular structure type and the dimensions of structural elements, we must also take into account the homogeneity of structure.

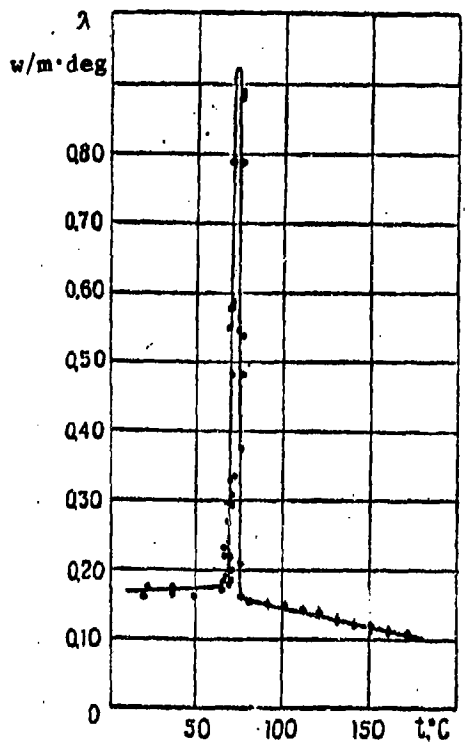

Figure 1. Thermal conductivity of caprolactam as a function of temperature: •, Values obtained in the present study; ϕ, Values found in [4]

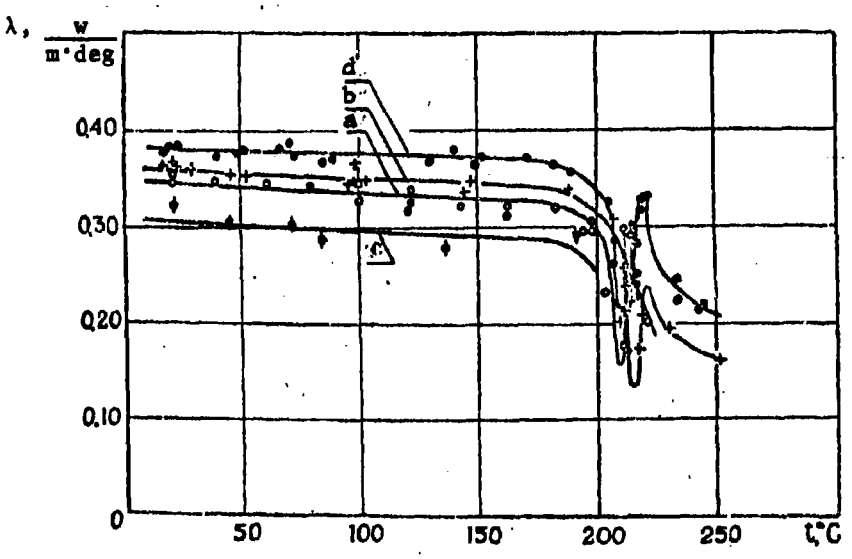

Figure 2. Thermal conductivity of polycaproamide as a function of temperature for various molecular weights: a, M = 18,000; b, M = 21,000; c, M = 25,000; d, M = 32,000

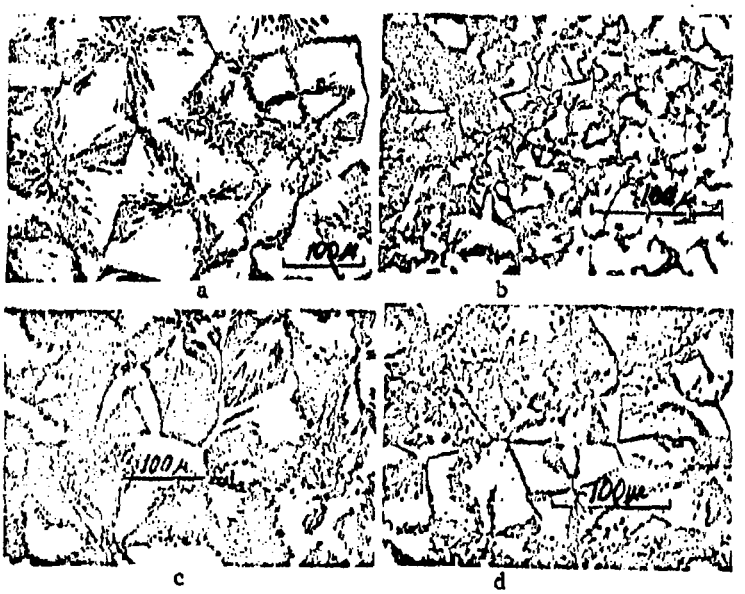

GRAPHIC NOT REPRODUCIBLE

Figure 3. Microphotographs of the structure of test polycaproamide specimens: a, M = 18,000; b, M = 21,000; c, M = 25,000; d, M = 32,000

References

1. Chernobyl-skiy, I. I., M. I. Pavlishchev, K. G. Tertyshnik, and A. N. Piven', *Khimicheskoye Mashinostroyeniye*, No. 2, 1965.
2. Knappe, W., *Kunststoffe*, Vol. 51, No. II, p. 707, 1961.
3. Eirman, K., *Koll.-Z. u. Z.-Polymere*, Vol. 201, p. 3, 1965.
4. Golubev, I. F., *Trudy GIAP*, No. 7, 1957.
5. Mandel'kern, L., *Krystallizatsiya Polimerov*, [Crystallization of Polymers], Khimiya Press, Moscow-Leningrad, 1966.